Exact Maps in Density-Functional Theory

vorgelegt von
Diplom-Physikerin
Tanja Dimitrov
geb. in Berlin

Von der Fakultät II – Mathematik und Naturwissenschaften
der Technischen Universität Berlin
zur Erlangung des akademischen Grades

Doktor der Naturwissenschaften
Dr. rer. nat

genehmigte Dissertation

Promotionsausschuss:

Vorsitzender: Prof. Dr. rer. nat. Mario Dähne
1. Gutachter: Prof. Dr. rer. nat. Andreas Knorr
2. Gutachter: Prof. Dr. rer. nat. Angel Rubio

Tag der wissenschaftlichen Aussprache: 09. Februar 2017

Berlin 2017

ABSTRACT

Providing sufficient accuracy at low-computational cost, not surprisingly, density-functional theory (DFT) is a standard tool in theoretical material science. Similarly, quantum-electrodynamical density-functional theory (QEDFT) provides a promising route to describe experiments at the interface of quantum optics and quantum chemistry. Formally, in the Kohn-Sham (KS) formulation of DFT and QEDFT the exact many-particle Schrödinger equation is replaced by a set of coupled non-linear one-particle differential equations. The electron-electron, the electron-ion and the electron-photon interactions of the interacting system are mimicked by their corresponding effective KS potential with an, in principle unknown exchange-correlation (xc) term. In practice, DFT and QEDFT require approximations for this xc potential. The quality of which fully determines how much the DFT and QEDFT observables deviate from the exact ones. Understanding the shortcomings and improving the quality of approximate functionals makes the study of the exact functional of model systems indispensable.

Here, we employ exact diagonalization for the Hamiltonian of different types of real-space lattice models in one spatial dimension to access the ground-state wave function, and thus to explicitly construct the exact functionals of DFT and QEDFT. To study the functional behavior of purely electronic systems, we consider two singlet-state electrons moving in an external potential with two connected atomic wells of variable depth and distance. To study coupled electron-photon systems, we consider the Rabi Hamiltonian with variable electron-photon coupling strength. By varying the model parameters, we systematically construct the functionals for systems from weak to strong coupling between the building blocks of the global system. Using the concept of the effective density-to-potential map, we discuss the intrasystem steepening which is an exact condition on the xc functional that captures the static correlation present in the system and carve out how it relates to the well-known intersystem derivative discontinuity. We further construct arbitrary observables as functionals of the internal variables which are directly affected by such features of the effective density-to-potential map. By constructing the reduced dipole map in the four-particle case of coupled electron-photon system, we show that the density-to-potential map helps to identify and understand recently discovered physical effects in the field of strongly coupled electron-photon systems.

This work provides a contribution to the development of approximate functionals required in practical density-functional calculations of arbitrary experimentally accessible observables. Both the intrasystem steepening and the intersystem derivative discontinuity play a crucial role for systems with highly-localized electrons. Including both features in approximate functionals will improve the accuracy of DFT evaluation of observables for such systems. Those results provide novel insight into the properties of the exact xc potentials in QEDFT. This work opens a new route to construct new functionals using coarse-grained or embedding approaches within the general and exact frameworks of DFT and QEDFT.

ZUSAMMENFASSUNG

Die Dichtefunktionaltheorie (DFT) ermöglicht computergestützte Berechnungen von Materialeigenschaften mit ausreichend hoher Rechengenauigkeit bei geringer Rechenzeit. Eine ähnlich vielversprechende Methode ist die quantenelektrodynamische Dichtefunktionaltheorie (QEDFT), die eine Beschreibung von Experimenten an der Schnittstelle zwischen der Quantenoptik und der Chemie erlaubt. In der Kohn-Sham Formulierung der DFT sowie der QEDFT wird die Vielteilchen Schrödingergleichung durch ein System von gekoppelten Einteilchengleichungen ersetzt. Sowohl die Elektron-Elektron, die Elektron-Ion als auch die Elektron-Photon Wechselwirkung wird in den gekoppelten Einteilchengleichungen durch ihr jeweiliges effektives Kohn-Sham-Potenzial beschrieben. Im Allgemeinen ist der Austausch-Korrelations (xc) Anteil des Kohn-Sham-Potenzials jedoch unbekannt und muss genähert werden. Inwieweit die DFT-Rechnungslösungen von den exakten Observablen abweichen, hängt von der Qualität der gewählten Näherung ab. Die Kenntnis der Eigenschaften von Funktionalen der Modelsysteme sind entscheidend um Näherungen für ein konkretes physikalisches System besser einzuordnen und die DFT-Näherungen qualitativ zu verbessern. Mittels exakter Diagonalisierung des Hamiltonians berechnen wir den Grundzustand von Modelsystemen im diskretisierten ein-dimensionalen Ortsraum und können somit die exakten DFT- und QEDFT-Funktionale berechnen. Wir untersuchen die Funktionale von rein elektronischen Systemen mit zwei Elektronen im Singletzustand, die sich im externen Potenzial zweier Molekültöpfe mit variablen Abstand und variabler Potenzialtopftiefe bewegen. Die Funktionale der gekoppelten Elektron-Photon Systeme werden unter Verwendung des Rabi Hamiltonians mit variabler Elektron-Photon Kopplungstärke untersucht. Die Modelparameter erlauben uns systematisch die Kopplungsstärke zwischen den einzelnen Systembestandteile zu variieren und deren zugehörigen Funktionale zu untersuchen. Unter Zuhilfenahme der effektiven Dichte-zu-Potenzialabbildung, diskutieren wir den intra-systemaren Anstieg, der die Korrelation im System beschreibt. Wir diskutieren wie sich dieser zu der bekannten Ableitungsunstetigkeit der DFT verhält. Darüberhinaus berechnen wir die Funktionalabhängigkeit ausgewählter Observablen, die durch die Eigenschaften der Dichte-zu-Potenzial Abbildung bestimmt ist. Wir kommen zu dem Schluss, dass die Dichte-zu-Potenzial Abbildung einen wesentlichen Beitrag zum Verständis der kürzlich untersuchten physikalische Effekte im starken Kopplungslimit beiträgt. Die im Rahmen der Dissertation untersuchten Eigenschaften exakter Funktionale können zur Entwicklung von den in der DFT und QEDFT erforderlichen Näherungsfunktionalen herangezogen werden. Der intra-systemare Anstieg und die Ableitungsunstetigkeit spielen eine zentrale Rolle für stark lokalisierte Vielteilchensysteme und sollten daher zur Verbesserung für die Näherungen dieser Systeme berücksichtigt werden. Die in der Arbeit gezeigten Ergebnisse geben einen Einblick in die Eigenschaften der xc-Potenziale der QEDFT, die zur Funktionalentwicklung im Rahmen von eingebetteten Theorien und Grobkornnäherungen herangezogen werden können.

CONTENTS

1 INTRODUCTION

Modern high-technology applications including electronic, magnetic and optical devices require the selection and design of materials with tailored mechanical, thermal, electronic, optic and magnetic material properties. Elasticity, electrical or thermal conductivity, wettability and polarizability represent, among other physical, chemical and engineering properties, the most prominent "properties of desire" involved in the development of new materials. Nowadays, there are approximately in between 40.000 to 80.000 different materials known that can be potentially used for technical applications [1] such as photovoltaics, thermoelectricity and plastic materials. The search for new materials is driven by experimental and theoretical material science, where the latter allows to *determine* and to *predict* the material properties without the need to explicitly perform a measurement process in an experimental setup.

The different measurement methods used in experimental material science give informations about the materials atomic nature and their spatial structure, the materials atomic bonding, the materials lattice defects and their microscopic architecture [1] that determine the physical and chemical properties of different materials. The theoretical models used in material science complement the insight gained by the measurement process, allow to guide the experimental search for new materials and further, also allow to determine the properties of materials that are not directly accessible by experimental measurement processes.

Theoretical models are based on mathematical equations that capture the geometry, the chemical and physical properties of the system and how they evolve in time. Since chemical and physical *processes* such as the altering or the formation of new chemical bonds, the emission or absorption of a photon, or the scattering of particles can change the properties of materials in space and time, it is of fundamental importance to determine the length- and time scales that form the "boundaries" of the system under consideration and that allow us to separate the system from its environment. Theoretical models assign a descriptor to the system, where the descriptor is defined by a set of initial properties of the system. It can be distinguished between (i) a complete descriptor that contains all informations that we can possibly obtain about a system, e.g. the ground-state wave function in quantum mechanics, and (ii) a reduced descriptor that contains a minimal number of properties related to the system that is sufficient for the description of any quantities of interest, e.g. the electronic density of the system.

The time-evolution of the systems properties and hence, of the systems descriptor is modeled by the equations of motion that follow the laws of classical or quantum mechanics [2]. The quantum-mechanical description of processes is usually required for processes that take place below or at the atomic length scale, the

typical length scale of the quantum world. Such quantum mechanical processes are the underlying processes of many experimental measurement instruments, e.g. of scanning tunneling microscopes [3] (STM) and nuclear magnetic resonance (NMR) spectrometers [4], of many technical devices, e.g. transistors [5, 6], light-emitting diodes (LEDs) [7], and solar cells [8], and of many processes that happen in nature, e.g. the photosynthesis [9] and the vision process of birds [10]. The physical behavior of these microscopic processes clashes with the intuitive laws we know from classical physics. This bizarre behavior of the quantum world directly affects the macroscopic properties of the world that surrounds us. Macroscopic quantum effects include e.g. superconductors [11], suprafluidity [12–14], or squeezed spin states [15, 16].

The discovery of the fundamental laws of the quantum world, the description of which required to go beyond the concepts of classical physics, dates back to the beginning of the 20th century. From the discovery of the black body radiation in 1900, to the Franck-Hertz experiment [17] over the Stern-Gerlach experiment [18, 19] to the double-slit experiments of light and matter, among many others, the field of quantum mechanics was driven by a wide range of experiments which ultimately led to the fundamental theoretical concepts of quantum mechanics. In particular, experimental observations such as the photoelectric effect [20, 21] and the Compton effect [22] revealed the quantized nature of light, postulated by Albert Einstein in 1905 [23]. Matter waves postulated by Louis de Broglie which assign particles with momentum p a wave-length $\lambda_{\mathrm{DB}} = \frac{h}{p}$ have been experimentally confirmed for electrons [24], atoms and dimers [25], neutrons [26] and even for large molecules such as the C60 fullerenes [27].

The wave-particle duality and the quantization of light and matter, Heisenbergs uncertainty condition, the concept of spin and entanglement are just a few concepts of this bizarre quantum world which seem to turn our world upside down. Some aspects of these quantum mechanical concepts such as interference become plausible in the context of Schrödingers wave mechanics [28, 29], or in the formally equivalent concept of matrix mechanics [30] introduced by Heisenberg, Jordan and Born [31–33]. In contrast to the mathematical rigorous formulation of quantum mechanical concepts, the interpretation of some quantum-mechanical quantities remains a controversial aspect of the theory that has started off with the famous Einstein-Bohr debate [34–37]. A particular delicate aspect is the concern about the fundamental nature of the quantum mechanical states of a system. However, this is only one of the many puzzling aspects in the theory of quantum mechanics, which has led to the various interpretations of the theory itself, including the Copenhagen interpretation [38], the statistical interpretation [39], the many-world interpretation [40, 41] and the interpretation by Bohm [42, 43]. The different interpretations may shine light on different aspects of the theory. Each of which may help to obtain a clearer picture of this bizarre quantum world and how it relates to the world that surrounds us.

The tools provided by the quantum mechanical framework give direct access to properties of many-body systems that can not be described within the frame-

work of classical mechanics. Theoretical methods derived from first principle quantum mechanics are called ab-initio methods. Ab-initio wave function based methods that allow the quantum description of the matter include coupled cluster theory [44], Møller-Plesset perturbation theory [45] and multi-reference approaches [46]. Such wave function based methods encounter the curse of dimension that refers to the exponential growth of the computational complexity with increasing particle number [46, 47]. DFT is an exact reformulation of Schrödinger wave mechanics that allows to describe the system by the three-dimensional electronic ground-state density, i.e. a fundamental descriptor of significantly lower dimension. In principle, DFT is an ab-initio method that scales with the three-dimensional density. In practice, DFT comes at the price hidden in the search of reliable approximations to the exchange-correlation potential.

Besides the quantum description of matter, quantum theory is also considered about the quantum description of the electromagnetic field. The combined quantum treatment of matter and fields allows to describe and predict theoretically the outcome of experiments at the interface of quantum chemistry and quantum optics. Recent experiments [48–55] at the interface of chemistry, material science and quantum optics, in the new field of quantum electrodynamics (QED) chemistry, have been able to modify the chemical landscape of systems by placing the system into an optical cavity. Of particular interest is the strong coupling regime between the matter and the electromagnetic fields, which leads to the formation of new hybrid matter-field states of novel character further broadening the variety of potential material candidates. Such systems can be theoretically studied by the recently developed exact framework of QEDFT.

Nowadays, ground-state DFT is a standard tool in material science and quantum chemistry [56–60]. Similarly, the framework of QEDFT provides a promising route for the theoretical description of experimental setups within the field of QED chemistry. The quality of practical DFT and QEDFT applications depends on the quality of the approximations to the unknown exchange-correlation functional. Approximate functionals can be found by fitting adjustable parameters to experimental or ab-initio data or by generalizing exact constraints originally derived from model systems [61]. In this work, we discuss an exact condition on the exchange-correlation functional in DFT and QEDFT that is relevant for systems consisting of well separated but mutually-interacting fragments.

This thesis is structured into eight chapters. Chap. 2 gives a brief overview over the concepts in interacting many-particle physics. Chap. 3 deals with density-based methods including the framework of DFT and QEDFT. Chap. 4 deals with the concepts of DFT on a lattice. In Chap. 5, we validate our program with reference data of a stretched H_2 molecule confined to one spatial dimension. We use these reference data as a starting point to introduce the well-known delocalization error of the local-density approximation (LDA) that directly translates from the density to the energies in the dissociation curve. In Chap. 6, we introduce the concepts of the effective density-to-potential map and the intrasystem steeping in correlated electron-electron systems. These findings are generalized to corre-

lated electron-photon systems in Chap. 7. Finally, Chap. 8 provides a summary of this thesis and gives an outlook on how our results can be used to improve the quality of approximate functionals in DFT and QEDFT.

Part I

THEORETICAL FOUNDATIONS

Here, we give an overview about the theoretical landscape in which this thesis is placed. Basic concepts and theoretical methods of non-relativistic quantum mechanics including wave function and density based methods are introduced. In particular, we focus on concepts relevant in ground-state density-functional theory and quantum electrodynamical density-functional theory. We briefly discuss some of the well-known shortcomings of approximate functionals and discuss existing approaches that aim to cure these shortcomings.

2 CONCEPTS IN INTERACTING MANY-PARTICLE PHYSICS

Theoretical material science allows to predict the material properties of a system using the ever increasing capacities of modern computers without the need to explicitly perform a measurement process in an experimental setup. Many material properties depend on the number of particles in the system and change whenever the particle number changes. Examples of such situations include charge transfer processes where the charge density is transferred among fragments within the system, photo-electron processes, where light absorption removes electrons from the system, e.g. an atom, molecule or solid, or exciton creation in solar cells, where electron-hole pairs are created. These changes in the particle number are only possible, if the system is in contact with its environment. Therefore, to accurately describe these processes within ab-initio methods, e.g. with density-functional theory introduced in Chap. 3, it is important to discuss the general concept of quantum systems, the partitioning of the physical system into system and environment, the concept of composite quantum systems and the related concepts of entanglement and correlation.

2.1 STATES OF MANY-PARTICLE QUANTUM SYSTEMS

Physical systems can be described by a complete descriptor given by a set of variables that carries all informations about the system and, in principle, allows to determine all its properties. In quantum mechanics such a descriptor is given by the complex probability wave function that depends on the position and spin coordinates of each particle. In static (time-independent) situations, typically the ground state of the system is considered. This state that is defined in the N-particle Hilbert space $\mathcal{H}_N$ is given by

$$\Psi(\vec{x}) = \Psi(\vec{r}_1\sigma_1, \vec{r}_2\sigma_2, \cdots, \vec{r}_N\sigma_N), \tag{1}$$

where

$$\vec{x} = (\vec{x}_1, \vec{x}_2, \cdots, \vec{x}_N) \tag{2}$$

denotes the collective space-spin variable of all particles and

$$\vec{x}_j = (\vec{r}_j, \sigma_j) \tag{3}$$

denotes the space-spin variable of the j-th particle in the system[1]. The wave function encounters the "curse of dimension" [47], since its complexity grows

1 We use the following notation for the integration over the spin-space variable:

$$\int d\vec{x} = \sum_{\sigma} \int d\vec{r}. \tag{4}$$

.

exponentially with the number of particles in the system. This exponential scaling is also known as the exponential wall in interacting many-body problems. We will later discuss how to (partly) circumvent the exponential wall, e.g. by using density-functional theory, where the wave function as basic descriptor of the system is replaced by the electron ground-state density n_{00}[2].

Definition 2.1.1: Ground-State Electron Density

The ground-state electron density of a pure state in the N-particle Hilbert space $\mathcal{H}_N$ is given as usual by

$$n_{00}(\vec{r}_1) = N \sum_{\sigma_1} \int d\vec{x}_2 \cdots \int d\vec{x}_N \Psi_0^*(\vec{x}_1, \vec{x}_2, \cdots, \vec{x}_N) \Psi_0(\vec{x}_1, \vec{x}_2, \cdots, \vec{x}_N), \tag{5}$$

with the ground-state wave function Ψ_0.

2.2 SCHRÖDINGER WAVE MECHANICS

The time-evolution of quantum-mechanical states is given by the time-dependent Schrödinger equation[3]

$$i\hbar\partial_t |\Psi\rangle = \hat{H}(t) |\Psi\rangle , \tag{6}$$

and the state at initial time t_0, i.e. the initial state $\Psi(t = t_0) = \Psi(t_0)$, whereas the stationary states of the system are defined by the eigenvalue problem

$$\hat{H} |\Psi_j\rangle = E_j |\Psi_j\rangle , \tag{7}$$

known as the static Schrödinger equation. Exact diagonalization of the Schrödinger equation gives access to the eigenvectors $|\Psi_j\rangle$ and the eigenvalues E_j of the eigenvalue problem defined in Eq. 7. Each eigenvector corresponds to a stationary eigenstate Ψ_j and each eigenvalue E_j to an eigenenergy of the system. In particular, the eigenstate with the lowest eigenenergy E_0, is the ground-state $|\Psi_0\rangle$ of the many-particle system. Alternately, the stationary eigenstates and eigenenergies can be found by applying the variational principle

$$E_0 \leq E_j = \frac{\langle \Psi_j | \hat{H} | \Psi_j \rangle}{\langle \Psi_j | \Psi_j \rangle}, \tag{8}$$

where the eigenenergy E_j is greater or equal to the ground-state energy E_0, i.e. the lowest eigenvalue of the system.

2.3 OPERATORS AND MEASUREMENT PROCESSES

The measurement process itself can change the state and hence, the properties of the system. Both, the system and the measurement apparatus form a composite

2 We use double numbered subscripts for expectation values and transition matrix elements as formally defined in Eq. 9. This allows us e.g. to formally distinguish between the ground-state density n_{00}, the first excited density n_{11} and the transition density between the ground-state and the first-excited state n_{01} within a compact notation.

3 Throughout this chapter we use SI units unless stated otherwise.

quantum system. From left to right, Fig. 1 illustrates the time-evolution of the measurement-detector system. Before the measurement the initial state of the combined system is a factorizable state. During the measurement process - provided the system is not in an eigenstate of the detector - the state of the system becomes an entangled state [62, 63]. The theoretical analogue to the experimen-

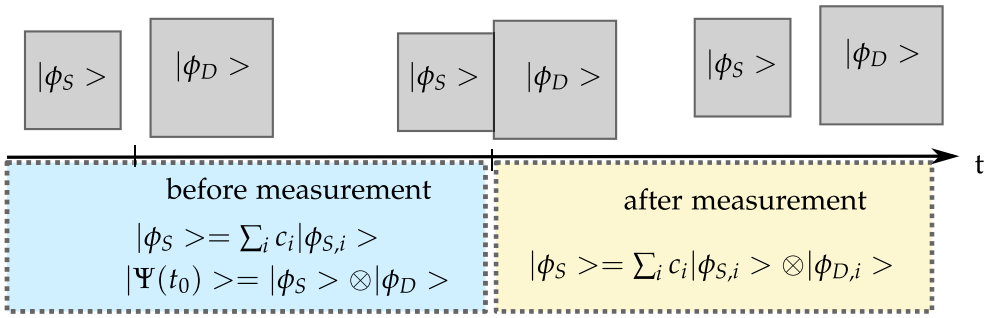

Figure 1: Measurement process in time. Before the measurement process the state of the combined system is a product state of the eigenstates of the detector and state of the system. During the measurement process the system and the detector interact. Provided the system is not in an eigenstate of the detector, during the measurement process the state of the system is an entangled state.

tal measurement process is the concept of operators $\hat{O}$ that act on the state of the system. Assuming the state vector is not an eigenstate of the considered operator, the operator changes the state of the system. Quantities measured in experiment can be formally connected to transition matrix elements and to expectation values $\mathcal{O}$ of arbitrary operators $\hat{O}$ defined in the N-particle Hilbert space $\mathcal{H}_N$, i.e. for pure states given by

$$\mathcal{O}_{jj'} = \langle \Psi_j | \hat{O} | \Psi_{j'} \rangle = \int d\vec{x} \Psi_j^*(\vec{x}) \hat{O} \Psi_{j'}(\vec{x}), \tag{9}$$

where the matrix elements are in the case of $j \neq j'$ the transition matrix elements and in the case of $j = j'$ the expectation values, respectively. Expectation values are measurable if they are real, which is fulfilled by hermitian operators $\hat{O} = \hat{O}^\dagger$, and under space-time reflection ($\mathcal{PT}$) symmetry also for non-hermitian operators [64, 65]. Recently, it has been shown that complex expectation values can also be measured via weak values [66].

Specific examples of expectation values that are directly accessible in experiments are the expectation values of the spin operators $\hat{S}_z$ and $\hat{S}^2$, the particle number operator $\hat{N}$ and the Hamilton operator $\hat{H}$. These expectation values are characteristic properties of the considered state Ψ_j. In particular, the ground state Ψ_0 of the system - that we have earlier introduced as complete descriptor of the system - contains the configuration and all informations we can possibly obtain about the system in its ground-state. We can directly access quantities such as the spin, the spin projection on the z-axis and the particle number of the ground state of the system by evaluating the following expectation values,

$$N = \langle \Psi_0 | \hat{N} | \Psi_0 \rangle, S_z = \langle \Psi_0 | \hat{S}_z | \Psi_0 \rangle, \text{ and } S^2 = \langle \Psi_0 | \hat{S}^2 | \Psi_0 \rangle, \tag{10}$$

where $\hat{N}$, $\hat{S}^2$, and $\hat{S}_z$ as usual denote the particle number operator, the square of the spin operator and the projection on the z-direction of the spin operator, respectively. Specific examples of transition matrix elements are the transition dipole matrix elements that are used in spectroscopy [67]

$$d_{jj'} = \langle \Psi_j | \hat{d} | \Psi_{j'} \rangle = \int d\vec{x} \Psi_j^*(\vec{x}) \hat{d} \Psi_{j'}(\vec{x}) \tag{11}$$

wherein the dipole operator is defined as

$$\hat{d} = \sum_{i=1}^{N} q_i \hat{\vec{r}}_i. \tag{12}$$

with q_i denoting the charge of the particle, i.e. for the electrons $q_i = -e$. Transition matrix elements and expectation values of operators allow us to access the properties of a system by using the concept of states. In principle, the framework of density-functional theory tells us that we can express properties of the system as functional of the density without the need to directly construct the wave function for the evaluation of expectation values and transition matrix elements. Examples of expectation values with trivial functional dependency on the electron density include the dipole moment

$$d_{00} = \int d\vec{r} n_{00}(\vec{r}) \hat{d} \tag{13}$$

and the particle number

$$N = \int d\vec{r} n_{00}(\vec{r}). \tag{14}$$

In general, the functional form of arbitrary observables is not known. One common example is the unknown xc functional that is missing to fully determine the functional form of the ground-state energy and band gaps. In practice, the missing part of the xc functional has to be approximated, e.g. by fitting parameters to model systems, to known experimental or ab-initio data. Clearly, the so obtained functionals are not universal and while giving excellent results for a certain system, they may completely fail for other ones. The functional search for other observables includes e.g. the search for the kinetic energy functional $T[n]$. In Chap. 5-7, we illustrate the explicit density dependence of selected observables for model systems and discuss an exact condition that approximate functionals should fulfill to accurately describe systems from weak-to strong correlation within the framework of DFT.

2.4 COMPOSITE QUANTUM SYSTEMS

Practical real physical systems ranging from microscopic particles to large-scale macroscopic objects are in contact with their environment, e.g. with an external bath. However, the partitioning of the physical space into system and environment is arbitrary. Typically, the length- and time-scale of the processes of interest that change the properties of the system determine how the system is portioned. If the system-environment interaction is very weak, and the system

approximately does not exchange any properties with its environment, we can approximately describe the system as an isolated system. In contrast, open quantum system are systems that are in contact with their environment.
Of particular interest are composite quantum systems such as molecular fragments or surface-interface interactions among others. These composite systems are build by fragments that are individual quantum systems. While the entire composite system can be considered as an isolated system with fixed integer particle number N, fractional amounts of the charge density δn and energy can be transferred among its fragments. As we will see in Chap. 3, in ground-state density-functional theory, observables such as the ground-state energy are expressible in terms of the ground-state density. A specific cut along the ground-state density is the integrated charge density over the entire system, i.e. the particle number of the (sub-)system. Since most properties of a system change with the particle number, it is of great use to study the density dependence of observables along the cut in N. For closed and isolated systems with non-degenerate ground-state, the values of N can only take integer values that correspond to the particle number of different, disconnected systems. Therefore, the density dependence of observables along the cut in N is a discontinuous function that only has values at integer particle number. The situation changes if a coupling between the initially disconnected systems is introduced. Then, each system forms an open system and the particle number of the individual subsystems can change in time. In particular, the particle number of each subsystem can also take fractional values. Consequently, the functional behavior along the cut in N becomes a continuous function for the regarded subsystem. One particular case are open systems with degenerate ground-state. For such systems the functionals along the cut in N show a straight-line behavior that change slope at integer values of N [68].

BIPARTITE QUANTUM SYSTEMS In the following we consider the special case of bipartite quantum systems $S = S_1 + S_2$ that are formed of two subsystems S_1 and S_2 as illustrated in Fig. 2. From the left to the right, Fig. 2 shows the time-

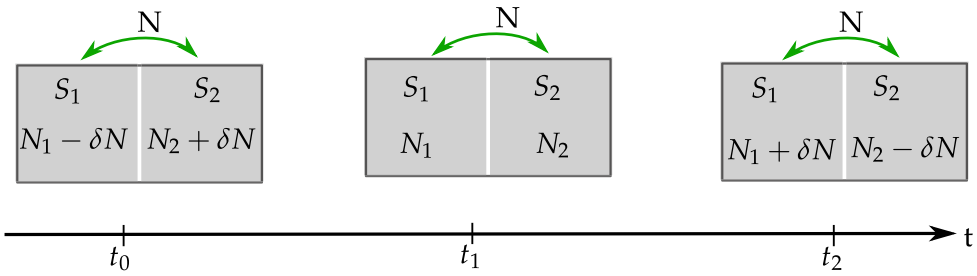

Figure 2: The exchange of particles within a bipartite system formed of two separate subsystems S_1 and S_2 is a process that happens in real-time t. The particle number of the combined system $N = N_1 + N_2$ is at every time-step integer and fixed, while the particle number within the subsystems can take fractional values.

evolution of such a bipartite system from an initial time t_0 to a final time t_2. As

indicated by the green arrows, both subsystems can exchange particles in time. Assuming the total system S is not in contact with its environment, the particle number $N = N_1 + N_2$ of the total system is conserved at arbitrary time steps. Due to the coupling between the subsystems charge density can be transferred among both fragments. As a consequence, the particle number of each subsystem can take fractional values. Here, the particle number of subsystem S_1 changes from initially $N_1 - \delta N$ at t_0 to $N_1 + \delta N$ at t_2, while the particle number of the subsystem S_2 changes from initially $N_2 + \delta N$ to $N_2 - \delta N$. Such processes in which the particle number of the fragments within a system changes in time are the underlying concept of the earlier mentioned processes such as the charge transfer processes between fragments of molecules.

2.5 ENTANGLED STATES OF COMPOSITE MANY-PARTICLE QUANTUM SYSTEMS

One of the most counterintuitive aspects within the theory of quantum mechanics is the concept of entanglement. For composite quantum systems, entanglement characterizes complex many-body states, where the fragments of the system have interacted in the past and for which the measurement of one quantum subsystem influences the experimental outcome of the other one [69]. In bipartite quantum systems $S_1 + S_2$ with the combined tensor product state space $\mathcal{H} = \mathcal{H}_{S_1} \otimes \mathcal{H}_{S_2}$ [70], entangled states as defined in Def. 2.5.1 can emerge.

Definition 2.5.1: Bipartite entangled states

A state, which is not factorizable into a product state of its subsystems, i.e. $|\Psi_{S_1 S_2}\rangle \neq |\Psi_{S_1}\rangle \otimes |\Psi_{S_2}\rangle$, is called an entangled state and the properties of both subsystems are correlated.

The concept of entanglement has been already introduced by Einstein [34] and Schrödinger [71], but until now the measurement of entanglement remains a long-standing problem [72–75]. However, a good measure for the entanglement in bipartite pure states is the entropy of entanglement [76]. The properties of an entangled state are correlated. In particular, it is distinguished between dynamic correlation [77] as defined in Def. 2.5.2, i.e. the correlation between the motion of particles, and static correlation [78, 79] as defined in Def. 2.5.3, i.e. the correlation in the region of near-degenerate states of the system.

Definition 2.5.2: Dynamical correlation

Dynamical correlation is due to the instantaneous repulsion of interacting electrons, e.g. the Coulomb interaction [77, 80].

Definition 2.5.3: Static correlation

The correlation in the region of near-degenerate states of the system such as in stretched H_2 is called static correlation. In the case of stretched H_2 the exact two-particle wave function becomes close to a superposition of two single Slater determinants [78, 79].

In this work, we are concerned with the static correlation in the system that can be characterized by the correlation entropy [81–83]

$$S = -\sum_{j=1}^{\infty} n_j \ln n_j, \tag{15}$$

where the occupation numbers n_j are the eigenvalues of the reduced one-body density matrix [84] that is given by

$$\rho_{\text{1RDM}}(\vec{r}_1, \vec{r}_1') = \sum_{\sigma_1, \sigma_1'} \int d\vec{x}_2 ... d\vec{x}_N \Psi^*(\vec{x}_1, \vec{x}_2, ..., \vec{x}_N) \Psi(\vec{x}_1', \vec{x}_2, ..., \vec{x}_N). \tag{16}$$

In spectral representation, the reduced density matrix can be written in terms of its eigenfunctions and eigenvalues as

$$\rho_{\text{1RDM}}(\vec{r}_1, \vec{r}_1') = \sum_j n_j \phi_j^*(\vec{r}_1) \phi_j(\vec{r}_1'), \tag{17}$$

where the eigenfunctions of the reduced one-body density matrix are the natural orbitals ϕ_j [85].

The correlation entropy is a measure of the Slater rank, which is given by the amount of Slater determinants required to exactly decompose the state [72, 86]. For pure states the correlation entropy is zero and for fully mixed states it reaches its maximum value [81–83]. In this work, we refer to coupled subsystems as weakly-correlated if the ground state of the system is well approximated by a single Slater determinant, otherwise we refer to the systems as strongly-correlated. Entangled many-body states fully capture the correlation present in composite quantum-mechanical systems with no classical analogue.

In Chap. 6, we introduce the concept of effective density-to-potential maps and the related concept of the intra-system steepening that allow to characterize how the correlation between subsystems is captured within DFT and QEDFT. We will see that the intrasystem steepening characterizes the static correlation between subsystems within the global system.

2.6 PARTICLES IN AN ELECTROMAGNETIC FIELD: FIELD QUANTIZATION

The eigenstates of the hydrogen atom in free space are the eigenstates of the composite electron-photon system described by the Hamiltonian of the entire system including the particles, i.e. the electrons and ions, as well as the internal and external electromagnetic fields present in the system. In the following, we briefly sketch the formal way allowing the full quantum treatment of the standard Hamiltonian of the combined system of charged particles in an electromagnetic field. We start by specifying the fields with its corresponding field variables relevant for the systems considered in this work.

Classical electromagnetic field - Maxwell equations At each point in space time the electromagnetic field is characterized by an electric and a magnetic field

$\vec{E}(\vec{r},t)$ and $\vec{B}(\vec{r},t)$, both of which are coupled through the Maxwell equations, i.e. the following set of coupled first-order partial differential equations given in SI units [87, 88]

$$\vec{\nabla} \times \vec{B}(\vec{r},t) - \frac{1}{c^2}\partial_t \vec{E}(\vec{r},t) = \mu_0 \vec{j}(\vec{r},t) \tag{18}$$

$$\vec{\nabla} \times \vec{E}(\vec{r},t) + \partial_t \vec{B}(\vec{r},t) = 0 \tag{19}$$

$$\vec{\nabla} \cdot \vec{B}(\vec{r},t) = 0 \tag{20}$$

$$\vec{\nabla} \cdot \vec{E}(\vec{r},t) = \frac{\rho(\vec{r},t)}{\epsilon_0} \tag{21}$$

with the current density $\vec{j}(\vec{r},t)$, the charge density $\rho(\vec{r},t)$, and with μ_0 and ϵ_0 denoting the magnetic permeability and electric permittivity in vacuum [4], respectively. In the following, we introduce the vector potential $\vec{A}(\vec{r},t) : \mathbb{R}^3 \times \mathbb{R} \to \mathbb{R}^3$ and the scalar potential $U(\vec{r},t) : \mathbb{R}^3 \times \mathbb{R} \to \mathbb{R}$. Using the Helmholtz theorem, the magnetic field

$$\vec{B}(\vec{r},t) = \vec{B}_{\parallel}(\vec{r},t) + \vec{B}_{\perp}(\vec{r},t) = \vec{\nabla} \times \vec{A}(\vec{r},t) \tag{22}$$

can be decomposed into its longitudinal curl-free $\vec{B}_{\parallel}$ and its transverse divergence-free part $\vec{B}_{\perp}$. The Maxwell equation of Eq. 20

$$\vec{\nabla} \cdot \vec{B}(\vec{r},t) = 0 = \vec{\nabla} \cdot (\vec{B}_{\parallel}(\vec{r},t) + \vec{B}_{\perp}(\vec{r},t)) \implies \vec{B}_{\parallel}(\vec{r},t) = 0 \tag{23}$$

is fulfilled if the longitudinal part of the magnetic field vanishes. The reformulation of the electric field in terms of the potentials reads [89]

$$\vec{E}(\vec{r},t) = -\vec{\nabla} U(\vec{r},t) - \partial_t \vec{A}(\vec{r},t) \tag{24}$$

and inserted together with Eq. 22 into Eq. 18 and Eq. 21 leads to [87]

$$-\epsilon_0 \left[\Delta U(\vec{r},t) + \vec{\nabla} \cdot \partial_t \vec{A}(\vec{r},t) \right] = \rho(\vec{r},t) \tag{25}$$

and

$$\vec{\nabla} \times \vec{\nabla} \times \vec{A}(\vec{r},t) + \mu_0 \epsilon_0 \partial_t^2 \vec{A}(\vec{r},t) + \mu_0 \epsilon_0 \vec{\nabla} \partial_t U(\vec{r},t) = \mu_0 \vec{j}(\vec{r},t). \tag{26}$$

In the following, we distinguish between internal and external sources of the electromagnetic field leading to the internal and external contributions of the potentials

$$\vec{A}(\vec{r},t) = \vec{A}_{\text{int}}(\vec{r},t) + \vec{A}_{\text{ext}}(\vec{r},t), \tag{27}$$

$$U(\vec{r},t) = U_{\text{int}}(\vec{r},t) + U_{\text{ext}}(\vec{r},t). \tag{28}$$

For both, the internal and the external potentials, we still have the freedom of the gauge function as can be seen in Eq. 29 and Eq. 30. For both fields, we choose the Coulomb gauge. This particular gauge automatically leads in the case of the internal field to the instantaneous Coulomb interaction between particles. For the external fields, we additionally apply the dipole approximation.

4 In SI units the magnetic permeability and the electric permittivity in vacuum are equal to $\mu_0 = 4\pi \times 10^{-7} (kgmA^{-2}s^{-2})$ and $\epsilon_0 = \frac{10^7}{4\pi c^2} (A^2 s^4 kg^{-1} m^{-3})$ [87].

Gauge freedom: The Coulomb gauge Both, the magnetic and the electric field, remain invariant under the following local gauge transformation on the vector and the scalar potential [90]

$$\vec{A}(\vec{r},t) \rightarrow \tilde{\vec{A}}(\vec{r},t) = \vec{A}(\vec{r},t) + \vec{\nabla}\mathcal{F}(\vec{r},t) \tag{29}$$

$$U(\vec{x},t) \rightarrow \tilde{U}(\vec{r},t) = U(\vec{r},t) - \partial_t \mathcal{F}(\vec{r},t) \tag{30}$$

in which $\mathcal{F}(\vec{r},t)$ is an arbitrary scalar gauge function.

In **Coulomb gauge**, we choose $\mathcal{F}(\vec{r},t)$ such that the longitudinal part of the internal part of the vector potential vanishes, i.e. $\vec{A}_{\parallel} = 0$. This leads to the following condition on the vector potential

$$\vec{\nabla} \cdot \vec{A} = 0. \tag{31}$$

We note, this condition fixes one degree of freedom of the vector potential, i.e. the two remaining degrees of freedom are the two (transversal) polarization directions of $\vec{A}_{\perp}$.

GAUGE FOR THE INTERNAL FIELDS: THE COULOMB GAUGE Integrating the Laplace equation (Poisson equation) given in Eq. 25 and using the Coulomb condition for the internal part of the vector potential, i.e. $\vec{A}_{\text{int},\parallel} = 0$, directly leads to the scalar potential [89]

$$U_{\text{int}}(\vec{r},t) = \frac{1}{4\pi\epsilon_0} \int d\vec{r}' \frac{\rho(\vec{r}',t)}{|\vec{r}-\vec{r}'|}, \tag{32}$$

i.e. the Coulomb potential. The Coulomb interaction is an instantaneous interaction that is commonly used in the standard Hamiltonian e.g. in quantum chemistry or solid state physics to describe the electric particle-particle interaction.

Lagrange density Starting point for the derivation of the correlated electron-photon Hamiltonian is the Lagrange density given by

$$\mathcal{L} = \mathcal{L}_R + \mathcal{L}_P + \mathcal{L}_{R-P}, \tag{33}$$

in which the $\mathcal{L}_R$ denotes the Lagrange density of the free electromagnetic field, $\mathcal{L}_P$ denotes the energy of the electrons, and $\mathcal{L}_{R-P}$ denotes the interaction of the particles with the field, see e.g. Ref. [91].

In the Lagrange density of fields $\mathcal{L}(\phi_\beta(\vec{r},t), \partial_t\phi_\beta(\vec{r},t), t)$, the index β denotes different components of the field. In the case of the Lagrange density of the matter system, there are two different components. The components are given by the Schrödinger field $\Psi(\vec{r},t)$, which needs to fulfill the Schrödinger equation of Eq. 6, and its complex conjugate $\Psi^*(\vec{r},t)$. In the case of the electromagnetic field there are four components, i.e. the three components of the vector potential $\vec{A}(\vec{r},t)$ and the scalar potential $U(\vec{r},t)$.

LAGRANGE DENSITY OF THE SCHRÖDINGER FIELD The Lagrange density for the Schrödinger field Ψ for a single electron is given by [92]

$$\mathcal{L}_P = \frac{i\hbar}{2}\left(\Psi^*\partial_t\Psi - \Psi\partial_t\Psi^*\right) - \frac{\hbar^2}{2m}\nabla\Psi\cdot\nabla\Psi^* - V(\vec{r},t)\Psi^*\Psi \tag{34}$$

LAGRANGE DENSITY OF THE FREE RADIATION FIELD In the absence of external sources, where the current density $\vec{j}(\vec{r},t)$ and the charge density $\rho(\vec{r},t)$ in Eq. 18 and Eq. 21 are set to zero, the Lagrange density reads

$$\mathcal{L}_R = \frac{\epsilon_0}{2}\left(\vec{\nabla}U(\vec{r},t) + \frac{d}{dt}\vec{A}(\vec{r},t)\right)^2 - \frac{1}{2\mu_0}\left(\nabla\times\vec{A}(\vec{r},t)\right)^2. \tag{35}$$

In the Coulomb gauge of Eq. 31, the Lagrange density of the free radiation field reduces to

$$\mathcal{L}_R = \frac{\epsilon_0}{2}\left(\frac{d}{dt}\vec{A}(\vec{r},t)\right)^2 - \frac{1}{2\mu_0}\left(\nabla\times\vec{A}(\vec{r},t)\right)^2. \tag{36}$$

or using the electric field $\vec{E}$ and the magnetic field $\vec{B}$

$$\mathcal{L}_R = \frac{\epsilon_0}{2}\left(\vec{E}^2(\vec{r},t) - c^2\vec{B}^2(\vec{r},t)\right). \tag{37}$$

PARTICLE-RADIATION INTERACTION OF THE LAGRANGE DENSITY IN MINIMAL COUPLING The corresponding interaction term of the Lagrange density of a system consisting of particles in an external electromagnetic field [90, 93] is given in **minimal coupling** by

$$\mathcal{L}_{R-P} = \vec{j}(\vec{r},t)\vec{A}(\vec{r},t) - \rho(\vec{r},t)U(\vec{r},t) \tag{38}$$

where the charge density is [93]

$$\rho(\vec{r},t) = \Psi^*(\vec{r},t)\Psi(\vec{r},t) \tag{39}$$

and the current density is given by [93]

$$\vec{j}(\vec{r},t) = \frac{1}{m}\mathrm{Re}\left(\Psi^*(\vec{r},t)\left[\frac{\hbar}{i}\vec{\nabla} - q\vec{A}(\vec{r},t)\right]\Psi(\vec{r},t)\right). \tag{40}$$

The total Lagrange density $\mathcal{L}$ for correlated matter-field systems is given in Def. 2.6.1.

Definition 2.6.1: Lagrange density of the Maxwell-Schrödinger field

$$\begin{aligned}\mathcal{L} = &\left[\frac{i\hbar}{2}\left(\Psi^*(\vec{r},t)\partial_t\Psi(\vec{r},t) - \Psi(\vec{r},t)\partial_t\Psi^*(\vec{r},t)\right)\right.\\ &\left.-\frac{\hbar^2}{2m}\vec{\nabla}\Psi(\vec{r},t)\cdot\vec{\nabla}\Psi^*(\vec{r},t) - V(\vec{r},t)\Psi^*(\vec{r},t)\Psi(\vec{r},t)\right]\\ &+\frac{\epsilon_0}{2}\left(\vec{E}^2(\vec{r},t) - c^2\vec{B}^2(\vec{r},t)\right) + \vec{j}(\vec{r},t)\vec{A}(\vec{r},t) - \rho(\vec{r},t)U(\vec{r},t)\end{aligned} \tag{41}$$

Conjugated momentum density of the field We define the set of conjugated variables by introducing the conjugated momentum density of the field, i.e.

$$\Pi_{\phi_\beta}(\vec{r},t) = \frac{\partial\mathcal{L}(\vec{r},t)}{\partial\dot{\phi}_\beta(\vec{r},t)}, \tag{42}$$

where $\phi_\beta \in \{A_j, U, \Psi, \Psi^*\}$. Using the Lagrange density of Eq. 36 and the relation of Eq. 24, in Coulomb gauge the conjugated momentum of the vector field $\vec{A}$ is given by the two transversal components of the electric field

$$\Pi_{A_j}(\vec{r}, t) = -\epsilon_0 E_{\perp,j}(\vec{r}, t). \tag{43}$$

The conjugated momentum of the Schrödinger field $\Psi(\vec{r}, t)$ is its conjugated complex [89]

$$\Pi_\Psi(\vec{r}, t) = \frac{i\hbar}{2}\Psi^*(\vec{r}, t), \tag{44}$$

and

$$\Pi_{\Psi^*}(\vec{r}, t) = -\frac{i\hbar}{2}\Psi(\vec{r}, t). \tag{45}$$

Lagrange function of the fields Integration of the Lagrange density given in Eq. 33 then leads to the Lagrange function describing interacting particles including the electromagnetic field, i.e.

$$L = L_P + L_R + L_{R-P} = \int \mathcal{L} d^3\vec{r} \tag{46}$$

with the Lagrangian of the particles L_P, the Lagrangian of the electromagnetic field L_{R-P}, and the Lagrangian of the interaction between the Schrödinger and the Maxwell field L_{R-P} [90]. The Lagrange function L and the Hamilton function H can be connected via the Legendre transformation [90]

$$H = \int d\vec{r} \sum_j \Pi_{\phi_\beta}(\vec{r}, t)\partial_t \phi_\beta(\vec{r}, t) - L. \tag{47}$$

Quantization of the field variables We replace all field variables ϕ_β by their corresponding quantum operators. For the fields, the following formal replacements take place

$$\phi_\beta(\vec{r}, t) \to \hat{\phi}_\beta(\vec{r}, t) \tag{48}$$
$$\Pi_{\phi_\beta}(\vec{r}, t) \to \hat{\Pi}_{\phi_\beta}(\vec{r}, t). \tag{49}$$

The Heisenberg operators $\hat{\phi}_\beta$ and $\hat{\Pi}_{\phi_\beta}$ now obey the following commutation relation

$$[\hat{\phi}_\beta(\vec{r}, t), \hat{\Pi}_{\phi_{\beta'}}(\vec{r'}, t)] = i\hbar\delta_{\beta\beta'}(\vec{r} - \vec{r'}). \tag{50}$$

For the particles, the replacement procedure given in Eq. 48 and Eq. 49 applied to the Schrödinger field, leads straightforward to the framework of second quantization. For the Schrödinger field the Heisenberg operators $\hat{\Psi}^\dagger(\vec{r}, t)$ and $\hat{\Psi}(\vec{r}, t)$ create and annihilate particles at time t and position $\vec{r}$, respectively.

THE QUANTIZED SCHRÖDINGER FIELD: FIRST AND SECOND QUANTIZATION
Field operators of second quantization create or annihilate particles in states of a N-particle Hilbert space. The resulting states are element of the $(N \pm 1)$-particle Hilbert space. Therefore, states of second quantization are defined in a direct sum of the different N-particle Hilbert spaces $\mathcal{F} = \mathcal{H}_0 \oplus \mathcal{H}_1 \oplus \mathcal{H}_2 \ldots \mathcal{H}_N$, i.e. the Fock space. In position representation, field operators create or annihilate particles with spin σ at position $\vec{r}$ and time t, where $\hat{\Psi}^\dagger_\sigma(\vec{r},t)$ and $\hat{\Psi}_\sigma(\vec{r},t)$ denote the creation and annihilation operator, respectively. Second quantization is an exact reformulation of first quantization taking states with different particle numbers into account. One-particle operators rewrite as

$$\hat{O}_{2nd}(t) = \int_{\mathcal{V}} d\vec{x} \hat{\Psi}^\dagger_\sigma(\vec{r},t) \hat{O}_{1st}(\vec{r},t) \hat{\Psi}_\sigma(\vec{r},t), \tag{51}$$

whereas two-particle operators rewrite as

$$\hat{O}_{2nd}(t) = \int_{\mathcal{V}} \int_{\mathcal{V}} d\vec{x} d\vec{x}' \hat{\Psi}^\dagger_\sigma(\vec{r},t) \hat{\Psi}^\dagger_{\sigma'}(\vec{r}',t) \hat{O}_{1st}(\vec{r},\vec{r}',t) \hat{\Psi}_\sigma(\vec{r},t) \hat{\Psi}_{\sigma'}(\vec{r}',t). \tag{52}$$

We expand the field operators in a complete set of m single particle basis functions

$$\hat{\Psi}_\sigma(\vec{r},t) = \sum_m \phi_m(\vec{r}) \hat{c}_{m\sigma}(t), \tag{53}$$

$$\hat{\Psi}^\dagger_\sigma(\vec{r},t) = \sum_m \phi^*_m(\vec{r}) \hat{c}^\dagger_{m\sigma}(t), \tag{54}$$

where the operator $\hat{c}^\dagger_m$ creates a particle in the m-th basis function.

Density operator in second quantization In second quantization, the density operator in real-space representation is given by

$$\hat{n}_{\text{2nd}}(\vec{r},t) = \int_{\mathcal{V}} d^3\vec{x} \hat{\Psi}^\dagger_\sigma(\vec{r}',t) \hat{n}(\vec{r}) \hat{\Psi}_\sigma(\vec{r}',t) = \sum_\sigma \hat{\Psi}^\dagger_\sigma(\vec{r},t) \hat{\Psi}_\sigma(\vec{r},t), \tag{55}$$

where the density operator in first quantization is given by $\hat{n}(\vec{r}) = \sum_j \delta(\vec{r} - \vec{r}_j)$.

THE QUANTIZED ELECTROMAGNETIC FIELD The transversal potential operators, $\hat{\vec{A}}$ and $\hat{\vec{E}}$ of the Maxwell field obey the following commutation relation [89]

$$[\hat{A}_\beta(\vec{r},t), \hat{E}_{\beta'}(\vec{r'},t)] = i\hbar \delta_{\perp,\beta\beta'}(\vec{r} - \vec{r'}), \tag{56}$$

where $\delta_{\perp,\beta\beta'}$ denotes the transversal delta function [94]. Additionally, $\hat{A}$, $\hat{E}$ and $\hat{B}$ are usually expanded into a set of eigenmodes of the geometry of the cavity or

in free space into plane waves. The expansion with the quantization volume V can be explicitly written as follows [94]

$$\hat{\vec{A}}(\vec{r}) = \sum_k \sum_{\lambda=1,2} \left(\frac{\hbar}{2\epsilon_0 c|\vec{k}|V}\right)^{\frac{1}{2}} \vec{e}_{k\lambda} \left(\hat{a}_{k\lambda} \exp\left(\mathrm{i}\vec{k}\cdot\vec{r}\right) + \hat{a}^\dagger_{k\lambda} \exp\left(-\mathrm{i}\vec{k}\cdot\vec{r}\right)\right), \tag{57}$$

$$\hat{\vec{E}}_\perp(\vec{r}) = \sum_k \sum_{\lambda=1,2} \mathrm{i}\left(\frac{\hbar c|\vec{k}|}{2\epsilon_0 V}\right)^{1/2} \vec{e}_{k\lambda} \left(\hat{a}_{k\lambda} \exp\left(\mathrm{i}\vec{k}\cdot\vec{r}\right) - \hat{a}^\dagger_{k\lambda} \exp\left(-\mathrm{i}\vec{k}\cdot\vec{r}\right)\right), \tag{58}$$

$$\hat{\vec{B}}(\vec{r}) = \sum_k \sum_{\lambda=1,2} \mathrm{i}\left(\frac{\hbar k}{2\epsilon_0 c V}\right)^{1/2} \vec{k}' \times \vec{e}_{k\lambda} \left(\hat{a}_{k\lambda} \exp\left(\mathrm{i}\vec{k}\cdot\vec{r}\right) - \hat{a}^\dagger_{k\lambda} \exp\left(-\mathrm{i}\vec{k}\cdot\vec{r}\right)\right), \tag{59}$$

where the classical vector field amplitude $\vec{A}_{k\lambda}$ of the classical vector field potential of $\vec{A}$ in Eq. 22 has been replaced by the quantum operator $\hat{\vec{A}}_{k\lambda}$ [94]

$$A^{(*)}_{\vec{k}\lambda} \xrightarrow{\wedge} \hat{\vec{A}}^{(\dagger)}_{\vec{k}\lambda} = \sqrt{\frac{\hbar}{2\epsilon_0 V \omega_k}}\, \hat{a}^{(\dagger)}_{\vec{k}\lambda}. \tag{60}$$

Here the operators $\hat{a}_{k\lambda}$ and $\hat{a}^\dagger_{k\lambda}$ create and annihilate photons with the polarization direction λ in the mode of frequency ω and wave vector k. The normalized wave vector is given by

$$\vec{k}' = \frac{\vec{k}}{|\vec{k}|} \tag{61}$$

and ω and $\vec{k}$ are related by the dispersion relation $\omega_k = c|\vec{k}|$

Hamiltonian for quantized matter We now consider matter that consists of coupled K nuclei and N electrons. The nuclei have spatial coordinates $\vec{R}$, masses M, charges Q and integer (half-integer) spin. Accordingly nuclei follow bosonic (fermionic) statistics. The N electrons have coordinates $\vec{r}$, masses m, charge $q = -e$, half-integer spin and follow fermionic statistics. Employing Eq. 47 yields the coupled electron-nuclei Hamiltonian in second quantization

$$\begin{aligned}
\hat{H}_P(t) = &\int_{\mathcal{V}} d\vec{x} \hat{\Psi}^\dagger_\sigma(\vec{r},t) \hat{t}_\mathrm{e}(\vec{r}) \hat{\Psi}_\sigma(\vec{r},t) + \int_{\mathcal{V}} d\vec{X} \hat{\Psi}^\dagger_\sigma(\vec{R},t) \hat{t}_\mathrm{n}(\vec{R}) \hat{\Psi}_\sigma(\vec{R},t) \\
&+ \int_{\mathcal{V}}\int_{\mathcal{V}} d\vec{X} d\vec{X}' \hat{\Psi}^\dagger_\sigma(\vec{R},t) \hat{\Psi}^\dagger_{\sigma'}(\vec{R}',t) \hat{v}_\mathrm{n\text{-}n}(\vec{R},\vec{R}') \hat{\Psi}_\sigma(\vec{R},t) \hat{\Psi}_{\sigma'}(\vec{R}',t) \\
&+ \int_{\mathcal{V}}\int_{\mathcal{V}} d\vec{x} d\vec{x}' \hat{\Psi}^\dagger_\sigma(\vec{r},t) \hat{\Psi}^\dagger_{\sigma'}(\vec{r}',t) \hat{v}_\mathrm{e\text{-}e}(\vec{r},\vec{r}') \hat{\Psi}_\sigma(\vec{r},t) \hat{\Psi}_{\sigma'}(\vec{r}',t) \\
&+ \int_{\mathcal{V}}\int_{\mathcal{V}} d\vec{x} d\vec{x}' \hat{\Psi}^\dagger_\sigma(\vec{r},t) \hat{\Psi}^\dagger_{\sigma'}(\vec{R}',t) \hat{v}_\mathrm{e\text{-}n}(\vec{r},\vec{R}') \hat{\Psi}_\sigma(\vec{r},t) \hat{\Psi}_{\sigma'}(\vec{R}',t),
\end{aligned} \tag{62}$$

with

$$\hat{t}_{\mathrm{e}}(\vec{r}) = \frac{(-i\hbar\vec{\nabla}_r)^2}{2m}, \tag{63}$$

$$\hat{t}_{\mathrm{n}}(\vec{R}) = \frac{(-i\hbar\vec{\nabla}_R)^2}{2M}, \tag{64}$$

$$\hat{v}_{\text{n-n}}(\vec{R},\vec{R}') = \frac{QQ'}{4\pi\epsilon_0|\vec{R}-\vec{R}'|}, \tag{65}$$

$$\hat{v}_{\text{e-e}}(\vec{r},\vec{r}') = \frac{e^2}{4\pi\epsilon_0|\vec{r}-\vec{r}'|}, \tag{66}$$

$$\hat{v}_{\text{n-e}}(\vec{R},\vec{r}) = -\frac{Qe}{4\pi\epsilon_0|\vec{R}-\vec{r}|}. \tag{67}$$

The operators in first quantization are explicitly given in Eq. 68-72.

MATTER HAMILTONIAN IN FIRST QUANTIZATION For completeness, we also explicitly state the reformulation of the matter Hamiltonian in first quantization according to the relations given in Eq. 51 and Eq. 52. The kinetic energy of the N electrons is written as

$$\hat{T}_{\mathrm{e}} = \sum_{j=1}^{N} \hat{t}_e(\vec{r}_j), \tag{68}$$

with position $\vec{r}_j$ of the j-th electron, whereas the second term represents the kinetic energy of the K nuclei

$$\hat{T}_{\mathrm{n}} = \sum_{\alpha=1}^{K} \hat{t}_{\mathrm{n}}(\vec{R}_\alpha). \tag{69}$$

The potential energy operator including the nuclei-electron attraction writes

$$\hat{V}_{\text{n-e}} = \sum_{\alpha=1}^{K}\sum_{j=1}^{N} \hat{v}_{\text{n-e}}(\vec{R}_\alpha,\vec{r}_j), \tag{70}$$

the nuclei-nuclei repulsion

$$\hat{V}_{\text{n-n}} = \sum_{\alpha,\beta=1;\alpha<\beta}^{K} \hat{v}_{\text{n-n}}(\vec{R}_\alpha,\vec{R}_\beta), \tag{71}$$

and the electron-electron repulsion

$$\hat{V}_{\text{e-e}} = \sum_{j,k=1;j<k}^{N} \hat{v}_{\text{e-e}}(\vec{r}_j,\vec{r}_k). \tag{72}$$

Hamiltonian for quantized matter in an external field Including the electromagnetic field the Hamiltonian of the full system reads

$$\hat{H} = \hat{H}_P + \hat{H}_{\mathrm{R}} + \hat{H}_{\text{R-P}}. \tag{73}$$

The Hamiltonian of the free radiation field can be described by a sum of independent harmonic oscillators each of them representing one field mode [95], i.e.

$$\hat{H}_{\mathrm{R}}(t) = \frac{\epsilon_0}{2} \int_{\mathcal{V}} d\vec{r} \left(\hat{\vec{E}}_{\perp}^2(\vec{r},t) - c^2 \hat{\vec{B}}^2(\vec{r},t) \right) \tag{74}$$

$$= \hbar \sum_k \sum_{\lambda=1,2} \omega_k \left(\hat{a}_{k\lambda}^{\dagger}(t) \hat{a}_{k\lambda}(t) + \frac{1}{2} \right), \tag{75}$$

where we have used Eq. 58 and Eq. 59. In momentum gauge and in the minimal coupling

$$\vec{p} \to \vec{p} - e\vec{A}, \tag{76}$$

the matter-field coupling is given by

$$\hat{H}_{\text{R-P}}(t) = \int_{\mathcal{V}} d\vec{r} \left[\hat{\vec{j}}(\vec{r},t) \hat{\vec{A}}(\vec{r},t) - \hat{\rho}(\vec{r},t) \hat{U}(\vec{r},t) \right]. \tag{77}$$

In light-matter coupled problems, the dipole approximation (long-wavelength approximation) and the change of the frame to the so-called length gauge (multipol gauge) are typically used[5]. This change of gauge can be obtained generally by using the Power-Zienau-Woolley transformation [94, 96–98]. The resulting Hamiltonian for the light-matter interaction reads in the new gauge explicitly as

$$\hat{\mathcal{H}}_{\text{R-P}}(t) = \frac{1}{\epsilon_0} \int_{\mathcal{V}} d\vec{r} \hat{\vec{E}}_{\perp}(\vec{r},t) \cdot \hat{\vec{P}}_{\perp}(\vec{r},t) + \frac{1}{2\epsilon_0} \int_{\mathcal{V}} d\vec{r} |\hat{\vec{P}}_{\perp}(\vec{r},t)|^2, \tag{78}$$

where $\hat{\vec{P}}_{\perp}$ is the transversal part of the polarization operator of the system. The polarization operator of the electrons in the dipole approximation is given by the dipole operator, i.e. $\hat{P} = -\sum_i e\hat{r}_i$.

2.7 THE BORN-OPPENHEIMER APPROXIMATION

In general many-body calculations where electrons and nuclei are treated, typically the Born-Oppenheimer approximation is applied. This approximation partly decouples [99] the electronic from the nuclear degrees of freedom by exploiting the large mass differences of electrons and nuclei. This mass difference naturally implies different time scales of these particles and thus allows to significantly simplify the problem. In general, the many-body wave function can be written as a superposition of nuclear and electronic parts [100]

$$\Psi_j(\vec{R}_1,...,\vec{R}_K;\vec{r}_1\sigma_1,...,\vec{r}_N\sigma_N) = \sum_k \Psi_{jk}^{\mathrm{n}}(\vec{R}_1,...,\vec{R}_K) \Psi_k^{\mathrm{e}}(\vec{R}_1,...,\vec{R}_K;\vec{r}_1\sigma_1,...,\vec{r}_N\sigma_N), \tag{79}$$

with the position R_l of the l-th nuclei and spin-orientation σ of the j-th electron [101]. In this expansion, the exact wave function is then typically approximated

5 In general, the dipol approximation is applicable if the size of the considered matter system is small in comparison to the wave length of the electromagnetic field. Beyond dipole treatment is required e.g. for very large molecules or molecular clusters.

by only one expansion coefficient, i.e. the adiabatic Born-Oppenheimer approximation. Hence, the Schrödinger equation decouples in one equation for the electrons and one equation for the nuclei. For a given set of fixed (clamped) nuclei $\vec{R}_\alpha$, the static electronic Schrödinger equation

$$\hat{H}_\mathrm{e}\Psi_k^\mathrm{e}(\vec{R}_1,...,\vec{R}_K;\vec{r}_1\sigma_1,...,\vec{r}_N\sigma_N) = (\hat{T}_\mathrm{e}+\hat{V}_\text{n-e}+\hat{V}_\text{e-e})\Psi_k^\mathrm{e}(\vec{R}_1,...,\vec{R}_K;\vec{r}_1\sigma_1,...,\vec{r}_N\sigma_N) \tag{80}$$

$$= E_k(\vec{R}_1,...,\vec{R}_K)\Psi_k^\mathrm{e}(\vec{R}_1,...,\vec{R}_K;\vec{r}_1\sigma_1,...,\vec{r}_N\sigma_N) \tag{81}$$

depends on the three spatial coordinates of each electron and allows to calculate the electronic wave function Ψ_k. The electronic eigenenergies $E_k(\vec{R}_1,...,\vec{R}_K)$ contribute to the potential energy surfaces that also include the nuclear potential $V_\text{n-n}(\vec{R}_1,...,\vec{R}_K)$ given by Eq. 71. However, the dimension of the many-electron Schrödinger equation increases exponentially with the number of electrons [101] and approximate schemes for solving it are required. One of these approximations is the Hartree-Fock theory introduced in Sec. 2.8. Alternatively, density-functional theory can be used to calculate these potential-energy surfaces.

2.8 THE HARTREE-FOCK METHOD

The Hartree-Fock method, in which the N-electron problem is replaced by N coupled one-electron ones, is a wave-function based variational method optimizing the single-particle orbitals of a single Slater determinant such that the total energy of the system becomes minimal [102, 103].

The variational principle for the energy allows to find stationary points of the expectation value of the Hartree-Fock Hamiltonian with respect to small variations in the orbitals $\phi_j \to \phi_j + \delta\phi_j$,

$$\delta E = \delta \langle\Psi| \hat{H}_\mathrm{HF} |\Psi\rangle = 0. \tag{82}$$

As ansatz for the many-body wave function serves a single Slater-determinant

$$\Psi(\vec{r}_1,\cdots,\vec{r}_N) = \frac{1}{\sqrt{N!}}\begin{vmatrix} \phi_1(\vec{r}_1) & \cdots & \phi_1(\vec{r}_j) & \cdots & \phi_1(\vec{r}_N) \\ \vdots & \ddots & \vdots & & \vdots \\ \phi_j(\vec{r}_1) & \cdots & \phi_j(\vec{r}_j) & \cdots & \phi_j(\vec{r}_N) \\ \vdots & & \vdots & \ddots & \vdots \\ \phi_N(\vec{r}_1) & \cdots & \phi_N(\vec{r}_j) & \cdots & \phi_N(\vec{r}_N) \end{vmatrix}, \tag{83}$$

which is an antisymmetrized product of single-particle orbitals, typically of Slater-$\phi(\vec{r}) \propto e^{-a\vec{r}}$ or Gaussian-type $\phi(\vec{r}) \propto e^{-a\vec{r}^2}$ [104]. Due to the antisymmetrization of the Slater determinant the Pauli exclusion principle is naturally fulfilled. The orbital $\phi_j(\vec{r}_N)$ corresponds to the j-th orbital occupied by the N-th electron and the factor $\frac{1}{\sqrt{N!}}$ ensures the normalization of the total wave function.

Instead of solving one N-particle Schrödinger equation, each of the N-coupled single-particle Hartree Fock equations

$$\hat{H}_{\mathrm{HF}} \left|\phi_j\right\rangle = \hat{H}(\vec{r}_j) + \hat{v}_{\mathrm{hx}} \left|\phi_j\right\rangle = \epsilon_j \left|\phi_j\right\rangle \tag{84}$$

need to be solved self-consistently. The Hartree and the non-local exchange term

$$\hat{v}_{\mathrm{hx}} = \frac{e^2}{4\pi\epsilon_0} \sum_{n=1}^{\mathrm{occ}} \left\langle\phi_n\right| \frac{1}{|\vec{r}_j - \vec{r}_n|} \left|\phi_n\right\rangle - \left|\phi_n\right\rangle \left\langle\phi_n\right| \frac{1}{|\vec{r}_j - \vec{r}_n|} \tag{85}$$

couple each of the j-th single-particle orbitals to all remaining occupied orbitals. The term

$$\hat{H}(\vec{r}_j) = -\frac{\hbar^2}{2m}\vec{\nabla}^2_{r_j} - \frac{e}{4\pi\epsilon_0} \sum_{\alpha=1}^{K} \frac{Q_\alpha}{|\vec{r}_j - \vec{R}_\alpha|} \tag{86}$$

includes the kinetic operator for the j-th electron plus its potential energy in the field of all nuclei. All particle-particle interactions are mimicked by a self-consistent net field created by all charges in the system [102].

To solve the Hartree-Fock equations, it is necessary to specify the form of the spin orbitals, which are either a set of restricted closed-shell spin orbitals or a set of unrestricted open-shell spin orbitals [105].

In a self-consistent scheme, the one-particle orbitals of this ansatz are varied until the resulting Slater-determinant minimizes the energy of the system

$$E_0 = \left\langle\Psi_0\right| \hat{H}_{\mathrm{HF}} \left|\Psi_0\right\rangle \leq \left\langle\Psi\right| \hat{H}_{\mathrm{HF}} \left|\Psi\right\rangle \tag{87}$$

and therefore, within the Hartree-Fock scheme, represents the best possible approximate ground-state wave function of the system that consists of a single Slater determinant. Alternatively, E_0 can also be expressed directly in terms of the single-particle orbitals [99]

$$E_0 = \frac{1}{2} \sum_{j=1}^{\mathrm{occ}} \epsilon_j + \left\langle\phi_j\right| \hat{H}_{\mathrm{HF}} \left|\phi_j\right\rangle . \tag{88}$$

The Hartree-Fock method scales with N^4 , where N denotes the number of basis functions [104]. For large distances in molecular dissociation processes, the Hartree-Fock wave function described by a Slater determinant does not reduce to the proper atomic limit [77], but for a range of problems, the Hartree-Fock method is in good agreement with experiments leading to an error of the energy which is below 1 %. The limitation of the energy accuracy is associated with the electron correlation problem [106]. The accuracy of other observables such as the molecular dipole moments, the electric polarizabilities, the electronic excitation energies and force constants among others is usually within 5-10 % [107]. The Hartree-Fock method considers exchange by the antisymmetrization and considers the Coulomb repulsion by taking the spatial average over all remaining electron positions.

3

DENSITY-BASED METHODS

Ground-state DFT [56–59, 108, 109] and time-dependent density-functional theory (TDDFT) [110–114] provide an exact framework to the many-body problem in quantum mechanics. Given an interacting N-particle system, the essence of ground-state DFT is to replace the $3N$-dimensional wave function by a fundamental descriptor of significantly lower dimension, i.e. the three-dimensional electronic ground-state density. The framework of DFT that formally underpins such a replacement is given in Sec. 3.2. Meanwhile, a variety of extensions to ground-state and time-dependent DFT have been developed that are nowadays used to study all different kinds of many-body problems. For example, systems coupled to an external magnetic field can be described in the framework of current-spin density functional theory (CSDFT), where the fundamental descriptors are given by the density $n(\vec{r})$, the magnetization $m(\vec{r})$ and the paramagnetic current $\vec{j}_p$ [115]. Typically, here the particles are treated in the non-relativistic limit, which is overcome by relativistic density-functional theory (RDFT). A particular new branch is QEDFT that generalizes the concepts of DFT and TDDFT. QEDFT overcomes the classical treatment of the electromagnetic field by treating the particles as well as the photons on the same theoretical footing, e.g. relevant for systems in a cavity. In Sec. 3.3 we discuss how ground-state DFT can be formally extended to fractional particle numbers and introduce the concepts relevant in QEDFT. Having the theoretical setup at hand, Sec. 3.4 describes how the Kohn-Sham approach makes use of the formal concepts presented in Sec. 3.2 and Sec. 3.3. Together with the approximations to the xc functional discussed in Sec. 3.5, the Kohn-Sham approach establishes DFT as a practical tool in computational science.

3.1 FORMAL SETUP OF GROUND-STATE DENSITY-FUNCTIONAL THEORY

Usually in the electronic structure theory community the matter is treated within the framework of many-body quantum theory, while the electromagnetic fields are treated within the framework of classical electromagnetic field theory. In such a treatment, the feedback of the electrons to the electrodynamic field is neglected. The considered Hamiltonian of Eq. 81 in first quantization is given by

$$\hat{H}_e = \sum_{i=1}^{N} -\frac{\hbar^2}{2m}\vec{\nabla}_i^2 + \sum_{i=1}^{N} v(\vec{r}_i) + \frac{1}{2}\sum_{i\neq j}^{N} \frac{e^2}{4\pi\epsilon_0|\vec{r}_i - \vec{r}_j|} \tag{89}$$

and reads in second quantization

$$\begin{aligned}\hat{H}_e = &\sum_{\sigma} \int d\vec{r}\hat{\Psi}_\sigma^\dagger(\vec{r}) \left(-\frac{\hbar^2}{2m}\vec{\nabla}^2 + V(\vec{r})\right) \hat{\Psi}_\sigma(\vec{r}) \\ &+ \frac{e^2}{4\pi\epsilon_0}\sum_{\sigma,\sigma'} \int\int d\vec{r}d\vec{r}'\hat{\Psi}_\sigma^\dagger(\vec{r})\hat{\Psi}_{\sigma'}^\dagger(\vec{r}')\frac{1}{|\vec{r}-\vec{r}'|}\hat{\Psi}_{\sigma'}(\vec{r}')\hat{\Psi}_\sigma(\vec{r}).\end{aligned} \tag{90}$$

The complexity in solving the exact many-body problem corresponding to the Hamiltonian in Eq. 89 and in Eq. 90 still goes beyond the technological capabilities of nowadays available computers making further simplifications necessary. In the following, we will show that DFT exploits the one-to-one correspondence between the local potential $v(\vec{r})$ and the electronic ground-state density $n_{00}(\vec{r})$ introduced in Def. 2.1.1.

3.2 CONCEPTS IN GROUND-STATE DENSITY-FUNCTIONAL THEORY

The formal setup of DFT relies on the existence and uniqueness of the density-to-potential map. While Sec. 3.2.1 introduces the Hohenberg-Kohn theorems which guarantee the uniqueness of this map, Sec. 3.2.2 is considered with the v-and N-representability conditions which assure its existence. In Eq. 102 we introduce the variational principle as a formal prescription on how to find the ground-state energy of the system. However, the search for the minimum of the energy functional is performed over the domain of all trial densities - including those which are not generated by an external potential, i.e. unphysical densities. This is the so-called interacting v-representability problem.

One practical way to circumvent the v-representability problem is the Levy-Lieb constrained search introduced in Sec. 3.2.3. Here, additional constraints within the variational principle restrict the domain of the search to the subset of N-representable densities. Sec. 3.2.4 discusses a more formal way to handle the v-representability problem, i.e. to reformulate DFT in terms of the Legendre transformation.

3.2.1 *The Hohenberg-Kohn theorem*

The theoretical foundations of density-functional theory were laid by the pioneering work of Walter Kohn and Pierre Hohenberg [109]. For isolated systems in an arbitrary local real-space potential with non-degenerate ground-state and for fixed particle-particle interaction, Kohn and Hohenberg established the fundamental maps required to solve the many-body quantum problem in a computational efficient way. The theoretical foundations of density-functional theory are encapsulated into two fundamental theorems known as the Hohenberg-Kohn theorems given in Theo. 3.2.1 and Theo. 3.2.2.

Fig. 3 depicts the exact maps relevant in ground-state density functional theory, i.e. the maps between the set of the ground-state wave functions $\mathcal{P} = \{\Psi_0^j(\vec{r})\}$, the set of the local potentials $\mathcal{V} = \{v^j(\vec{r})\}$, and the set of the ground-state densities $\mathcal{N} = \{n_{00}^j(\vec{r})\}$, where the different elements in the set are labeled by j. Each element j illustrated as a black-filled circle in Fig. 3 corresponds to a function in real-space $\vec{r}$ as indicated for the density and potential in Fig. 6.

The static many-body Schrödinger equation of Eq. 7 defines a map

$$\mathcal{A} : \mathcal{V} \to \mathcal{P},\ v^j(r) \mapsto \Psi_l^j(r) \tag{91}$$

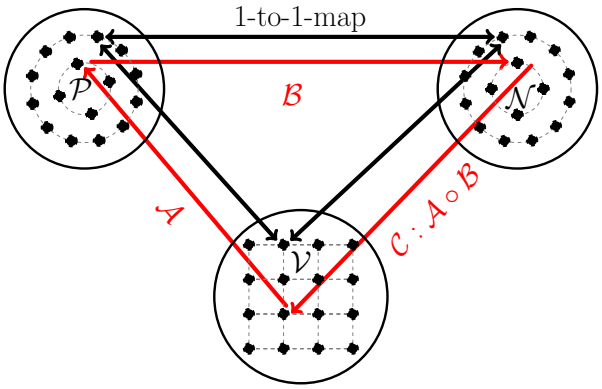

Figure 3: Schematic illustration of the one-to-one map between elements in the set of local potentials $\mathcal{V}$, the set of non-degenerate N-electron ground-state wave function $\mathcal{P}$, and the set of ground-state electron densities $\mathcal{N}$. Assuming N- and v-representability, every element in $\mathcal{V}$ has an exact one-to-one equivalent in $\mathcal{N}$ and $\mathcal{P}$, where each element indicated as black-filled circle represents a function in real-space $\vec{r}$. This figure is adapted from Ref. [116].

that connects elements from the set of local external potentials to its image in the set of ground-state wave functions ($l = 0$) and in the set of excited-state wave functions ($l \neq 0$). The map

$$\mathcal{B} : \mathcal{P} \to \mathcal{N}, \ \Psi_0^j(\vec{r}) \mapsto n_{00}^j(\vec{r}) \tag{92}$$

connects elements in the set of the ground-state wave functions to elements in the set of ground-state electron densities by exploiting Eq. 5. The v-representability condition [117–121] discussed in Sec. 3.2.2 assures that the map

$$\mathcal{C} : \mathcal{A} \circ \mathcal{B} : \mathcal{V} \to \mathcal{N}, \ v^j \mapsto n_{00}^j \tag{93}$$

between elements in the set of local potentials $\mathcal{V}$ and elements in the set of ground-state densities $\mathcal{N}$ is surjective, i.e. that every element j in the set of $\mathcal{N}$ is generated by an element in the set of $\mathcal{V}$ [122]. An illustration of surjective, but not injective maps is given in Fig. 4[1]. By restricting the co-domain of the map $\mathcal{C}$ to the set of v-representable densities, the v-representable condition guarantees the surjectivity and hence, the existence of the combined map $\mathcal{C} : \mathcal{A} \circ \mathcal{B}$. Note, surjectivity of map $\mathcal{A}$ requires that every wave function in the set $\mathcal{P}$ is generated by an external potential in the set $\mathcal{V}$. Similarly, the surjectivity of the map $\mathcal{B}$ requires that every density in the set $\mathcal{N}$ is generated by a wave function in the set $\mathcal{P}$. The surjectivity of the map $\mathcal{B}$ restricts the set $\mathcal{N}$ to the set of densities that are N-representable, while the surjectivity of the map $\mathcal{C}$ additionally restricts the set $\mathcal{N}$ to the set of densities that are v-representable.

Hohenberg and Kohn proved under certain restrictions that a surjective map $\mathcal{A}$ and a surjective map $\mathcal{B}$ is injective. Together with the existence of the map assured by the v- and N-representability condition all maps in Fig. 3 become bijective. The injectivity of map $\mathcal{A}$ implies that any distinct potentials in the set

1 Non-uniqueness is a common problem e.g. in spin-DFT [123].

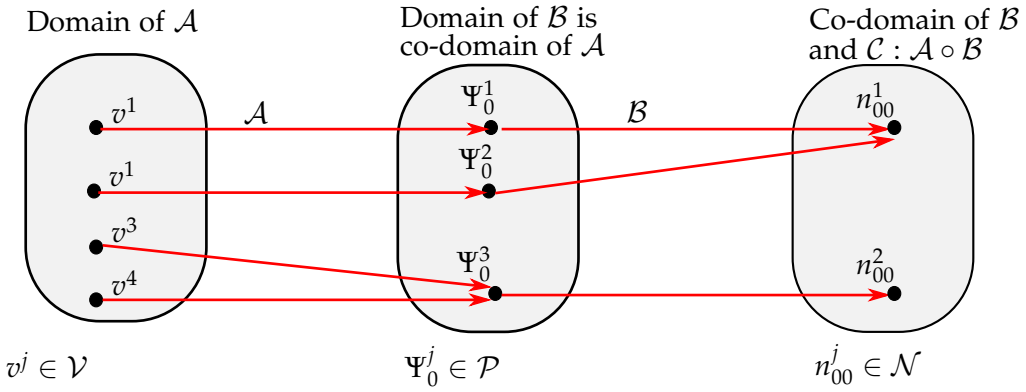

Figure 4: Non-unique maps. Schematic illustration of the surjective, but not injective map $\mathcal{C} : \mathcal{A} \circ \mathcal{B}$. Red arrows depict the map between elements marked as black-filled circles from their domain onto their co-domain. Surjective maps allow that the image in the co-domain corresponds to distinct elements in the domain. The map $\mathcal{A}$ maps the set of local potentials $\mathcal{V}$ to the set of non-degenerate N-electron ground-state wave function $\mathcal{P}$, and the map $\mathcal{B}$ maps the set $\mathcal{P}$ onto the set of ground-state electron densities $\mathcal{N}$. Every element in the co-domain has at least one element in its corresponding domain. This is assured for the map $\mathcal{B}$ by the N-representability condition, while the map $\mathcal{C}$ additionally requires the v-representability condition.

$\mathcal{V}$ that lead to a non-degenerate ground-state of the system always generate distinct ground-state wave functions in the set $\mathcal{P}$, i.e. if $v^j \neq v^{j'}$ then $\Psi_0^j \neq \Psi_0^{j'}$. The injectivity of map $\mathcal{B}$ implies that distinct non-degenerate ground-states never generate the same ground-state density, i.e. if $\Psi_0^j \neq \Psi_0^{j'}$ than $n_{00}^j \neq n_{00}^{j'}$, see also Ref. [124].

From the bijectivity of the maps $\mathcal{A}$ and $\mathcal{B}$ directly follows that also the map $\mathcal{C}$ is bijective and therefore, that the map $\mathcal{C}$ is fully invertible. Mathematically, the domain and the co-domain of the map $\mathcal{C}$ can be swapped implying that the external potential of a physical system $v(\vec{r})$ is fully determined by its electron ground-state density $n_{00}(\vec{r})$.

From the uniqueness of the map $\mathcal{C}$ (up to an additive constant) follows that the map is invertible and we can write

$$\mathcal{C}^{-1} : \mathcal{N} \to \mathcal{V},\ n_{00}^j \mapsto v^j. \tag{94}$$

The one-to-one correspondence between n_{00}^j and v^j is the essence of the first Hohenberg-Kohn theorem [109] in Theo. 3.2.1.

Theorem 3.2.1: First Hohenberg-Kohn Theorem

For isolated systems in an arbitrary local real-space potential with non-degenerate ground-state and for fixed particle-particle interaction, the map between the local potential and the electron density of the system is (up to an additive constant) unique, i.e.

$$v(\vec{r}) \underset{\text{1-to-1}}{\longleftrightarrow} n_{00}(\vec{r}). \tag{95}$$

In other words, the ground-state electron density $n_{00}[v]$ is a unique functional of the external potential and vice versa $v[n_{00}]$.

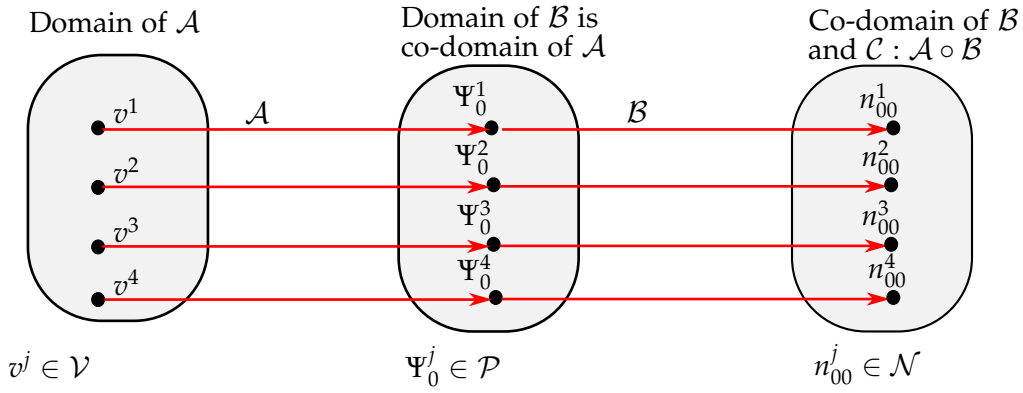

Figure 5: Schematic illustration of the bijective map between elements marked as black-filled circles from their domain onto their co-domain as proven by Hohenberg-Kohn. The map $\mathcal{A}$ maps the set of local potentials $\mathcal{V}$ to the set of non-degenerate N-electron ground-state wave functions $\mathcal{P}$, and the map $\mathcal{B}$ maps the set $\mathcal{P}$ onto the set of ground-state electron densities $\mathcal{N}$. The surjectivity of the map $\mathcal{C}:\mathcal{A}\circ\mathcal{B}$ is assured by the v-representability condition, Hohenberg-Kohn proved that the the map $\mathcal{C}$ is also injective, and hence bijective. Every element in $\mathcal{C}$ has exactly one corresponding element in the set $\mathcal{A}$ and $\mathcal{B}$.

In general, where the domain of $\mathcal{B}$ also contains degenerate ground-state wave functions, the inversion of map $\mathcal{B}$, i.e.

$$\mathcal{B}^{-1}:\mathcal{N}\to\mathcal{P},\ n_{00}^j(r)\mapsto\Psi_l^j(r) \tag{96}$$

is not unique making it impossible to construct the ground-state wave function of a system given solely its electronic ground-state density and without solving the Schrödinger equation [125]. In the case of degenerate ground-state wave functions, the "ground-state density uniquely determines a manifold of degenerate states", each of which "uniquely determines the potential" [123]. As example Ref. [123] provides the non-interacting Li atom, in which the external potential generates a unique density that corresponds to distinct wave functions. However, for non-degenerate ground-state wave functions, the map $\mathcal{B}$ defines a functional $\Psi_{00}[n_{00}]$. Note, the wavefunctional $\Psi\left(\alpha(\vec{r}),n_{00}(\vec{r})\right)$ further depends on the choice of an arbitrary gauge function $\alpha(\vec{r})$. In the Hohenberg-Kohn theorem, the gauge function is set to zero and the wave function solely depends on the ground-state density [126].

The wavefunctional allows to express expectation values of arbitrary operators $\hat{O}$ as functionals of the ground-state density, i.e.

$$\mathcal{O}_{ii}[n_{00}] = \langle \Psi_i[n_{00}] | \hat{O} | \Psi_i[n_{00}] \rangle . \tag{97}$$

In particular, the total energy of the system can be defined in terms of the density of the system, i.e.

$$E[n[v(\vec{r})]] = \langle \Psi_0[n] | \hat{T} + \hat{V}_{\text{e-e}} + \hat{V} | \Psi_0[n] \rangle \tag{98}$$

$$= \int v(\vec{r}) n[v(\vec{r})] d\vec{r} + F_{\text{HK}}[n[v(\vec{r})]], \tag{99}$$

with the Hohenberg-Kohn functional as in Def. 3.2.1.

Definition 3.2.1: Universal Hohenberg-Kohn Functional

The expectation value of the kinetic energy operator $\hat{T}$ and the electron-electron interaction operator $\hat{V}_{\text{e-e}}$ is called the universal Hohenberg-Kohn functional, i.e.

$$F_{\text{HK}}[n[v(\vec{r})]] = \langle \Psi[n[v(\vec{r})]] | \hat{T} + \hat{V}_{\text{e-e}} | \Psi[n[v(\vec{r})]] \rangle \tag{100}$$

$$= E[n[v(\vec{r})], N] - \int v(\vec{r}) n[v(\vec{r})] d\vec{r}. \tag{101}$$

The Hohenberg-Kohn functional has no explicit dependence on the external potential v^j, but has an implicit one via its dependence on the density $n_{00}[v]$. Therefore, the exact Hohenberg-Kohn functional is universal, i.e. it is able to accurately describe different systems ranging from molecules to solids [127], while its functional form remains the same. In contrast to the wavefunctional, the Hohenberg-Kohn functional is a unique functional with well-defined domains and analytic properties [125].

Theorem 3.2.2: Second Hohenberg-Kohn Theorem

The energy functional has its minimum at the ground-state density of the interacting-system. The variational principle reads

$$E_{00} = E[n_{00}] \leq E[n] = F_{HK}[n] + \int v(\vec{r}) n(\vec{r}) d\vec{r}. \tag{102}$$

In general, the explicit density dependence of arbitrary observables is unknown and the lack of general recipes on how to derive explicit density functionals of arbitrary operators can hamper practical DFT applications. In this work, we illustrate the explicit density dependence of arbitrary observables as functional of the density for our specific model systems. Constructing the explicit density map illustrates what was proven by Hohenberg and Kohn. This is not only of educational value, but also allows to get new insight, e.g. by studying on how signatures of the density-to-potential map show in arbitrary density functionals.

3.2.2 *Existence of the maps: N- and v-representability condition*

Under the assumptions of the Hohenberg-Kohn theorem discussed in Sec. 3.2.1, the theorem guarantees that if the density-to-potential map of a system exists, it is a unique, fully invertible map. Nevertheless, the Hohenberg-Kohn theorem does not say anything about the existence of this map. Further, the Hohenberg-Kohn functional does not tell us if the density that minimizes the energy functional gives us back a true physical quantity, i.e. that the resulting density originates from an (i) antisymmetric many-body wave function corresponding to the ground-state of an arbitrary (ii) local external potential [57]. Condition (i) and (ii) are the so-called N and v-representability condition. The exact Hohenberg-Kohn functional is the smallest N-representable functional [128, 129]. In detail, it is distinguished between the (i) interacting, the (ii) non-interacting, the (iii) pure-state and the (iv) ensemble v-representability condition. Each of which refers to the question whether the density of (i) an interacting system, of (ii) an non-interacting system, of (iii) a pure ground-state Ψ_0 or of (iv) an statistical ensemble is generated by an external potential, respectively.

The interacting v-representability guarantees not only the existence of the density-to-potential map, but also guarantees that the density that minimizes the energy functional represents a true physical quantity. While the interacting v-representability condition complements the first Hohenberg-Kohn theorem and therefore, further consolidates the formal framework of DFT, the non-interacting v-representability condition is essential for practical DFT calculations. The essence of usual DFT calculations is to replace the interacting system by a much simpler auxiliary non-interacting one, i.e. the Kohn-Sham approach discussed in detail in Sec. 3.4. The Kohn-Sham approach solely works if a non-interacting potential exists that reproduces the density of the interacting system, i.e. the non-interacting v-representability condition [130].

Given its fundamental importance, we briefly review under which conditions a ground-state density is v- or N-representable.

For the electron density the N-representability problem is solved, since any non-negative, differentiable, normalized function can be written in terms of some antisymmetric wave function, and therefore is N-representable. Herein, differentiability ensures that the kinetic energy is finite, i.e. $\int |\vec{\nabla}\sqrt{n(\vec{r})}|^2 < \infty$ [131, 132].

Unfortunately, assuring v-representability of a given density is a more difficult task. As pointed out by Mel Levy in Ref. [133] "countless" non-v-representable densities appear "in the neighborhood of ensemble-v-representable densities". So is there any hope? The answer is: it depends. As shown in Ref. [120], in infinite-dimensional space not every density is v-representable. Fortunately, there are several ways around the v-representable problem. In its original formulation, the Hohenberg-Kohn theorems were restricted to pure-state v-representable densities. The first examples of non-v-representable densities that have been brought up by Ref. [134] and Ref. [135] are not pure-state but at least ensemble-

v-representable. For such densities it is sufficient to enlarge the domain of the variational search to the set of trial densities that are constructible as convex combination of the degenerate densities, i.e. the set of ensemble-v-representable trial densities. However, in general, it is not clear how to restrict the domain to the set of v-representable densities.

The Levy-Lieb constrained search [135, 136][2] introduced in Sec. 3.2.3 circumvents the v-representability problem by modifying the domain of the search to the set of trial densities that are N-representable. Note, in Ref. [120] it is shown that not every N-representable density is ensemble v-representable. However, if the density in the constrained search is v-representable then the energy minimum equals the Hohenberg-Kohn functional [139]. A more formal way to circumvent the v-representability is to reformulate DFT in terms of the Legendre-transformation as discussed in Sec. 3.2.4. Provided that the Legendre transformation exists, it immediately follows that each density corresponds to a conjugated external potential [125, 135, 140–142].

Going from infinite-dimensional space to finite-dimensional space, it could be shown [57, 119, 121, 130, 143, 144] that any differentiable, normalized and strictly positive fermionic or bosonic density is ensemble-v-representable. In this thesis, we explicitly construct the density maps by exact diagonalization of model Hamiltonians in finite dimension. By construction each density corresponds to an external potential and to a N-particle wave function, and hence is N- and v-representable. In general, exact diagonalization is numerically not feasible. Alternatively, the density maps can be found by applying the Levy-Liebs constrained search formalism to our model system. While the normalization constrained in the search assures that the trial densities are N-representable, the finite dimension of the lattice assures that any positive normalized density that minimizes the energy functional is also v-representable. The N- and v-representability also assures the existence of the Legendre transformation that is discussed in Sec. 3.2.4.

3.2.3 *Levy-Lieb constrained search*

There is no systematic procedure that allows to restrict the domain of trial densities to the set of v-representable ones [137, 138]. One way to handle the v-representability problem is the constrained search formalism of Levy and Lieb. The Levy-Lieb constrained search restricts the domain to the set of N-representable trial densities and therefore, simply circumvents the v-representability problem. The single minimization principle as in Eq. 8 is replaced by a minimization procedures that is performed by two separate steps [138] as can be seen in Def. 3.2.2.

2 Note, the domain of the search in Eq. 102 goes over all trial densities that are positive definite and integrate to the particle number of the system, for further details see e.g. Ref. [137, 138]. Therefore, the domain of the variational search in Eq. 102 also includes the subset of densities that are not generated by an external potential, i.e. the set of non-v-representable densities [138].

Definition 3.2.2: Levy-Lieb constrained search

The Levy-Lieb constrained search is given by

$$E_{00} = \min_{n} \left[\inf_{\Psi \to n} \langle \Psi[n(\vec{r})] | \, \hat{T} + \hat{V}_{\text{e-e}} \, | \Psi[n(\vec{r})] \rangle + \int v(\vec{r}) n[v(\vec{r})] d\vec{r} \right] . \quad (103)$$

The inner minimization

$$Q_{\text{HK}}[n(\vec{r})] = \inf_{\Psi \to n} \langle \Psi[n(\vec{r})] | \, \hat{T} + \hat{V}_{\text{e-e}} \, | \Psi[n(\vec{r})] \rangle \quad (104)$$

searches for the minimum of the expectation value of kinetic energy plus electron-electron interaction operator over the domain of all N-representable wave function. Therefore, the inner minimization assures that the density stems from an antisymmetric wave functions. The outer minimization

$$E_{00} = \min_{n} \left[Q_{HK}[n] + \int v(\vec{r}) n[v(\vec{r})] d\vec{r} \right] \quad (105)$$

further restricts the domain to the set of densities that integrate to the particle number of the system. The domain of the search in Eq. 105 still includes the subset of densities that are not generated by an external potential, i.e. the set of non-v-representable densities [137]. Provided that the minimizing density is v-representable, the functional defined in Eq. 104 is equal to the Hohenberg-Kohn functional, i.e. $Q_{\text{HK}}[n(\vec{r})] = F_{\text{HK}}[n(\vec{r})]$ [139]. Formally, the Levy-Lieb constrained search for pure states can be extended to ensembles [145, 146].

3.2.4 *DFT in terms of the Legendre transformation*

A more formal way to handle the v-representability problem is given by the reformulation of the Hohenberg-Kohn variational problem in terms of the Legendre transformation [125, 135, 140–142]. In the Legendre transformation framework of DFT, the Hohenberg-Kohn functional is defined as

$$F_{\text{HK}}[N, n(\vec{r})] = - \inf_{v} \left[\int n(\vec{r}) v(\vec{r}) d\vec{r} - E[v(\vec{r})] \right] , \quad (106)$$

where the old variable

$$n_{00}(\vec{r}) = \left[\frac{\delta E}{\delta v(\vec{r})} \right]_{N} , \quad (107)$$

is replaced by the derivative of the old functional $E[N, v(\vec{r})]$ with respect to the old variable $v(\vec{r})$ at constant particle number N. This leads to a generalized variational principle for a fixed local potential over a set of trial densities [125].

Taking the Legendre transformation of the Hohenberg-Kohn functional yields

$$E[N, v(\vec{r})] = \inf_{n} \left[\int n(\vec{r}) v(\vec{r}) d\vec{r} + F_{\text{HK}}[n(\vec{r})] \right] , \quad (108)$$

where the conjugated variable is given by

$$v(\vec{r}) = -\left[\frac{\delta F_{\mathrm{HK}}}{\delta n}\right]_N . \tag{109}$$

The question whether the density that minimizes the energy functional $E[N, n(x)]$ is v-representable can be replaced by asking whether the Legendre transformation of the energy functional $E[N, v(\vec{r})]$ exists [135]. Further the Legendre transformation allows a formal proof of the convexity of $F_{HK}[n]$ in n, which is a necessary criterion for the existence of the global minima of the system and therefore formally underpins Theo. 3.2.2.

The differential form of $E[N, v]$ is given by

$$dE = \mu dN + \int n(\vec{r})\delta v(\vec{r})d\vec{r}. \tag{110}$$

While the electronic ground-state density of Eq. 107 describes the local response to perturbations in the energy functional with respect to the external potential for fixed particle number, the chemical potential

$$\mu = \left[\frac{\delta E}{N}\right]_{v(\vec{r})}, \tag{111}$$

describes the global response of the system to changes with respect to the total particle number for fixed external potential [147].

The existence of the Legendre transformation allows a change of variables from the external potential $v(\vec{r})$ to the ground-state density $n_{00}(\vec{r})$ in the concave energy functional $E[v(\vec{r})]$ in v. By construction, the Legendre formalism of DFT assures v-representability of the density.

3.3 EXTENSIONS TO THE CONCEPTS OF GROUND-STATE DFT

The concepts introduced in Sec. 3.2 provide a powerful theoretical framework. In its original formulation DFT is restricted to a subset of physical interesting problems, but its mathematical rigor and its success in practical applications rapidly lead to a variety of extensions. This work is mainly concerned with processes in which the particle number of the system changes adiabatically in time. Note, the concepts introduced so far are valid for fixed particle number. Therefore, Sec. 3.3.1 introduces the concept of the intrasystem derivative discontinuity, an exact concept for infinitesimally weak coupled system-bath complexes with degenerate ground-state. Using the concept of the derivative discontinuity, DFT is able to describe processes in which the particle number of the system can change gradually in time. Sec. 3.3.1 extends the Hohenberg-Kohn formalism to finite temperature that in general lifts the degeneracy of the ground-state.

3.3.1 *DFT for fractional particle numbers*

In its original formulation the Hohenberg-Kohn theorems are valid for isolated systems with fixed particle number N. In particular, the particle number can be

expressed in terms of the ground-state density $N[n_{00}]$. The description of observables that explicitly depend on the particle number of the system such as the ionization energy, the electron affinity or the band gap of the system require to extend the concepts introduced so far, where the particle number was kept fixed at constant integer value. Along the lines of Hohenberg-Kohns original formulation of DFT, density functionals are only defined for the set of discrete integer values N. Each fixed value of N corresponds to one minimization procedure that yields the real-space ground-state density of the considered system. By construction, these density functionals show a discontinuous behavior along the cut of N that only have values at integer particle number N.

INTERSYSTEM DERIVATIVE DISCONTINUITY For systems with a degenerate ground-state, these discontinues values at integer N can be connected via straight lines introducing an infinitesimally weak coupling from the system to an external bath [68]. The coupling formally allows to consider the system as an open quantum system that can change its particle number gradually in time, and therefore the value of N can take fractional values.

Considering a two-fold degenerate density with the density $n_{00,1}$ corresponding to a N-particle system and the density $n_{00,2}$ corresponding to a $N+1$ particle system, functionals along the cut in N can be constructed as convex combination

$$F = (1-\omega)F_N + \omega F_{N+1} \tag{112}$$

with the mixing parameter $0 \leq \omega \leq 1$ as has been shown by Ref. [68, 148]. We like to highlight that this straight-line behavior is only exact in the limit of an exact degeneracy of the ground-state. Nevertheless, with caution this straight-line behavior is a very good approximation for systems with a near-degeneracy of the ground-state. Such near-degenerate density functionals approach the straight-line behavior of the functionals as constructed in Eq. 112, while the eigenenergies of the system approaches a real degeneracy, i.e. the transition from an avoided crossing to a real-crossing of the eigenergies. However, the mixing in the degenerate subspace of the ground-state densities results in a functional dependency along the cut in N that is given by straight lines, which change their slopes at integer values of N [68, 148]. At points where the slope changes, the derivatives of the density functionals constructed as in Eq. 112 show the well-known intersystem derivative discontinuity. Contrarily, functionals along the cut in the variable N that correspond to systems with a near-degenerate ground-state always have a well-defined gradient. A text-book example is the derivative discontinuity of the Hohenberg-Kohn functional along the cut in the variable N (linked to the so-called band-gap problem in DFT). In this work, we illustrate also other observables as functional of N and illustrate their straight-line behavior for systems with a real-degenerate ground-state. Further, we illustrate how the near-degeneracy lifts the derivative discontinuity and leads to functionals that have a well-defined gradient along the cut in the variable N.

Definition 3.3.1: Straight-line behavior & derivative discontinuity

The straight-line behavior refers to the functional behavior of the energy functional along the cut in the variable N. This is an exact condition for systems with degenerate ground-state for which the density can be constructed as convex combination in the degenerate subspace [68, 148]. The derivative of $E[N]$ with respect to the particle number becomes discontinuous at integer values of N, where the slope of $E[N]$ changes its values. The change in the slope of $E[N]$ corresponds to the energy that is required to add or to remove a particle from the system.

THE MERMIN-THEOREM The Mermin theorem naturally allows the treatment of systems with fractional particle numbers within the framework of DFT by generalizing the Hohenberg-Kohn theorem to finite temperatures. For a grand-canonical ensemble at a given temperature and chemical potential,

(i) the map between the external potential $v(\vec{r})$ and the equilibrium density $n^{eq}(\vec{r})$ is bijective, i.e.

$$v(\vec{r}) \leftrightarrow n^{eq}(\vec{r}) = \mathrm{Tr}\left\{\hat{\rho}_{eq}\hat{n}\right\} \tag{113}$$

(ii) and the equilibrium density minimizes

$$\Omega[n] = F_{\mathrm{M}}[n](\mu, T) - \mu\hat{N} + \sum_j v_j n_j \tag{114}$$

with the universal Mermin-functional

$$F_{\mathrm{M}}[n](\mu, T) = \mathrm{Tr}\left\{\hat{\rho}_{eq}[n]\left(\hat{T} + \hat{W} + k_B T \ln(\hat{\rho}_{eq}[n])\right)\right\} \tag{115}$$

The equilibrium density-matrix is defined as

$$\hat{\rho}_{eq} = \frac{e^{-\beta\left(\hat{H}-\mu\hat{N}\right)}}{\mathrm{Tr}\left\{e^{-\beta\left(\hat{H}-\mu\hat{N}\right)}\right\}} \tag{116}$$

and minimizes $\Omega(\hat{\rho}) = \mathrm{Tr}\left\{\hat{\rho}\left(\hat{H} + k_B T \ln(\hat{\rho}) - \mu\hat{N}\right)\right\}$ such that $\Omega(\hat{\rho}_{eq}) = E - TS - \mu N = -k_B T \ln Z$ is the grand-canonical potential with E the internal energy, S the entropy and $Z = \mathrm{Tr}\left\{e^{-\beta\left(\hat{H}-\mu\hat{N}\right)}\right\}$ the partition function [149].

PARTITIONING OF THE SYSTEM Another way to treat fractional particle numbers using density-based methods is given by density-based fragment techniques [150] including partitioning density-functional theory (PDFT) [151] , subsystem DFT [152] and quantum mechanical embedding theories based on the density matrix such as density-matrix embedding theory (DMET) [153]. The underlying concept of such density-based fragment techniques [150] is the partitioning of the total system - that is too complex to be described fully quantum-mechanically - into its usually smaller, easier traceable subunits that then can be treated fully quantum-mechanically. Such procedures are commonly used to partition large molecules into its atomic subsystems or molecular fragments [154]. Among the

many partitioning schemes that can be found in literature, we like to highlight the Hirshfeld partitioning scheme [155] that divides the system such that the information distance between different fragments is minimized [156] and the Bader partitioning scheme [157] that divides the system into fragments with sharp boundaries whenever the charge density perpendicular to the boundary surface passes a minima [156]. The decomposition of the total system into such "chemical building blocks" reduces the computational cost and usually offers an alternative route to gain further insight about the system [158]. Formally, the density can be written as a sum over all of j subsystem-densities $n_{00,j}(\vec{r})$, i.e.

$$n_{00}(\vec{r}) = \sum_{j=1}^{S} n_{00,j}(\vec{r}), \tag{117}$$

where S denotes the number of subsystems within the system. Without external constraints this partitioning of the density is not unique [152].

3.3.2 *DFT for coupled electron-photon systems*

QEDFT generalizes the concepts of ground-state DFT to correlated electron-photon problems. Within the framework of QEDFT the matter as well as the fields can be described quantum mechanically in an computationally efficient manner. In particular, QEDFT allows to theoretically describe experiments at the interface of quantum optics and quantum chemistry, where the considered systems within QEDFT are typically located in an optical cavity [114]. For example, QEDFT allows to describe experiments that modulate the chemical properties of molecules inside a cavity.

Concepts in quantum optics include exact diagonalization of model Hamiltonians and the reduced density matrix formulation among others. A complementary view is now offered by the framework of QEDFT. QEDFT allows to describe the quantum nature of electrons and photons on the same quantized footing. It is an exact reformulation of the following Schrödinger equation [159–161] containing N electrons interacting with N_p photon modes with frequency ω_α with $\alpha = k\lambda$ and $\hat{\vec{P}} = -e\sum_{i=1}^{N}\vec{r}_i$

$$\hat{H}(t) = \hat{H}_e(t) + \hat{H}_p(t) \tag{118}$$

$$\hat{H}_e(t) = \sum_{i=1}^{N}\left(-\frac{\hbar^2}{2m}\vec{\nabla}_i^2 + v_{\text{ext}}(\vec{r}_i, t)\right) + \frac{e^2}{4\pi\epsilon_0}\sum_{ij,i>j}\frac{1}{|\vec{r}_i - \vec{r}_j|} \tag{119}$$

$$\hat{H}_p(t) = \frac{1}{2}\sum_{\alpha=1}^{N_p}\left[\hat{p}_\alpha^2 + \omega_\alpha^2\left(\hat{q}_\alpha + \frac{\vec{\lambda}_\alpha}{\omega_\alpha}\cdot\hat{\vec{P}}\right)^2\right] + \frac{j_{\text{ext}}^\alpha(t)}{\omega_\alpha}\hat{q}_\alpha. \tag{120}$$

and allows to describe e.g. electrons in an optical cavity. The variable p_α and q_α describe the photon field and the photon displacement variable q_α is here the displacement of the α-th harmonic oscillator associated to the photon mode. It is directly proportional to the electric displacement field observable of the α-th mode. The effective strength of the electron-photon interaction is given by the

electron-photon interaction parameter $\vec{\lambda}_\alpha$.
The mathematical rigorous formulation of QEDFT can be found in Refs. [159, 162, 163] and in the following, we briefly summarize, what is necessary in the framework of the current work. QEDFT is based on the one-to-one correspondence between sets of conjugated pairs of variables, i.e. between the set of the external potential for the electrons and the photons ($v_{\text{ext}}(\vec{r},t)$ and $j^{(\alpha)}_{\text{ext}}(t)$), and the set of the electron density $n(\vec{r},t)$ and photon analogue $q_\alpha(t)$, i.e.

$$(v_{\text{ext}}(\vec{r},t), j^{(\alpha)}_{\text{ext}}(t)) \underset{1:1}{\longleftrightarrow} (n(\vec{r},t), q_\alpha(t))\,. \tag{121}$$

The photon quantity

$$q_{k\lambda}(t) = \langle\Psi(t)|\,\hat{q}_{k\lambda}\,|\Psi(t)\rangle = \sqrt{\frac{\hbar}{2\omega_{k\lambda}}}\,\langle\Psi(t)|\,\hat{a}^\dagger_{k\lambda} + \hat{a}_{k\lambda}\,|\Psi(t)\rangle\,, \tag{122}$$

where $\hat{a}^\dagger_{k\lambda}$ and $\hat{a}_{k\lambda}$ are the creation and annihilation operators introduced in Sec. 2.6 and $\hat{q}_{k\lambda}$ denotes the displacement of the k-th harmonic oscillator associated to the photon mode. It is directly proportional to the electric displacement field observable of the k-th mode as in Eq. 58. The theoretical foundations of DFT for correlated electron-photon systems are given by Ref. [114, 159, 162, 163]. As in electronic DFT, we can exploit the one-to-one correspondence to setup a Kohn-Sham construction that allows to simulate the many-body dynamics by a non-interacting system. The latter system is naturally computationally more appealing. However, this replacement comes with a prize, namely the typically xc potential emerges and has to be approximated in all practical applications. Neglecting this xc potential leads to the mean-field potential that is identical to a classical Maxwell-Schrödinger simulation [164, 165]. However, also first approximations to the xc potential of correlated electron-photon systems are already on the market such as the optimized effective potential approximation [160].

The Hilbert space of the corresponding ground-state wave function of the coupled electron-field system is equal to $\mathcal{H} = \mathcal{H}_{ph} \otimes \mathbb{1} + \mathbb{1} \otimes \mathcal{H}_e + \mathcal{H}_{ph} \otimes \mathcal{H}_e$. The dimension of the Hilbert space of the system increases with the number of electrons and photon modes within the system, the number of photons within each mode and with the number of polarization directions of the electromagnetic field. For example a cavity system that considers a two-dimensional electron that is sampled on a real-space grid with 20 points in each direction and coupled to a single-photon mode that can host up to 200 photons with two polarization directions has already a Hilbert space of dimension $20 \times 20 \times 200 \times 200 = 16\,000\,000$. Contrarily, in the Kohn-Sham approach of QEDFT, the electronic equations of motion partially decouple from the photonic ones. The remaining dimension of the problem stated above is 20×20 for the electrons and 200×2 for the photons. Both systems are still coupled via $n(\vec{r},t)$ and $q_\alpha(t)$ and have to be solved self-consistently.

3.4 DFT IN PRACTICE

While Sec. 3.2 and Sec. 3.3 are concerned with the formal framework of DFT, the present section is devoted to the concepts that bring the formal framework of DFT

to a practical level. A major contribution to the practicability of DFT is given by the KS scheme. In the KS scheme, the interacting many-body system is replaced by the auxiliary non-interacting Kohn-Sham system introduced in Sec. 3.4.1. The exact Kohn-Sham potential is able to fully mimic the electron-electron interaction in all of its facets.

3.4.1 *The non-interacting Kohn-Sham system*

From the Hohenberg-Kohn (HK) theorem in Theo. 3.2.1 follows that - for fixed interaction $V_{\text{e-e}}$ - the electron ground-state density fully determines the external potential and vice versa. Therefore, the high-dimensional wave function can be replaced by the three-dimensional ground-state density reducing the dimension of the problem drastically. The Kohn-Sham approach is a numerically feasible scheme that allows to find the ground-state density of a system without solving the interacting many-body Schrödinger equation but only solving sets of (coupled) non-interacting equations.

THE ELECTRONIC KOHN-SHAM EQUATIONS The principle idea of the Kohn Sham approach is to introduce an effective potential v_{ks} that allows to replace the interacting many-body Hamiltonian with $V_{\text{e-e}} \neq 0$ by an auxiliary non-interacting one with $V_{\text{e-e}} = 0$ as illustrated in Fig. 6. Assuming interacting and non-interacting v-representability, the map

$$v \overset{V_{\text{e-e}}\neq 0}{\longleftrightarrow} n_{00} \overset{V_{\text{e-e}}=0}{\longleftrightarrow} v_{ks} \tag{123}$$

exists and the Kohn-Sham Hamiltonian of the auxiliary system of non-interacting particles can be written as sum of the one-particle Hamiltonians,

$$\hat{H}_{ks}([n],\vec{r}) = \sum_j \hat{h}_{ks}([n],\vec{r}) = \sum_j \left(-\frac{\hbar^2}{2m}\vec{\nabla}_j^2 + v_{\text{ks}}([n],\vec{r}) \right) \tag{124}$$

with the effective Kohn-Sham potential v_{ks} that mimics the electron-electron interaction

$$v_{\text{ks}}([n],\vec{r}) = v_{\text{ext}}(\vec{r}) + v_{\text{H}}([n],\vec{r}) + v_{\text{xc}}([n],\vec{r}). \tag{125}$$

These potentials are connected to the energy functional. The total energy as functional of the density $n(\vec{r})$ is formally defined as

$$E[n] = T_S + U[n] + E_{\text{xc}}[n] + \int d\vec{r} n(\vec{r}) v(\vec{r}) \tag{126}$$

in which the kinetic energy of noninteracting spin-less system is given by

$$T_S[n] = -\frac{\hbar^2}{2m}\sum_{j=1}^{N} \int d\vec{r} \phi_j^*(\vec{r}) \vec{\nabla}^2 \phi_j(\vec{r}), \tag{127}$$

the classical Coulomb energy (Hartree energy) by

$$U[n] = \frac{e^2}{8\pi\epsilon_0} \int d\vec{r} \int d\vec{r'} \frac{n(\vec{r}) n(\vec{r'})}{|\vec{r} - \vec{r'}|}, \tag{128}$$

and the xc energy functional by

$$E_{xc}[n] = \int d\vec{r} n(\vec{r}) \epsilon_{xc}(n(\vec{r})), \tag{129}$$

where ϵ_{xc} is the xc energy density per particle. In practice, an expression for the total energy functional in terms of the Kohn-Sham eigenvalues is favorable. This expression is given as follows

$$E = \sum_{i}^{N} \epsilon_i + U[n] + E_{xc}[n] - \int \frac{\delta E_{xc}}{\delta n(\vec{r})} n(\vec{r}) d\vec{r}. \tag{130}$$

The functional derivative of the classical Coulomb energy U is connected to the Hartree-potential

$$v_H([n], \vec{r}) = \frac{\partial U[n]}{\partial n(\vec{r})}, \tag{131}$$

i.e. the electrostatic electron-electron repulsion term. Binding atoms to molecules and solids, the xc energy has the role of "natures glue" [166], its functional derivative is connected to the xc potential

$$v_{\mathrm{xc}}([n], \vec{r}) = \frac{\partial E_{\mathrm{xc}}[n]}{\partial n(\vec{r})}. \tag{132}$$

The corresponding Schrödinger-type equations are the Kohn-Sham equations

$$\hat{h}_{ks}(\vec{r}) \phi_j(\vec{r}) = \epsilon_j \phi_j(\vec{r}), \tag{133}$$

where the $\phi_j(\vec{r})$ are the one-particle Kohn-Sham orbitals that together can host up to two particles with opposite spin [167]. The set of orbitals form together the Kohn-Sham wave function [61]

$$\Psi_{\mathrm{ks}}(\vec{r}) = \frac{1}{\sqrt{N!}} det\{\phi_j(\vec{r})\}, \tag{134}$$

that is defined by a single Slater determinant [168], similarly to the Hartree-Fock wave function as defined in Eq. 83. Note, while the single Slater determinant in Hartree-Fock theory is chosen such that the energy is minimal, in DFT the Slater determinant is chosen such that it yields the exact many-body density. The density of the non-interacting system is given by

$$\sum_{i=1}^{N} |\phi_i(\vec{r})|^2 = n_{00}^{\mathrm{ks}}(\vec{r}), \tag{135}$$

where the sum goes over all occupied Kohn-Sham orbitals. The exact non-interacting Kohn-Sham potential reproduces the exact interacting many-body density as defined in Def. 2.1.1 and the density of the non-interacting system yields

$$n_{00}^{\mathrm{ks}}(\vec{r}) = n_{00}(\vec{r}). \tag{136}$$

In practice, the density is found by solving these equations self-consistently [169].

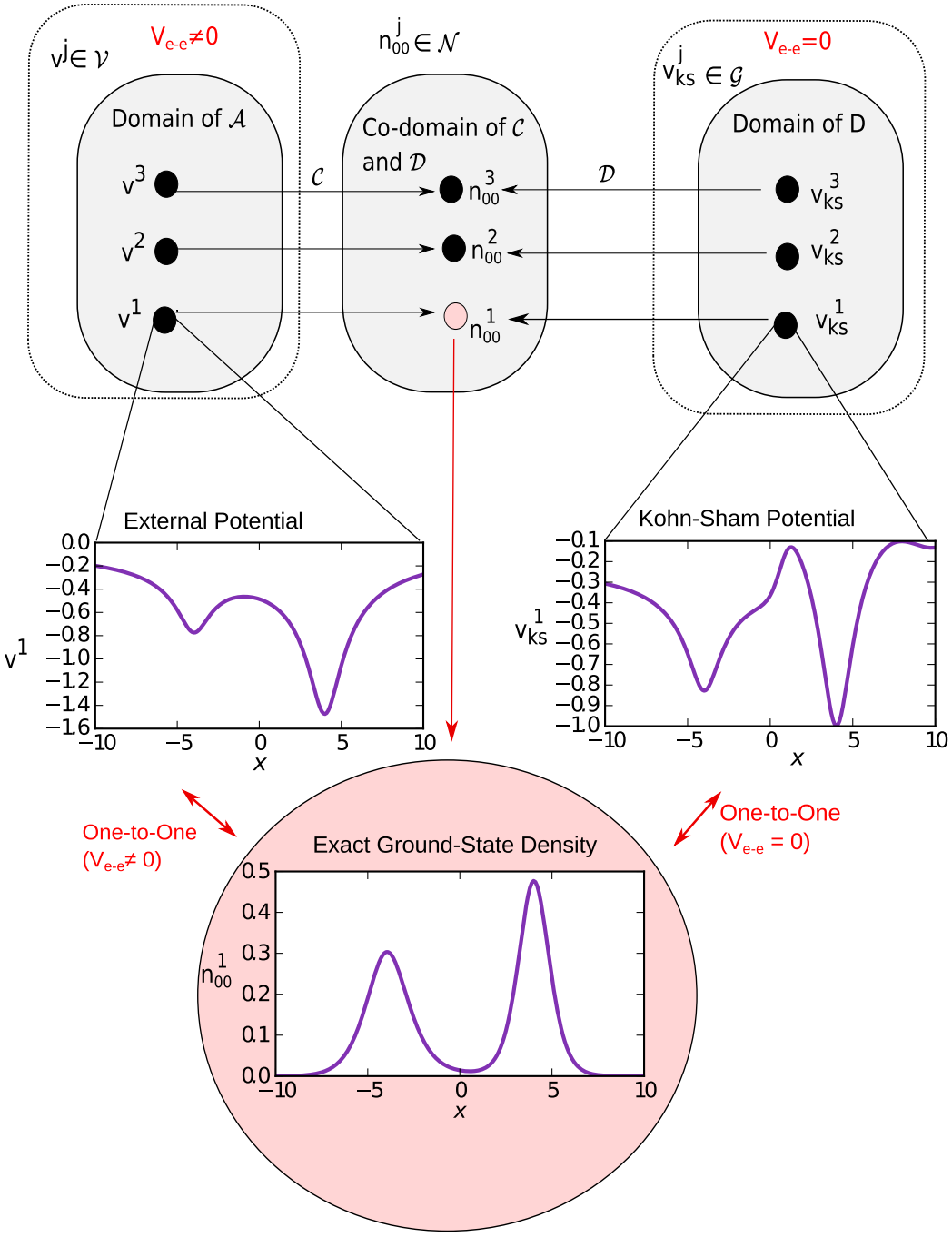

Figure 6: Schematic illustration of the bijective map $\mathcal{C}$ and $\mathcal{D}$ between elements marked as black-filled circles from their domain, i.e. the set $\mathcal{V}$ and $\mathcal{G}$, onto their co-domain, i.e. restricted to the set of interacting and non-interacting v-representable densities $\mathcal{N}$ assuring surjectivity of the maps $\mathcal{C}$ and $\mathcal{D}$. The prove of Hohenberg-Kohn holds for fixed electron-electron interaction $V_{\text{e-e}}$ and therefore, guarantees injectivity of both maps, i.e. the map from the set of potentials corresponding to interacting particles ($V_{\text{e-e}} \neq 0$) to the set of densities and from the set of Kohn-Sham potentials of the auxiliary non-interacting particles ($V_{\text{e-e}} = 0$) to the set of densities.

THE PHOTONIC KOHN-SHAM EQUATIONS In the Kohn-Sham approach of coupled matter-field Hamiltonians, the Kohn-Sham equation for the photons and for the matter partially decouple. In addition, to the electronic Kohn-Sham equations in Eq. 133- 135, we also have to consider the Kohn-Sham equations for the photons, i.e. given by

$$i\hbar\frac{\partial}{\partial t}\left|\chi_{k\lambda}(t)\right\rangle = \frac{1}{2}\left[\hat{p}_\alpha^2 + \omega_{k\lambda}^2\hat{q}_{k\lambda}^2\right]\left|\chi_{k\lambda}(t)\right\rangle + \frac{j_s^{(k\lambda)}(t)}{\omega_{k\lambda}}\hat{q}_{k\lambda}\left|\chi_{k\lambda}(t)\right\rangle, \tag{137}$$

where each of the orbitals $\chi_{k\lambda}(t)$ corresponds to one photon mode with the initial state $\chi_{k\lambda}(t_0)$. The effective KS potential $j_s^{(\alpha)}(t)$ of the photon is known explicitly and can be written as

$$j_s^{(k\lambda)}(t) = -\omega_{k\lambda}^2\vec{\lambda}_{k\lambda}\cdot\vec{d}(t) + j_{\text{ext}}^{(k\lambda)}(t) \tag{138}$$

where the total dipole moment of the electrons $\vec{d}(t) = \sum_i e\vec{r}_i(t)$ is the expectation value of the dipole operator introduced in Eq. 12. Both, the electronic and photonic Kohn-Sham equations are coupled via internal variables, i.e. the electronic density as defined in Eq. 135 and the photon analogue as defined in Eq. 122. Further, we have to add the contributions stemming from the correlated electron-photon interaction to the Kohn-Sham potential of Eq. 125, in which the electrons move. The Kohn-Sham potential of the coupled electron-photon system reads

$$v_{ks}^{e-ph} = v_{\text{KS}}([n],\vec{r}) + \sum_{k\lambda} v_{Mxc}^{k\lambda}([n,q_{k\lambda}],\vec{r}). \tag{139}$$

where $v_{Mxc}^{k\lambda}$ describes the mean-field xc potential as defined in Ref. [163, 170].

3.4.2 *Features of the exact Kohn-Sham system*

The xc potential as in Eq. 132 is the unknown ingredient in KS DFT. Since the advent of DFT, the search for approximations to the xc potential reproducing highly accurate electron densities for arbitrary systems remains a challenging task. There is no systematic route in finding improved approximate functionals, but various strategies in finding them are in use [61], e.g.

(i) fitting the approximate functionals to experimental or ab-initio data,

(ii) finding exact constraints of the exact functional by using basic quantum mechanics or

(iii) using machine learning as a practical tool.

Mathematical constraints of the exact functional Reliable approximate functionals should fulfill mathematical properties of the exact functional [128]. Mathematical properties of the exact functional of the auxiliary non-interacting system reflect the physical properties of the fully-interacting many-body system. One promising way to learn about such properties is to study the exact functional of specific model systems. The most prominent model system is the homogeneous

electron gas that lead to LDA discussed in Sec. 3.5. The LDA fulfills mathematical properties of the exact xc functional such as the normalization condition of the xc hole [171]

$$\int d\vec{r}' n_{xc}(\vec{r}, \vec{r} + \vec{r}') = -1, \tag{140}$$

which relates as follows to the exact xc energy functional

$$E_{xc} = \frac{e^2}{8\pi\epsilon_0} \int \int d\vec{r} d\vec{r}' \frac{n(\vec{r}) n_{xc}(\vec{r}, \vec{r}')}{|\vec{r} - \vec{r}'|}. \tag{141}$$

However, well-known shortcomings of the LDA in describing strongly-correlated systems indicate that certain mathematical properties of the exact xc functional are violated. Another important class of model systems are one-dimensional lattice model systems that have shown to be a reliable tool in studying the limit of strong-correlation in DFT [172]. Such simplified model systems allow to compute the exact maps relevant in DFT and have been used to analyze the exact one-to-one map between ground-state densities and potentials computed for a half-filled one-dimensional Hubbard chain in Ref. [173] using the Bethe ansatz, for the one-site and double-site Hubbard models in full Fock space in Ref. [174, 175] and for the two-electron Hubbard dimer via constraint search in Ref. [176], among others. In particular, Ref. [177, 178] could show that the time-dependent exact xc functional of the one-dimensional Hubbard dimer in the strongly-correlated limit develops the same step feature as the real-space one-dimensional model studied in Ref. [179].

3.4.3 *Exact Kohn-Sham system of two-particle systems in a singlet state*

Many exact properties of the exact xc potential have been found by studying the exact xc potential of simple model systems. In particular, the construction of the exact Kohn-Sham potential for two-particle systems unraveled how the characteristic real-space signatures of the exact auxiliary Kohn-Sham potential enforce the right electron localization in the system.

In their pioneering work Gritsenko and coworkers [180] constructed, decomposed and analyzed the exact auxiliary xc potential of various molecules such as LiH, BH and FH. Such two particle-systems have simply one doubly occupied Kohn-Sham orbital of the form [181]

$$\phi_{ks} = \frac{n_{00}^{\frac{1}{2}}}{\sqrt{2}}, \tag{142}$$

allowing to construct the corresponding Kohn-Sham potential. For two electrons in between two fragments, Ref. [182] provides the analytic form of the Kohn-Sham potential, i.e.

$$v_{ks} = \frac{\hbar^2}{2m} \frac{\vec{\nabla}^2 \sqrt{n(\vec{r})}}{\sqrt{n(\vec{r})}} + \epsilon_1. \tag{143}$$

Further the kinetic energy functional of two non-interacting particles, i.e. T_S, is equal to the Weizsäcker kinetic energy functional [101]

$$T_S^{2p} = \frac{\hbar^2}{8m} \int d\vec{r} \frac{\left|\vec{\nabla} n(\vec{r})\right|^2}{n(\vec{r})}. \tag{144}$$

While stretching the molecular fragments in space, Gritsenko et al. discovered that the exact xc potential develops characteristic real-space signatures, namely steps and peaks. By using optimized effective potential Ref. [183] showed that the exact Kohn-Sham system for atomic systems such as Be and Kr develops step features at inter-atomic shell regions. Further in Ref. [184] the position, the shape and the height of the step in the exact Kohn-Sham potential for few electron-systems is analyzed. Further, the peak has been found to suppress the quantum tunneling of the non-inertacting Kohn-Sham particles [182, 185].

3.5 APPROXIMATIONS TO E_{XC}

Practical DFT calculations rely on approximations to the xc functional in Eq. 129, the quality of which determines the accuracy of the DFT results. Approximate functionals can be found by a range of different strategies such as empirical fitting, exact constraints of model system, mixing of exact and approximate exchange, and local scaling among others. The quality of approximate functionals in use fully determines how much the approximate electron ground-state density deviates from the exact one, and hence fully determines the accuracy of the theoretically obtained observables. Unfortunately, approximate functionals lack reasonable error estimates and systematic procedures to improve them [186]. Further, quantum mechanics is full of surprises, and small changes in a quantum mechanical system may lead to a completely different behavior of the system. Most approximate functionals work well for a specific class of systems, but may completely fail for other physical systems or chemical environments. All in all, this hinders to judge their quality for arbitrary systems and arbitrary chemical environments - and hence, their universal validity.

Practical calculations therefore face the challenging problem of finding a region of trust for the approximate functionals in use. In literature provided data sets of (i) highly-accurate theoretical or (ii) experimentally obtained observables of well-studied systems allow to benchmark approximate functionals.

Local density approximation The local density approximation is the exact xc functional of the homogeneous electron gas (HEG), the density of which is given by [187]

$$n_{00}^{\mathrm{HEG}} = \frac{3}{4\pi \left(r_s r_b\right)^3} \tag{145}$$

with the Bohr radius r_b and with the Wigner-Seitz radius r_s, i.e. the radius of a sphere containing one electron [47]. The exact expression of the kinetic energy

functional of the uniform electron gas is given by the Thomas and Fermi [188] functional, i.e.

$$T^{\text{TF}} = \frac{3}{10}(3\pi^2)^{\frac{2}{3}} \int d\vec{r} n(\vec{r})^{\frac{5}{3}}. \tag{146}$$

The expression for the exact exchange for the homogeneous electron gas is given by [189, 190]

$$E_{\text{x}}^{\text{LDA}}[n] = -\frac{3}{2}\left(\frac{3}{4\pi}\right)^{\frac{1}{3}} \int d\vec{r} n(\vec{r})^{\frac{4}{3}}. \tag{147}$$

The exact expression of the correlation energy is exactly known in the low-density limit [191] and in the high density limit [192]. General correlation densities can be approximately found by quantum Monte Carlo (QMC) simulations [193] or by Møller-Plesset perturbation theory [194]. There exist different parameterization schemes based on the correlation energies obtained by QMC. In three dimensions, a common parameterization is the one of Vosko, Wilk, and Nusair that can be found in Ref. [195]. In this work, we study one-dimensional model systems. For the LDA in one-dimension we use a library of exchange and correlation functionals (libxc) [196] that has implemented the parameterization of Casula, Sorella and Senatore [197] for the correlation functional of one-dimensional systems and the Slater exchange [198]. In the LDA the xc energy as in Eq. 129 is approximately given by the xc energy of the HEG, i.e.

$$E_{xc}^{\text{LDA}}[n] = \int d\vec{r} n(\vec{r}) \epsilon_{xc}^{\text{HEG}}(n(\vec{r})). \tag{148}$$

Not surprisingly, the LDA accurately describes the xc energy of systems with uniform electron densities. However, practical density functional calculations also successfully apply the local density approximation to systems with non-uniform, slowly varying densities.

Jacobs ladder Jacobs ladder [199] is commonly used to illustrate the different levels of accuracy that is provided by approximate functionals. Starting at the lowest level with the LDAs, the next level in the hierarchy is associated with the general gradient approximation (GGA) [200, 201]. Originally, the meta-GGAs were introduced as the third level approximations and were followed at the fourth level by the hybrid-functionals. However, the recent development of the highly-accurate strongly constrained and appropriately normed (SCAN) meta-GGA [202, 203] has shown to keep up with the accuracy of hybrid functionals [204]. The hierarchy of approximate functionals in TDDFT can be similarly illustrated by Jacobs ladder [205]. Future developments of approximate functionals in QEDFT will lead to higher-level approximations that will allow to climb up the levels of accuracy described by Jacobs ladder.

Functional shortcomings and recent developments Functionals in DFT ranging from the LDAs [169], to the gradient expansions such as the GGAs, e.g. Perdew-Burke-Ernzerhof (PBE) [201] and the hybrid functionals such as B3LYP [206], to the orbital-functionals such as optimized effective potentials [207] and to

the range-separated hybrids such as HSE06 [208] have known shortcomings to model gaps of semiconductors [209], molecular dissociation curves [210], barriers of chemical reactions [211], polarizabilities of molecular chains [212, 213], and charge-transfer excitation energies, particularly between open-shell molecules [214]. Optimally-tuned range separated functionals [215], ensemble density functional theory [216, 217] and local scaling corrections [218], logarithmically enhanced factors in gradient approximations [219] and the particle-particle Random-phase approximation (RPA) [220] can diminish or even cure some of these shortcomings, but may also introduce further difficulties such as the RPA dissociation curve of H_2 that is able to capture the static correlation present in the system, but introduces an unphysical repulsion at large finite distances [221].

Shortcomings of approximate functionals show that some important qualitative features of the exact functional are (partially) violated. One common example is the delocalization error of approximate functionals such as LDA and GGAs that tend to artificially spread out the ground-state electron density in space when molecules are stretched in space [222]. In DFT, any observable is a functional of the ground-state density. Consequently, the delocalization error of the density directly transmits into observables as functional of the density. The particle number is a non-local quantity. Thus, integration of a delocalized density due to approximate functionals leads to a qualitative different behavior of the functionals along the cut in the variable N. As a consequence most approximations for the ground-state energy as functional of the particle number N are either concave or convex functions between integer N's [218, 223]. In the case of degenerate ground-state such approximate functionals violate the exact Perdew-Parr-Levy-Balduz condition [68]. The Perdew-Parr-Levy-Balduz condition states that the ground-state energy as a function of the particle number $E(N)$ is a linear function between integer N. The linearity of $E(N)$ leads to the well-known derivative discontinuity [68] and is one of the many exact conditions on the xc functional. Exact conditions on the xc-functional are a very useful tool in the development of new, improved functionals. In Chap. 5, we discuss an exact condition on the xc-functional that is relevant for systems consisting of well separated but mutually-interacting fragments, such as in stretched molecules. Among the approaches to model the limit of strongly correlated, low density systems with DFT we highlight the long range corrected hybrids [224], the generalization of the strictly correlated electron functional to fractional electron numbers [225–228] and the recently introduced local scaling correction, which imposes the linearity condition to local regions of the system, correcting both energies and densities and affirming the relevance of modelling fractional electron distributions to reduce the delocalization error [218].

One relatively new approach in the development of accurate functionals is the machine learning approach [229–232]. The functional of Ref. [230] that requires around 10^5 empirical numbers yields highly accurate densities in the closer region of the training sets. Machine learning is a promising route in evaluating and benefiting from the large amount of data reproduced by density functional calculations every single day.

Part II

METHODICAL PROCEDURE - CONSTRUCTING EXACT MAPS IN DENSITY-BASED METHODS

We introduce the model Hamiltonians and methodical procedure used within this thesis. Applying different simplifications to the many-body Hamiltonian introduced in the previous part of this thesis leads to the Hubbard and Soft-Coulomb Hamiltonian for purely electronic systems and the Rabi model for coupled light-matter interactions. We explain the procedure how the effective density-to-potential maps of such model systems can be constructed.

4 DENSITY-FUNCTIONAL THEORY ON A LATTICE

Static ground-state DFT has been originally introduced for systems in continuous real-space. However, in computational science, the continuous space variable is replaced by the discretized space variable, e.g. by an equidistant lattice, where different sites in the lattice are separated by the spacing Δr. Consequently, the wave function describing an independent particle j on the lattice becomes a n_s^3-dimensional vector. While the dimension of the N-particle wave function further increases with the number of particles in the system, the dimension of the ground-state density solely depends on the number of sites in the lattice making lattice DFT to an appealing tool. Schönhammer and Gunnarson made use of the concept of density functional theory on a lattice to investigate the band-gap problem of DFT [233, 234]. Nowadays, lattice DFT is a well-established method that provides a numerically feasible environment to investigate the exact properties and to test the quality of approximate exchange-correlation functionals. It has been generalized to a variety of different density-based methods, see e.g. the mathematical rigorous formulation of time-dependent current-density functional theory (TDCDFT) on a lattice provided by Ref. [235]. On a real-space grid with its site-localized basis functions, the continuous real-space ground-state density and potential are replaced by on-site densities and on-site potentials and integrals become a sum over the individual sites [233]. In this work, we consider one-dimensional lattice models, that require the following replacements

$$V(x) \to v(x_1, ..., x_k, ..., x_{n_s}) \tag{149}$$

$$n_{00}(x) \to (n_{00}(x_1), ..., n_{00}(x_{n_s})) \tag{150}$$

$$\int dx \to \sum_j \frac{1}{\Delta x}\,, \tag{151}$$

where x denotes the position vector in one dimension and Δx is the lattice spacing. As a consequence, the domain of density functionals $O[n_{00}(x)]$ is replaced by the set of the n_s on-site densities. Consequently, functionals of the on-site densities are given by

$$O[n_{00}(x)] \to O[n_{00}(x_1), ..., n_{00}(x_{n_s})]. \tag{152}$$

THE HIGH-DIMENSIONAL UNIQUE DENSITY-TO-POTENTIAL MAP In particular, the external potential is a unique functional of the density and can be expressed in terms of the density as defined in Theo. 3.2.1. For fixed electron-electron interaction, each of the potential v^j in the set of external potentials $\mathcal{V}$ has an exact one-to-one correspondent density vectors n_{00}^j in the set of ground-state densities $\mathcal{N}$ as depicted in Fig. 5. Each element j is now given by a vector that contains all on-site densities and one that contains all on-site potentials. Using this replacement the one-to-one map in one dimension explicitly writes

$$n_{00}^j = (n_{00}^j(x_1), ..., n_{00}^j(x_{n_s})) \leftrightarrow v^j = (v^j(x_1), ..., v^j(x_{n_s})). \tag{153}$$

Reliable approximate exchange-correlation functionals have to reproduce the features of the exact density-to-potential maps for different j. In particular the density-to-potential map has to capture the correlation within the system. In the present work, we construct and analyze the density-to-potential map of one-dimensional numerical feasible lattice Hamiltonians ranging from weak to strong correlation. We study how the features of correlation are captured in the density-to-potential map of lattice models.

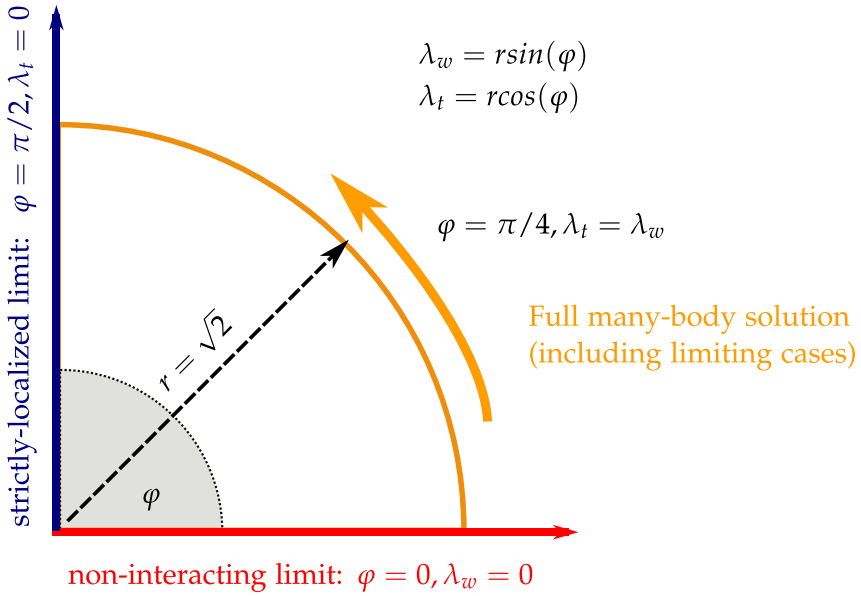

Figure 7: Illustration of the kinetic hopping probability λ_t and the strength of electron-electron interaction λ_w in polar representation for the lattice Hamiltonian used in this work as defined in Eqn. 155. This figure is adapted from Ref. [116].

FROM WEAK-TO-STRONG CORRELATION To study the density-to-potential map from weak-to-strong correlation, we introduce the parameter φ to the Hamiltonian of Eq. 62 that allows us to simultaneously tune the strength of the kinetic energy $\lambda_T T_e$ and the electron-electron repulsion $\lambda_W V_{\text{e-e}}$ via a single free parameter. In terms of polar coordinates, the strength of the kinetic hopping and the electron-electron repulsion can be written as

$$\lambda_t = r\cos(\varphi) \text{ and } \lambda_w = r\sin(\varphi). \tag{154}$$

Fig. 7 illustrates how we can gradually change the electron-electron correlation within the system by varying φ while the radius r is kept fixed. Here, without loss of generality, we use $r = \sqrt{2}$ and $\varphi \in [0, \frac{\pi}{2}]$. Additionally, we introduce the parameter μ, which serves as a Lagrange multiplier that shifts the ground-state of the system to blocks with different particle number N in Fock space. The Hamiltonian now writes

$$\hat{H}^{\varphi} = \hat{H}(\varphi) = \lambda_t(\varphi)\hat{T} + \lambda_w(\varphi)\hat{V}_{\text{e-e}} + \hat{V} + \mu\hat{N}. \tag{155}$$

A common concept is to introduce a hopping parameter t_0 to the kinetic operator. The hopping that describes the tunneling of the electrons along the sites in the lattice depends on the lattice spacing Δr. However, in this work we leave Δr fixed and modulate the strength of the electron-electron interaction and the kinetic hopping probability via the parameter λ_t and λ_w instead.

Non-interacting electron limit For $\varphi = 0$ implying that $\lambda_w = 0$, the Hamiltonian in Eq. 155 represents a system of non-interacting electrons. In this limit, the ground-state of the system can be written exactly in terms of a single Slater determinant. According to Sec. 2.4, where we have introduced the Slater-rank of the system as a measure of static correlation within the system, this limit corresponds to non-correlated electrons.

Site-localized electron limit In the limit $\varphi = \frac{\pi}{2}$, the kinetic hopping λ_t of the electrons in Eq. 155 vanishes. In this limit, where the tunneling probability of the electrons is set to zero, the electrons are "frozen" and strictly localized on the sites. Due to the zero-point oscillation energy, the kinetic energy of electrons can not be switched off in quantum mechanics. Setting the kinetic energy to zero implying a simultaneously sharp measurement of momentum and position of the electrons violates Heisenbergs uncertainty relation. Therefore this limit represents a classical description that is not suitable for electronic systems. However, mathematically, this limit is still justified and all quantities can be regarded as having a conditional dependency on the electronic position. We therefore use this limit to illustrate how the correlation in the system grows while the kinetic energy approaches zero and $\varphi \to \frac{\pi}{2}$. For $\varphi = \frac{\pi}{2}$, the Hilbert space of the electrons is solely connected via the electron-electron operator and the external potential operator. For a symmetric system the ground-state of fully site-localized electrons becomes degenerate allowing us to illustrate the concept of the derivative discontinuity for a specific model system. In the case of an exact degeneracy of the ground-state, the ground-state density of the system can be constructed as convex combination of the degenerate states. In this limit the straight-line behavior of ground-state density functionals as defined in Eq. 112 is an exact condition. The ground state of such strongly correlated systems is not well approximated by a single Slater determinant.

4.1 SOFT-COULOMB AND HUBBARD MODEL HAMILTONIAN

In Eq. 53-54, we demonstrated that the field operators can be expanded in a complete set of basis functions. However, in practical applications, the field operators of the Schrödinger field

$$\hat{\Psi}_\sigma(\vec{r}) \approx \sum_{i=1}^{X} \hat{c}_{i\sigma}\phi_i(\vec{r}) \tag{156}$$

are usually expanded in an finite set of X basis functions $\phi_i(\vec{r})$, i.e. an incomplete set of basis functions. The operators $\hat{c}^\dagger_{i\sigma}$ and $\hat{c}_{i\sigma}$ again correspond to the creation and annihilation of electrons with spin projection σ in the basis function ϕ_i. The

basis functions do not need to be necessarily orthogonal. For non-orthogonal basis function, the overlap matrix of the basis functions is defined as

$$S_{ij} = \int d^3r \phi_i^*(\vec{r})\phi_j(\vec{r}) \tag{157}$$

and the operators creating particles in state $\phi_i(\vec{r})$ are given by

$$\hat{a}_{i\sigma}^\dagger = \sum_j S_{ji}\hat{c}_{j\sigma}^\dagger. \tag{158}$$

Using the basis function expansion of the field operators as in Eq. 156, the Hamiltonian becomes

$$\hat{H} = \underbrace{\sum_{ij\sigma} t_{ij}\hat{c}_{i\sigma}^\dagger\hat{c}_{j\sigma}}_{\hat{T}} + \underbrace{\sum_{ij\sigma} v_{ij}\hat{c}_{i\sigma}^\dagger\hat{c}_{j\sigma}}_{\hat{V}} + \underbrace{\frac{1}{2}\sum_{ijkl\sigma\sigma'} w_{ijkl}\hat{c}_{i\sigma}^\dagger\hat{c}_{k\sigma'}^\dagger\hat{c}_{l\sigma'}\hat{c}_{j\sigma}}_{\hat{W}} \tag{159}$$

with the kinetic hopping probability

$$t_{ij} = \int d\vec{r}\phi_i^*(\vec{r})\left(-\frac{\hbar^2}{2m}\vec{\nabla}^2\right)\phi_j(\vec{r}), \tag{160}$$

the external potential

$$v_{ij} = \int d\vec{r}\phi_i^*(\vec{r})V(\vec{r})\phi_j(\vec{r}), \tag{161}$$

and the electron-electron repulsion

$$w_{ijkl} = \frac{e^2}{4\pi\epsilon_0}\int d\vec{r}\int d\vec{r}'\phi_i^*(\vec{r})\phi_j(\vec{r})\frac{1}{|\vec{r}-\vec{r}'|}\phi_k^*(\vec{r}')\phi_l(\vec{r}'). \tag{162}$$

The accuracy and the computational costs depend on the amount and the functional form of these basis functions. For detailed informations see Ref. [236].

To reduce the dimension of the many-electron problem, we additionally restrict ourselves to one spatial dimension. Therefore, we replace the position vector of an individual particle by x with $(x_1, ..., x_j, ..., x_{n_s})$ where j runs over all sites in the one-dimensional lattice. Further, we replace the derivative $\vec{\nabla}$ by ∂_x. As basis set for the field operators in Eq. 156, we choose Heaviside functions which are spatially localized over each site j to its neighboring site in the real-space grid, i.e.

$$\phi_j = \Theta(\Delta_x/2 - |x_j - x|). \tag{163}$$

The kinetic hopping term defined in Eq. 160 plus the external potential of Eq. 161 becomes

$$t_{ij} = \int dx\Theta(\Delta_x/2 - |x_i - x|)\left(\frac{-\hbar^2}{2m}\partial_x^2 + V(x)\right)\Theta(\Delta_x/2 - |x_j - x|). \tag{164}$$

Approximating the gradient in the hopping term by second-order finite difference, the hopping within the kinetic energy operator becomes a nearest neighbor

hopping term given by $t_0 = \frac{1}{m\Delta x^2}$. In second-order finite difference, the kinetic energy operator reads

$$\hat{T} = -\frac{t_0}{2}\sum_{l=1}^{M}\sum_{\sigma}\hat{c}^{\dagger}_{l,\sigma}\hat{c}_{l+1,\sigma} + \hat{c}^{\dagger}_{l+1,\sigma}\hat{c}_{l,\sigma} - 2\hat{c}^{\dagger}_{l,\sigma}\hat{c}_{l,\sigma}, \tag{165}$$

where $\hat{c}^{\dagger}_{l,\sigma}$ and $\hat{c}_{l,\sigma}$ denote creation and annihilation operators of an electron placed on site l with spin projection onto the z-axis σ. Besides the nearest neighbor hopping term, Eq. 165 also considers the on-site hopping term. Since the on-site hopping simply corresponds to a constant shift of the energy, model systems usually exclude this term. However, in this work we keep the term to allow for a consistent first and second quantized treatment of the Hamiltonian.

In one dimension the Coulomb potential as given in Eq. 162 encounters a singularity at $|\vec{r} - \vec{r}'| \to 0$. This singularity can be circumvented using the non-local soft-Coulomb electron-electron interaction [237, 238],

$$\hat{W}_{\mathrm{SC}} = \frac{e^2}{4\pi\epsilon_0}\sum_{l,m,\sigma,\sigma'}\frac{\hat{c}^{\dagger}_{l,\sigma}\hat{c}^{\dagger}_{m,\sigma'}\hat{c}_{m,\sigma'}\hat{c}_{l,\sigma}}{2\sqrt{(\Delta x(l-m))^2 + a}}. \tag{166}$$

Contrary to the on-site Hubbard interaction, the soft-Coulomb interaction also acts on particles located at different sites l and m with spins σ and σ'. In this work the softening parameter is set to $a = 1$.

The external potential is given by

$$\hat{V} = \sum_{l=1}^{n_s} v_l \hat{c}^{\dagger}_{l}\hat{c}_{l}, \tag{167}$$

that introduces a potential difference between the different sites in the lattice.

Similar to Ref. [239, 240], we study the purely electron-electron correlation for the following two set ups (i) and (ii) that differ by the choice of the external potential.

(I) TWO-SITE LATTICE MODEL As first setup (i) we consider the two-site lattice model in full Fock-space, where we use the parameter v_1 and v_2 in Eq. 167. Few-site lattice models allow us to perform exact diagonalization in the full Fock space of the model. Using a permutation operator, the Fock space can be sorted by different properties of the state e.g. by the particle number N and the spin S_z and S^2. In particular, we study two sites in the lattice, where the corresponding Fock space is spanned by the zero-, one-, two-, three- and four-particle basis functions as can be seen in Tab. 1. As a particular example, we study the two-particle singlet subspace of the two-site lattice model, i.e. we restrict ourselves to states that are labeled by the quantum numbers $N = 2$, $S^2 = 0$ and $S_z = 0$. Both, the vector of the collected on-site potentials in Eq. 149 and the vector of the collected on-site densities in Eq. 150 reduce to vectors with two components given by $v(\vec{x}) = (v(x_1), v(x_2))$ and $n_{00}(\vec{x}) = (n(x_1), n(x_2))$ respectively. Each of these components correspond to one site in the lattice, i.e. $x_{1/2}$ corresponds to

	$\|0\rangle$	$\|\uparrow\rangle$	$\|\downarrow\rangle$	$\|\uparrow\downarrow\rangle$
$\|0\rangle$	$\otimes$	$\otimes$	$\otimes$	$\otimes$
$\|\uparrow\rangle$	$\otimes$	$\otimes$	$\otimes$	$\otimes$
$\|\downarrow\rangle$	$\otimes$	$\otimes$	$\otimes$	$\otimes$
$\|\uparrow\downarrow\rangle$	$\otimes$	$\otimes$	$\otimes$	$\otimes$

$$
\begin{aligned}
|0\rangle \otimes |\uparrow\downarrow\rangle &= |0,\uparrow\downarrow\rangle = \hat{c}_{2\uparrow}\hat{c}_{2\downarrow}|0\rangle \\
|\uparrow\downarrow\rangle \otimes |0\rangle &= |\uparrow\downarrow,0\rangle = \hat{c}_{1\uparrow}\hat{c}_{1\downarrow}|0\rangle \\
|\uparrow\rangle \otimes |\downarrow\rangle &= |\uparrow,\downarrow\rangle = \hat{c}_{1\uparrow}|0\rangle + \hat{c}_{2\downarrow}|0\rangle \\
|\downarrow\rangle \otimes |\uparrow\rangle &= |\downarrow,\uparrow\rangle = \hat{c}_{2\uparrow}|0\rangle + \hat{c}_{1\downarrow}|0\rangle
\end{aligned}
\tag{168}
$$

Table 1: Left-hand side: full Fock-space of the two-site lattice model spanned by the basis states of both sites. The rows correspond to the basis state of one site and the columns to the basis states of the other site in the lattice. The vacuum-state is spanned by the tensor product shown in the upper left corner and the four-particle state by the tensor product shown in the lower right corner. The two-particle basis states are highlighted in red color. Right-hand side: Introducing the formal notation for the two-particle singlet basis states. Particle on different sites in the ket are separated by a comma.

the value at site $1/2$, respectively. Further the restriction to fixed particle number, here $N = 2$, on a two-site lattice naturally fixes one of the free parameters of the density. From Eq. 173 directly follows

$$N = n_{00}(x_1) + n_{00}(x_2) = 2. \tag{169}$$

Therefore, the density solely depends on one single free parameter given by the density difference between both sites

$$\delta n_{00} = n_{00}(x_1) - n_{00}(x_2). \tag{170}$$

The density difference between the sites can be introduced by applying an external potential difference between both sites given by $\delta v = v(x_1) - v(x_2)$. Using the parameter δv, we can shift the electron density from one site to another. The replacement of the on-site densities $n_{00}(x_1)$ and $n_{00}(x_2)$ by the particle number N and the occupation difference δn_{00} can be also understood as a rotation of the complete coordinate system [176].

(II) STRETCHING 1D-MOLECULAR FRAGMENTS As second setup (ii) we consider a many-site lattice model. Here, we restrict ourselves to the two electron spin-singlet states. As external potential we use

$$v_l = \frac{Z_1(\alpha)}{\sqrt{(x_l - \frac{d}{2})^2 + 1}} + \frac{Z_2(\alpha)}{\sqrt{(x_l + \frac{d}{2})^2 + 1}} + \frac{Z_1(\alpha)Z_2(\alpha)}{\sqrt{(d^2+1)}}, \tag{171}$$

$$Z_1(\alpha) = -\alpha, \quad Z_2(\alpha) = -(2-\alpha), \tag{172}$$

with two atomic wells that are spatially separated by the distance d. Increasing the value of d allows to imitate the bond-stretching of molecular wells in space. The depth of the individual wells Z_1 and Z_2 can be gradually changed by the parameter $\alpha \in [0, 2]$. In the limits $\alpha = 0$ and $\alpha = 2$ one of the wells vanishes and the potential corresponds to one atomic well with depth -2. For values in between, the potential resembles a molecule with two atomic wells with a potential difference δv between both wells. Here, we characterize the potential difference

between the molecular fragments by the value $\delta v = Z_1 - Z_2$, i.e. the difference between the minimal value of each potential well. The potential difference shifts electrons from one of the molecular wells towards the other.

Effective density-to-potential map For more than two sites in the lattice the density-to-potential map grows into a high-dimensional, untraceable object. A particular cut along the n_s-dimensional real-space density is the sum of all on-site densities

$$N = \sum_{j=1}^{n_s} n_{00}(x_j), \tag{173}$$

which corresponds to the particle number N of the lattice system that we have introduced in Eq. 14 for continuous systems. For observables depending on processes where the particle number within the system changes, it is of great use to study the functional behavior of the high-dimensional lattice functionals along the cut in N, i.e. $O[N]$.

To analyze how the correlation between subsystems is captured in the density-to-potential map, we partition the system into its subsystems which is a common concept in density-based fragment techniques [150] introduced in Sec. 3.3.1. In particular, we introduce the concept of the effective density-to-potential map. The effective density difference between subsystems within the system δn can be also understood as specific cut along the density.

4.2 TWO-SITE RABI-HUBBARD MODEL

To study how the relation between the electron-photon coupling to the electron-electron interaction reflects in the exact maps, we also study the case of two electrons coupled to a single photon mode.

As a system of interest, we here study a simple, but nontrivial model system, i.e. a two site model coupled to a single photon mode described by the Rabi-Hubbard Hamiltonian [160, 241]. The Rabi model has been heavily investigated in literature [242], e.g. recently in the context of photon blockade [243], geometric phases [244] or ultra-strong light-matter coupling [245]. In this work, we generalize the Rabi model that originally contains a single electron to a two site model that can contain also two interacting electrons. The electron-electron interaction is then described by the Hubbard interaction and the full Hamiltonian [1] reads as follows

$$\begin{aligned}\hat{H}_0 = &-\frac{t_0}{2}\sum_{\sigma=\uparrow,\downarrow}\left(\hat{c}^\dagger_{1,\sigma}\hat{c}_{2,\sigma} + \hat{c}^\dagger_{2,\sigma}\hat{c}_{1,\sigma}\right) + U_0\sum_{i=1,2}\hat{n}_{i,\uparrow}\hat{n}_{i,\downarrow} \\ &+ \omega\hat{a}^\dagger\hat{a} + \omega\lambda\hat{q}\hat{d} + \frac{j_{\text{ext}}}{\omega}\hat{q} + v_{\text{ext}}\hat{d}\end{aligned} \tag{174}$$

where the photon displacement coordinate is given by $\hat{q} = \sqrt{\frac{1}{2\omega}}\left(\hat{a} + \hat{a}^\dagger\right)$ and λ introduces a coupling between the electronic and photonic part of the system.

1 To obtain the Hamiltonian given in Ref. [170], replace $q \to -q$ and $j_{\text{ext}} \to -j_{\text{ext}}$.

The electronic part consists out of a two-site Hubbard model with the on-site parameter U_0, the hopping matrix element t_0, and $\hat{c}^\dagger_{i,\sigma}$ and $\hat{c}_{i,\sigma}$ creates or destroys an electron with spin σ on site i. The electron density operator on site i is given by $\hat{n}_i = \sum_\sigma \hat{c}^\dagger_{i,\sigma}\hat{c}_{i,\sigma}$. We furthermore specify the dipole moment of the electronic system by $\hat{d} = \hat{n}_1 - \hat{n}_2$. In this work, we analyze the single electron subspace, where naturally the effect of the electron-electron interaction disappears and the two electron subspace, where the strength of the electron-electron interaction is given by the Hubbard-U parameter U_0.
We emphasize that the Rabi-Hubbard Hamiltonian of Eq. 174 is in this form exactly identical to a two-site Holstein-Hubbard Hamiltonian that is routinely used in the electron-phonon community. The Holstein-Hubbard Hamiltonian has been studied, e.g. in the context of bipolarons [246–248].
We set the photon frequency equal to one, i.e. $\omega = 1$. Using the external variables v_{ext} and j_{ext}, we stepwise screen the external potential of the photons and electrons. For each fixed pair of the external potential(v_{ext}, j_{ext}), we diagonalize the Hamiltonian given in Eq. 174 using exact diagonalization [116, 249]. Each diagonalization gives us the corresponding ground-state wave function of the system denoted by $\Psi_0^{(v_{ext},j_{ext})}$. Using the exact wave function, we have access to the conjugated set of variables, i.e. $(\Delta n, q)$ by evaluating the corresponding expectation values

$$\Delta n = \left\langle \Psi_0^{(v_{ext},j_{ext})} \middle| \hat{n}_1 - \hat{n}_2 \middle| \Psi_0^{(v_{ext},j_{ext})} \right\rangle \tag{175}$$

and

$$q = \left\langle \Psi_0^{(v_{ext},j_{ext})} \middle| \hat{q} \middle| \Psi_0^{(v_{ext},j_{ext})} \right\rangle \tag{176}$$

corresponding to the electronic density and the photonic displacement coordinate. Screening the parameters v_{ext} and j_{ext} allows us to construct the complete map between the conjugated set of variables. Note, for the resonant case, we set the kinetic hopping probability, $t_0 = 1$. Following Ref. [163], we can exploit the one-to-one correspondence that is here given as

$$(v_{\text{ext}}, j_{\text{ext}}) \underset{1:1}{\longleftrightarrow} (\Delta n, q)\,. \tag{177}$$

Directly following up on Ref. [116], where we introduced the concept of the intrasystem steepening for purely electronic systems, here we analyze the map for a coupled electron-photon system. Further, we study how features of the exact map from the set of internal variables to the set of external variables translate to the purely photonic observables. As example we show the photon occupation $\hat{N} = \hat{a}^\dagger\hat{a}$ as functional of both densities. The photon occupation is connected to non vanishing Berry phases in Rabi models [250].
As can be deduced from the equations of motions for the photonic systems (e.q. Eq. 2 in Ref. [170].), we can establish a direct connection between q and Δn and j_{ext} for the ground-state ($\frac{\partial}{\partial t}q = \frac{\partial^2}{\partial t^2}q = 0$)

$$q = -\frac{\lambda}{\omega}d - \frac{1}{\omega^3}j_{\text{ext}}. \tag{178}$$

To clarify the role of the external potential of the photons j_{ext}, we depict the

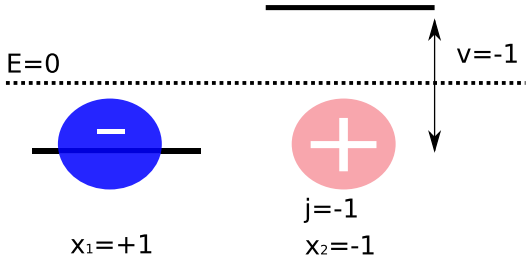

Figure 8: Schematic view on the two-side model: A negative external potential $v = -1$ introduces an energy difference between the two-sites. The electronic ground-state becomes localized on the left side. The external variable for the photon field, j can be interpret as classical charges. If $j = -1$, a positive classical charge is introduced to the system.

Rabi-Hubbard model in Fig. 8 for the case of a single electron in the system. If $j_{ext} = 0$ and a negative external potential $v_{ext} < 0$ acts on the system, the external potential introduces a energy gap between the two sites such that the electron becomes localized on one of the sites. The external potential for the photons j_{ext}, can now be interpret as classical external charges. This can be seen as follows: If, we introduce a classical positive charge to the system, this attractive term can counterbalance the effect of the external potential v_{ext} and that is exactly the case, if $j_{ext} < 0$.

The classical mean-field approximation to the correlated Hamiltonian of Eq. 174 reads as follows [170]

$$\hat{H}_{fm,0} = -\frac{t_0}{2}\sum_{\sigma=\uparrow,\downarrow}\left(\hat{c}^\dagger_{1,\sigma}\hat{c}_{2,\sigma} + \hat{c}^\dagger_{2,\sigma}\hat{c}_{1,\sigma}\right) + U_0\sum_{i=1,2}\hat{n}_{i,\uparrow}\hat{n}_{i,\downarrow} + \omega\lambda q\hat{d} + v_{\text{ext}}\hat{d} \tag{179}$$

$$\hat{H}_{ph,0} = \omega\hat{a}^\dagger\hat{a} + \omega\lambda\hat{q}d + \frac{j_{\text{ext}}}{\omega}\hat{q}, \tag{180}$$

where $d = \langle d\rangle$ and $q = \langle q\rangle$. To obtain the mean-field ground-state wave function, Eqns. 179-180 have to be solved either self-consistently, or Eq. 178 can be exploited leading to the following electronic equation

$$\hat{H}_{fm,0} = -\frac{t_0}{2}\sum_{\sigma=\uparrow,\downarrow}\left(\hat{c}^\dagger_{1,\sigma}\hat{c}_{2,\sigma} + \hat{c}^\dagger_{2,\sigma}\hat{c}_{1,\sigma}\right) + U_0\sum_{i=1,2}\hat{n}_{i,\uparrow}\hat{n}_{i,\downarrow} - \lambda^2 d\hat{d} + \tilde{v}_{\text{ext}}\hat{d} \tag{181}$$

with $\tilde{v}_{\text{ext}} = v_{\text{ext}} - \frac{\lambda}{\omega^2}j_{\text{ext}}$. In these equations, we apply the classical approximation only to the electron-photon interaction, while the electron-electron interaction is treated fully correlated. The classical (mean-field) approximation to the correlated Hamiltonian is equal to a Schrödinger-Maxwell approximation. We may expect that such a approximation works well for the studied model in the weak-coupling regime and in the limit of infinite coupling [160].

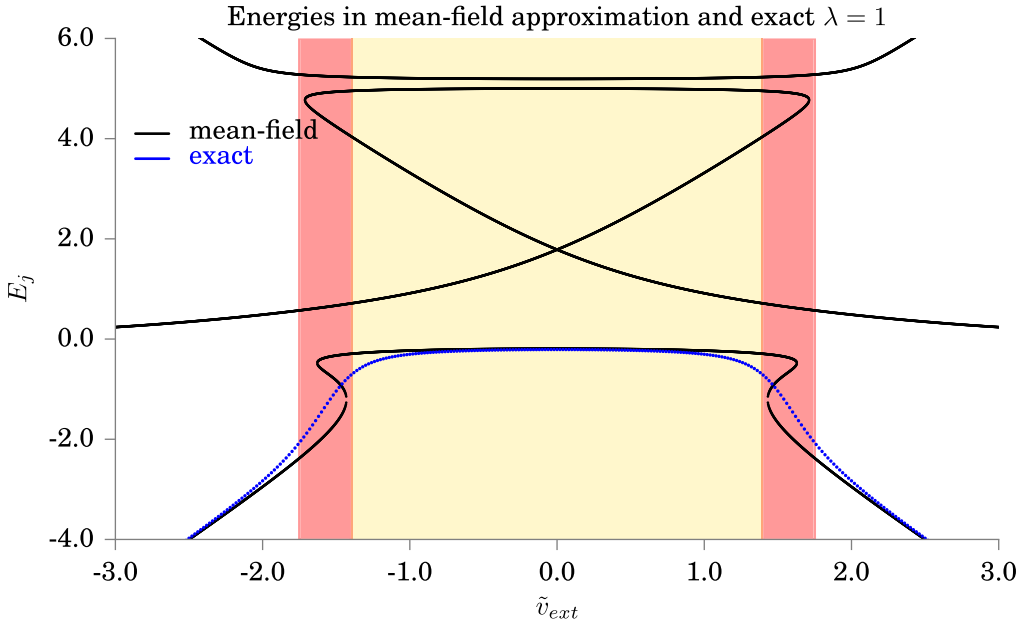

Figure 9: Energies for the two-site two electron Rabi-Hubbard model in mean-field approximation for $U_0 = 5, t_0 = 1, \omega = 1, \lambda = 1$ colored in black and the corresponding expectation value of $\hat{H}_{fm,0}$ evaluated with the exact ground-state wave function of the Hamiltonian in Eq. 174 colored in blue. Areas with more than three solutions in the mean-field approximation are highlighted in color.

MEAN-FIELD APPROXIMATION IN THE SINGLET SUBSPACE For the two-electron on two-sites case, the three singlet states basis functions are given by

$$|\phi_1\rangle = (|\uparrow\downarrow, 0\rangle) \tag{182}$$

$$|\phi_2\rangle = \frac{1}{\sqrt{2}} (|\uparrow, \downarrow\rangle - |\downarrow, \uparrow\rangle) \tag{183}$$

$$|\phi_3\rangle = (|0, \uparrow\downarrow\rangle) \tag{184}$$

The total wave function developed in this basis set that are not the eigenfunctions of the electronic Hamiltonian can be written using the configuration interaction (CI) coefficients

$$|\Psi\rangle = \alpha_1 |\phi_1\rangle + \alpha_2 |\phi_2\rangle + \alpha_3 |\phi_3\rangle . \tag{185}$$

In this basis, we can write the Hamiltonian using the following matrices:

$$\sum_{\sigma=\uparrow,\downarrow} \left(\hat{c}^\dagger_{1,\sigma} \hat{c}_{2,\sigma} + \hat{c}^\dagger_{2,\sigma} \hat{c}_{1,\sigma} \right) = \begin{pmatrix} 0 & 1/\sqrt{2} & 0 \\ 1/\sqrt{2} & 0 & 1/\sqrt{2} \\ 0 & 1/\sqrt{2} & 0 \end{pmatrix} \tag{186}$$

$$\sum_{i=1,2} \hat{n}_{i,\uparrow} \hat{n}_{i,\downarrow} = \begin{pmatrix} 1 & 0 & 0 \\ 0 & 0 & 0 \\ 0 & 0 & 1 \end{pmatrix} \tag{187}$$

$$\hat{d} = \begin{pmatrix} 2 & 0 & 0 \\ 0 & 0 & 0 \\ 0 & 0 & -2 \end{pmatrix}. \tag{188}$$

Using these explicit matrices, we can rewrite the Schrödinger equation into a set of nonlinear equations using the Hamiltonian $\hat{H}_{fm,0}$ of Eq. 181. In this way, we can obtain the mean-field eigenenergies and eigenvalues. Using

$$\hat{H}_{fm,0} |\Psi_i\rangle = E_i |\Psi_i\rangle , \tag{189}$$

and the normalization condition on the CI coefficients, we obtain the following four equations

$$-(\alpha_2 t_0)/2\sqrt{2} + \alpha_1(2\lambda\omega(-j_{ext}/\omega^3 - (2\alpha_1^2 - 2\alpha_3^2)\lambda\omega) + U_0 + 2v_{ext}) = \alpha_1 E_i \tag{190}$$

$$-(\alpha_1 t_0)/2\sqrt{2} - (\alpha_3 t_0)/2\sqrt{2} = \alpha_2 E_i \tag{191}$$

$$-(\alpha_2 t_0)/2\sqrt{2} + \alpha_3(-2\lambda\omega(-j_{ext}/\omega^3 - (2\alpha_1^2 - 2\alpha_3^2)\lambda\omega) + U_0 - 2v_{ext}) = \alpha_3 E_i \tag{192}$$

$$|\alpha_1|^2 + |\alpha_2|^2 + |\alpha_3|^2 = 1 \tag{193}$$

that have to be solved for $(\alpha_1, \alpha_2, \alpha_3, E_j)$. In Fig. 9, we plot all eigenenergies of the two-site two electron Rabi-Hubbard model in mean-field approximation along $\tilde{v}_{ext}$. We find although the electronic Hilbert space has only three basis functions there exist areas, where more than three eigenenergies E_j with corresponding stationary states are found, similar to Ref. [246]. The corresponding expectation value of $\hat{H}_{fm,0}$ evaluated with the exact ground-state wave function of the Hamiltonian in Eq. 174 is colored in blue and deviates significantly in the area highlighted in red, see Fig. 9.

Part III

RESULTS - INSIGHT FROM THE EXACT DENSITY MAPS

We fill the formally exact concepts of density-functional theory with live. For one-dimensional lattice models, we present the exact density-to-potential and the exact density-to-wavefunction map that underly the Hohenberg-Kohn theorem. Having the exact maps at hand, we are able to show expectation values and transition matrix elements of arbitrary operators as functionals of the electron ground-state density for the studied systems. We introduce the concept of the intrasystem steepening and discuss how it relates to the well-known derivative discontinuity.

5 MAPS IN GROUND-STATE DENSITY FUNCTIONAL THEORY

In this chapter, we introduce the delocalization error [222] for one-dimensional stretched molecules by reproducing the exact and LDA dissociation curve of hydrogen as provided by the reference calculations of Ref. [172]. This allows us to introduce this shortcoming of LDA by simultaneously validating our code. The reference data provided by Ref. [172] were obtained by Density-matrix renormalization group (DMRG).

5.1 EXACT REAL-SPACE DENSITY OF A MOLECULAR-LIKE SYSTEM

For fixed electron-electron interaction, the Hohenberg-Kohn theorem of Theo. 3.2.1 states that there is a one-to-one correspondence between the external potential and the ground-state density of the system. Therefore, the exact real-space density has to fully capture the correlation present in the system. For a few selected examples, we explicitly show how the static correlation between fragments of the system is captured in the real-space density of the system while the fragments are stretched in space.

REAL-SPACE DENSITY OF COUPLED SUBSYSTEMS As first example we study the maps of an one-dimensional real-space model system that describes two electrons in a singlet state moving in the one to two-well potential with variable height and distance of the wells as introduced in Eq. 171. To start we set $\alpha = 1$ in Eq. 171 and study the molecular potential of two wells of equal height implying that the potential difference is equal to $\delta v = Z_1 - Z_2 = 0$. We have chosen the real-space coordinate of each particle j as $L_{x_j} = -10.25 : 0.1 : 10.25$, i.e. $n_{x_j} = 206$ grid points in one direction. The upper panel of Fig. 10 shows the exact potential plus the electron-electron repulsion between the two electrons[1] as function of their real-space coordinates x_1 and x_2 while the distance from $d = 1$ to $d = 5$ between the molecular fragments increases from left to right. For each fixed distance d in the external potential, we diagonalize the corresponding Hamiltonian and obtain the basic descriptor of quantum wave mechanics, i.e. the ground-state wave function of the system $\Psi_0(x_1, x_2)$. In our example with $n_{x_1} = n_{x_2}$ grid points, the wave function $\Psi_0(x_1, x_2)$ already has a dimension of $n_{x_1} \times n_{x_2} = 42\,436$. The middle panel of Fig. 10 shows the corresponding conditional probability of finding one electron at a given configuration of the system. With increasing distance between the identical 'molecular wells', the system 'breaks' into two identical fragments that are correlated as long as the distance between both wells is finite. By tracing out one electronic coordinate, we obtain the ground-state density of the system, i.e. the one-dimensional real-space function as shown in the lower panel of Fig. 10. As one can see, the ground-state density only depends on one spatial coordinate reducing the degrees of freedom significantly while maintain-

1 The electron-electron interaction adds a repulsive part to the diagonal of the external potential.

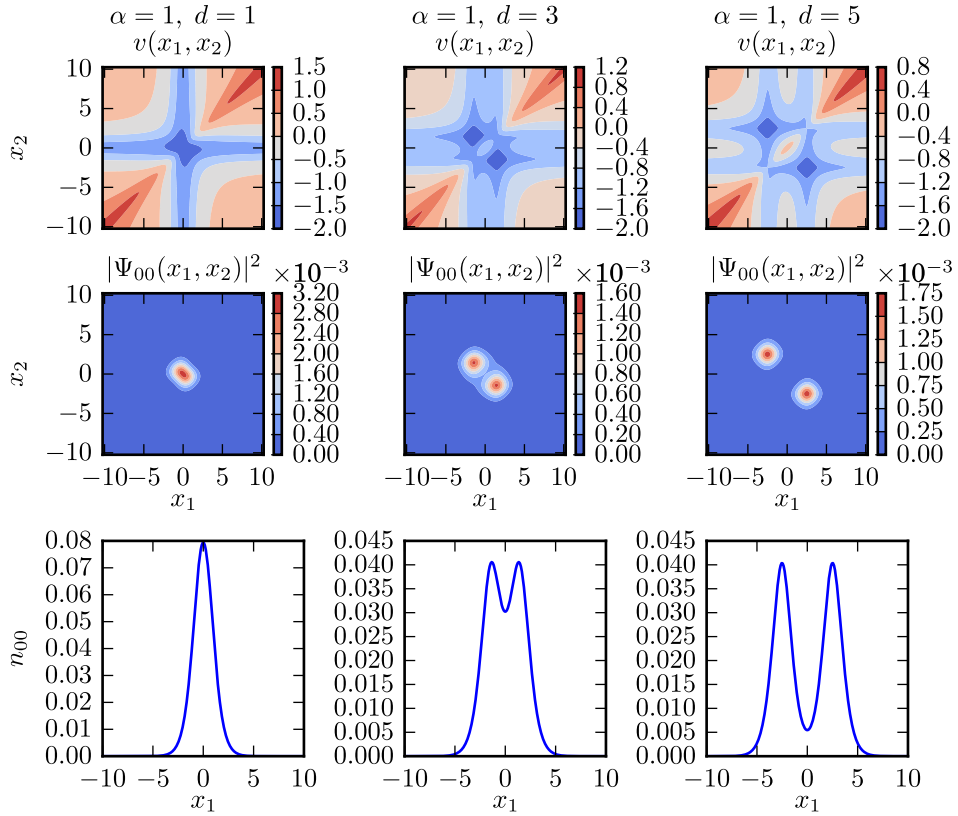

Figure 10: Two interacting electrons moving in the external potential of correlated identical fragments that are stretched in space from $d = 1$ to $d = 5$. The upper panel displays the external potential plus the electron-electron repulsion, the middle panel the corresponding conditional probability and the lower panel the ground-state density in real space.

ing the relevant information about the system. In contrast to Fig. 10, Fig. 11 shows the exact external potential, the exact conditional probability and the exact ground-state density for two non-interacting electrons, i.e. $\hat{W}_{SC} = 0$ in Eq. 166. Thus, missing the repulsive barrier to the diagonal of the external potential. In the absence of the electron-electron interaction between the particles, the density of the non-interacting particles in Fig. 11 smears out in the region between both fragments. The principle idea of Kohn-Sham DFT is to recover the exact ground-state density of the interacting system by introducing the Kohn-Sham potential, i.e. an auxiliary effective potential in which the non-interacting particles move and that fully mimics the electron-electron interaction. For two electrons the exact Kohn-Sham potential can be constructed using Eq. 143.

DISSOCIATION CURVE H_2 LDA lacks the static correlation between the subsystems within a system while the subsystems are stretched in space, e.g. relevant to describe the bond-stretching of closed-shell molecules. One common example to illustrate this shortcoming of LDA is the bond-stretching of the H_2 molecule [221]. Fig. 12 shows the exact versus the LDA ground-state energy as function of the distance d between the fragments, here the hydrogen atoms. We have reproduced

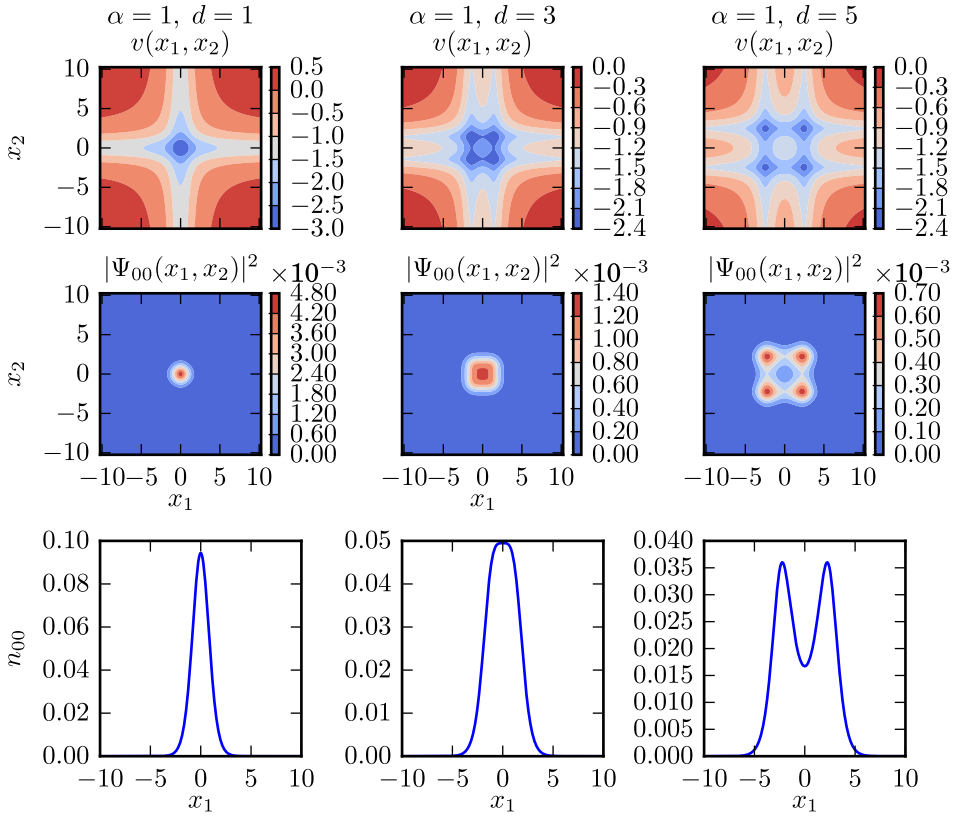

Figure 11: Two non-interacting electrons moving in the external potential of correlated identical fragments that are stretched in space from $d = 1$ to $d = 5$. The upper panel displays the external potential, the middle panel the corresponding conditional probability and the lower panel the ground-state density in real space.

the dissociation curve of hydrogen as provided by the reference calculations of Ref. [172] to validate our code. While the exact Kohn-Sham potential develops steps and peaks at large distances d, these real-space signatures that capture the correlation in the system are missing in the LDA Kohn-Sham potential. Since H_2 is a symmetric molecule with the same charge of each nuclei, for this case the exact real-space potential only develops peaks as can be seen in Fig. 13. In the case of asymmetric molecules the Kohn-Sham potential also shows a step feature [179]. The corresponding real-space ground-state densities for different selected values of d can be found in Fig. 13. From $d = 1$ to $d = 5$ the LDA density deviates from the exact density as the fragments are stretched in space. While the LDA is fairly accurate close to the minimum energy of the dissociation curve, large deviations occur for larger distances. As one can see, the LDA density artificially spreads the electronic density for increasing values of d. This illustrates the delocalization error of LDA that directly leads to the error for the binding energy at large distances as can be seen in Fig. 12.

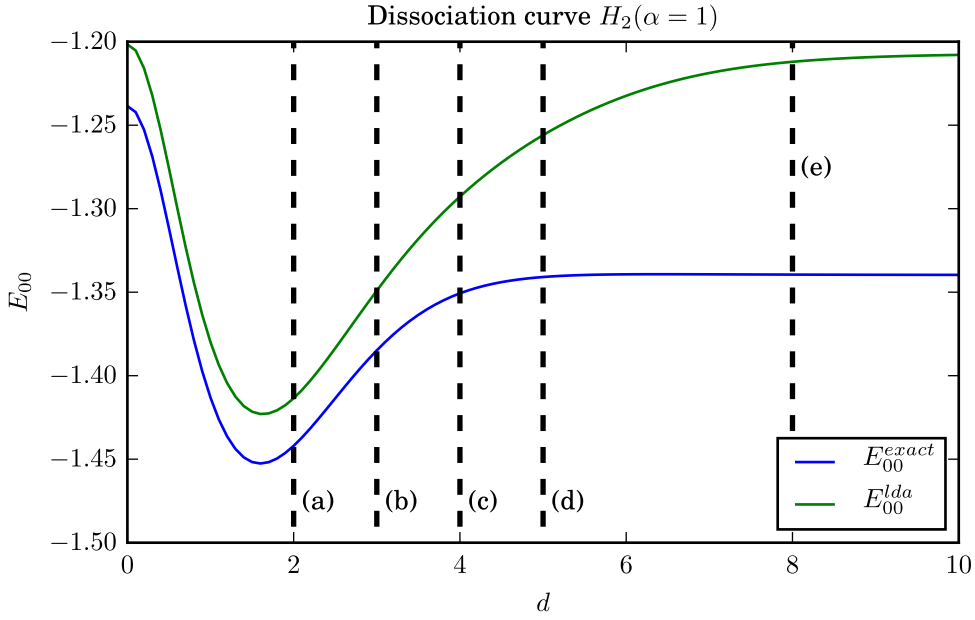

Figure 12: Dissociation curve of H_2 with the exact ground-state energy colored in blue and the LDA energy colored in green. From (a)-(e) the fragments are stretched in space. The corresponding exact and LDA densities and Kohn-Sham potentials can be found in Fig. 13.

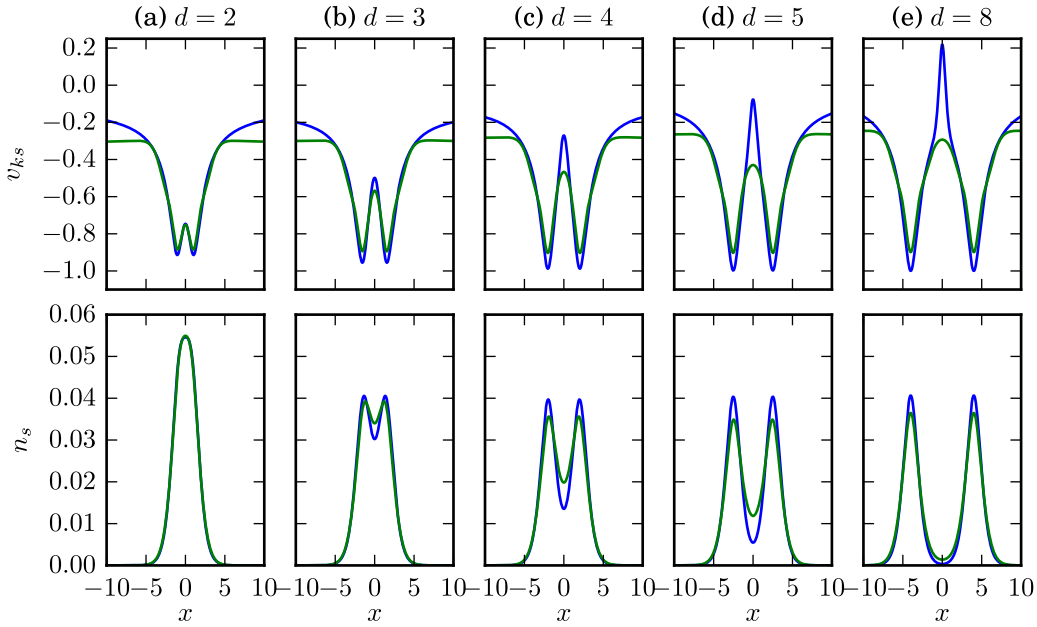

Figure 13: Electron ground-state densities and Kohn-Sham potentials of the one-dimensional H_2 while the fragments are stretched in space for different distances (a)-(e). Top panel: Exact Kohn-Sham potentials colored in blue and LDA potentials colored in green. Bottom panel: Exact densities colored in blue and LDA densities colored in green. The corresponding ground-state energies for the distances (a)-(e) can be found in Fig. 12.

6

INTRASYSTEM STEEPING OF EXACT DENSITY MAPS IN CORRELATED ELECTRON-ELECTRON SYSTEMS

Provided that the formal criteria of density functional theory such as v-and N-representability as introduced in Sec. 3.2.2 are fulfilled, practical DFT applications require the knowledge of explicit expressions of density functionals (i) and accurate approximations to the xc potential of the auxiliary Kohn-Sham system (ii) as discussed below.

(i) From the HK theorems follows that arbitrary observables are expressible in terms of the ground-state density. However, to make use of the ground-state density as basic descriptor it is necessary to find an explicit expression for the density dependence of the desired observable. For example the explicit density dependence of the ground-state energy functional is given by Eq. 130.

Due to the lack of a systematic procedure on how to determine the functional form, in general the density dependence of arbitrary observables remains unknown. Our work illustrates that arbitrary observables are functionals of the density by showing the density dependence of selected observables for our specific model system. We will see that features of the real-space ground-state density directly translate to the density functionals of other observables. However, it is not clear how to generalize the functionals constructed for our system to other systems nor it is known how to derive the functional expression of arbitrary observables.

(ii) Assuming the functional form is explicitly known as is the case for the ground-state energy functional given in Eq. 130, the quality of the approximate density entering the exact analytic expression fully determines the accuracy of the calculated observables. Herein, the quality of the approximate density is fully determined by the approximate xc functional. We illustrate how features of the exact density manifest in the density dependence of arbitrary observables.

6.1 GENERAL CONCEPTS: THE INTRASYSTEM STEEPENING AND THE INTERSYSTEM DERIVATIVE DISCONTINUITY OF THE EFFECTIVE DENSITY-TO-POTENTIAL MAP

Ground-state DFT considers the one-to-one correspondence between the exact ground-state density and the external potential in complete real-space. However, in the following, we like to introduce the concept of the *effective* density-to-potential map that allows us to judge whether the complete real-space density

The following chapter is based on the work T. Dimitrov, H. Appel, J. I. Fuks, and A. Rubio, "Exact maps in density functional theory for lattice models", New Journal of Physics **18**, 8, 083004 (2016) [116].

of approximate functionals correctly amounts for the static correlation between the subsystems within the interacting system. We discuss the intrasystem steepening and the intersystem derivative discontinuity, that are both features of the effective density-to-potential map and carry the relevant information about the correlation present in the system. In particular, we like to carve out how the intrasystem steepening differs to the widely in literature discussed intersystem derivative discontinuity of DFT. Both features, are features of the exact effective density-to-potential map that appear in the cuts of the density functionals, rather than in the density dependence of the functionals in complete real-space. Further, both features describe the electron localization over subsystems within a system and directly amount for the static correlation present in the system. The steps (1)-(6) in the paragraphs (A)-(C) sketch a systematic route on how to apply the concept of the effective density-to-potential map to systems that consist of j subsystems and how this concept allows us to judge the quality of approximate functionals.

(A) CONSTRUCTION OF THE EFFECTIVE DENSITY-TO-POTENTIAL MAP

- First, partition the system into its subsystems (basins), e.g. using a Bader partitioning scheme.
- Second, integrate the density over each subsystem and assign the integrated subsystem densities to the different basin, i.e. for j basins the densities $n_{00,1}, ..., n_{00,j}$, which we get by dividing the density into its subsystem densities as introduced in Eq. 117.
- Third, construct the effective density-to-potential map that now depends on all subsystem densities. The electron localization over different subsystems as well as the static correlation between two subsystems i and j is captured in the density difference $\delta n_{00,ij} = n_{00,i} - n_{00,j}$ as functional of the potential difference $\delta v_{kl} = Z_k - Z_l$, where Z_k and Z_l are the maximal depth of the external potential present in the considered basins k and l.

(B) FEATURES OF THE EFFECTIVE DENSITY-TO-POTENTIAL MAP

- Fourth, construct all possible effective density-to-potential maps.
- Fifth, find the maximum value of each of the the effective density-to-potential maps that define the tensor

$$f_{ijkl} = \max \left| \frac{\partial \delta n_{00,ij}}{\partial \delta v_{kl}} \right| . \tag{194}$$

  The tensor f_{ijkl} allows us to quantify the intrasystem steepening in terms of a mathematical more rigorous definition.

The tensor f_{ijkl} stores the maximum value of the gradient of all possible effective density potential maps in the system. Clearly, this value is not always unique since the number of maxima depend on the number of the particles in the system as well as on the collective behavior of particles and the choice of the partitioning of the system into its subsystems. Approaching a degeneracy of the ground-state

energy leads to increasing, but bounded values of the tensor f_{ijkl}. In the case of a real degeneracy of the ground-state density, the functional value of f_{ijkl} for given $ijkl$ diverges at integer N. The divergence of f_{ijkl} shows that infinitesimally small changes in the effective density-to-potential map have a significant influence on the electron localization over all building blocks within the global system. The divergence provides a clear criterion that the corresponding density-functionals of arbitrary observables along the cut in the density difference between the building blocks obey the straight-line behavior. Contrary, the functional behavior corresponding to finite values of f_{ijkl} have a well defined gradient along this cut related to the intrasystem steepening of the effective density-to-potential map. The concept of the intrasystem steepening has recently been introduced [116] and shown to hold for correlated electron-photon systems [251].

Definition 6.1.1: The intrasystem steepening

The intrasystem steepening refers to the steepness of the gradient of the effective density-to-potential map and is a measure for the static correlation between subsystems in a system. The intrasystem steepening directly tells us how strongly the changes in the external potential affect the electron localization over the subsystems within the system. In particular, a steep gradient indicates that small changes in the external potential lead to drastic changes in the density. In the limit of decoupled systems, the intrasystem steepening transitions into the well-known intersystem derivative discontinuity.

(c) JUDGING THE QUALITY OF APPROXIMATE FUNCTIONALS

- Sixth, repeat the first five steps using the density of approximate functionals. The comparison between the exact and the approximate tensor f_{ijkl} allows to judge whether the considered approximate functional correctly amounts for the static correlation present in the system.

6.2 ILLUSTRATING GENERAL CONCEPTS IN DFT WITH SPECIFIC MODEL SYSTEMS

6.2.1 *Construction of the effective density-to-potential map*

(I) Effective density-to-potential map of one-dimensional molecules For fixed distance d, we systematically tune the external potential given by the nuclear charge of both atoms in the molecule. Here, we vary the parameter α in discrete steps that allows us to simultaneously vary the nuclear charge of both atoms while keeping the total nuclear charge ($Z_1 + Z_2 = 2$) of the system fixed. For each external potential, we diagonalize the corresponding Hamiltonian. Therefore, we can directly access the exact ground-state wave function and density of the system. Each atom of the diatomic molecule can be regarded as fragment of the system. In the case of the hydrogen molecule, where $\alpha = 1$, the fragments are given by the individual hydrogen atoms. In the following, we apply the concept of the *effective density-to-potential map* that allows us to analyze the correlation between both fragments by a descriptor of significantly lower dimension. The

dimension of the new descriptor reduces from the number of sites in the lattice to the number of fragments in the system. Following the scheme (A)-(C) introduced in Sec. 6.1, first, we partition the system into its fragments. In the case of the diatomic molecule, we simply divide the real-space into its left and right-half space. Second, we sum the density over each half-space

$$n_{00,1} = \sum_{i=1}^{M/2} n_{00}(x_i) \text{ , and } n_{00,2} = \sum_{i=M/2+1}^{M} n_{00}(x_i). \tag{195}$$

We refer to each fragment as an *effective site* in real space. Then the density difference between the integrated densities of both fragments becomes a density difference between both effective sites, i.e.

$$\delta n_{00} = n_{00,1} - n_{00,2}. \tag{196}$$

In the case of a symmetric molecule, e.g. $\alpha = 1$ as in Fig. 13, the density difference between the effective sites is always zero. In other words the electron density over each half-space integrates to an integer value, i.e. two fragments with particle number $N = 1$. Third, we construct the effective density-to-potential map of our system. Therefore, we introduce a potential difference between the fragments that shifts density from one fragment to the other fragment within the system. Here, we define the effective potential difference as the difference between the minima of the wells given by $\delta v = Z_1(\alpha) - Z_2(\alpha)$. For each external potential, diagonalization of the Hamiltonian gives us back a real-space density. Fig. 14

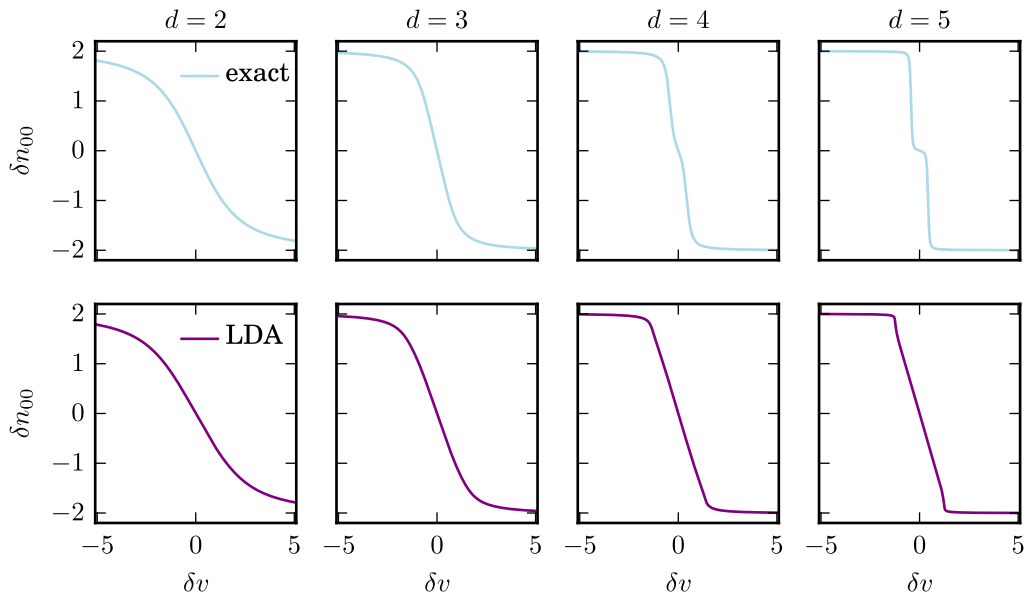

Figure 14: Effective density-to-potenial map of one-dimensional molecules that consist of at most two subsystems separated by the distance d. Top panel: constructed from the exact real-space densities similar to Ref. [239, 240]. Bottom panel: constructed from the LDA densities. The depth of the molecular wells varies from -5 to $+5$. This figure is adapted from Ref. [116].

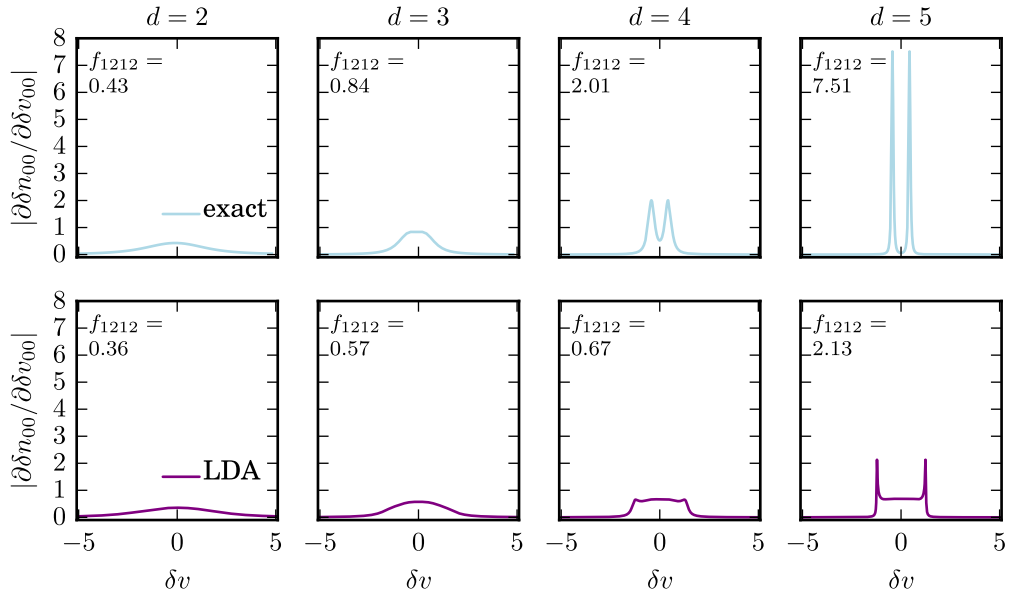

Figure 15: Derivative of the effective density-to-potenial map that we have shown in Fig. 14 with the tensor $f_{ijkl} = f_{1212}$, which is the maximum value of the derivative. Note, from left to right with increasing values of d, where the system "breaks" into two mutually interacting fragments the value of f_{0000} is not unique. Top panel: constructed from the exact real-space densities. Bottom panel: constructed from the LDA densities. The depth of the molecular wells varies from -5 to $+5$.

shows the resulting *effective* density-to-potential map for different distances d between the fragments. Each pair of the effective density and the effective potential is one point in the effective density-to-potential map of Fig. 14 as illustrated in Fig. 16 for the effective map $d = 8$. The corresponding derivative of the effective density-to-potential map with respect to the potential difference between both fragments is plotted in Fig. 15. Here, where we only have two subsystems, the tensor f_{ijkl} stores a single number for small distances and two numbers for larger distances, where the system "breaks" into two mutually, but interacting fragments. In our case $f_{ijkl} = f_{1212}$ depends on the density difference $\delta n_{00,12}$ and the potential difference δv_{12} between both fragments that we have earlier denoted by δn_{00} and δv. The local maxima correspond to the tunneling points [185]. The finite value of f_{1212} tells us that the gradient along the density difference between both fragments is well defined. From left to right in Fig. 15 with increasing distance between the fragments, the value of f_{1212} increases. The top panel in Fig. 15 corresponds to the derivative of the exact effective density-to-potential map. The increase of the value f_{ijkl} quantifies the intrasystem steepening that characterizes the electron localization over the fragments within the system. In contrast the divergence of the value f_{ijkl} would correspond to the well-known derivative discontinuity of the density-to-potential map along the cut in the variable δn_{ij}. The second row of Fig. 15 that displays the derivative of the LDA effective density-to-potential map shows that the intrasystem steepening is not well captured by the

LDA for large distances d, i.e. the LDA underestimates the electron localization over subsystems within the system.

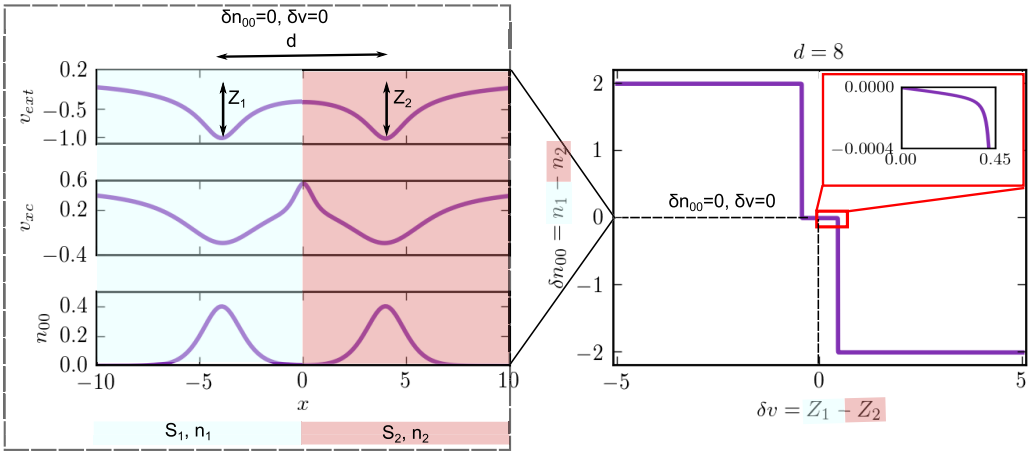

Figure 16: Effective density-to-potenial map constructed from the exact real-space densities and their corresponding external potentials of one-dimensional molecules that consist of at most two subsystems separated by the distance d, similar to Ref. [239, 240]. This figure is adapted from Ref. [116].

(II) Exact density-to-potential map of a two-site lattice model The dimension of the two-site model allows us to construct the exact density maps in complete Fock-space including the zero to four particle states. The exact density-to-potential map in complete real-space is determined by the pair δn_{00} and N. This allows us to study the functional behavior along the cut in the variable δn_{00} and N. For fixed particle number N of the total system, the effective density-to-potential map of the two-site model, i.e. δn_{00}-to-δv, coincides with the exact density-to-potential map in complete real-space. For the two particle singlet ground- and excited-states, Fig. 17 shows the density-difference as function of the potential difference between both sites for different values of φ.

6.2.2 *Analyzing the density-to-potential map*

Fig. 14 shows the effective density-to-potential map of exact solvable models of one-dimensional molecules, where the distance d between the fragments increases from $d = 2$ on the left to $d = 8$ at the right. Fig. 17 shows the ground- and excited-state density-to-potential map for the two-particle singlet states of the two-site lattice model. The qualitative behavior of the effective density-to-potential map in Fig. 14 is well captured by the density-to-potential map of the two-site lattice model shown in the first row of Fig. 17. We have imitated the bond-stretching of the molecules by increasing the angle φ from $\varphi = 0$ on the left to $\varphi = \frac{\pi}{2}$ on the right, where $\varphi \to \frac{\pi}{2}$ relates to the distance of the fragments as $d \to \infty$. As introduced in Eq. 154 and Eq. 155 the angle φ determines the ratio between the kinetic energy to the electron-electron interaction. From left to right, the system transitions from a non-correlated one in the non-interacting electron limit to a strongly-correlated one in the site-localized limit. From left to right, the

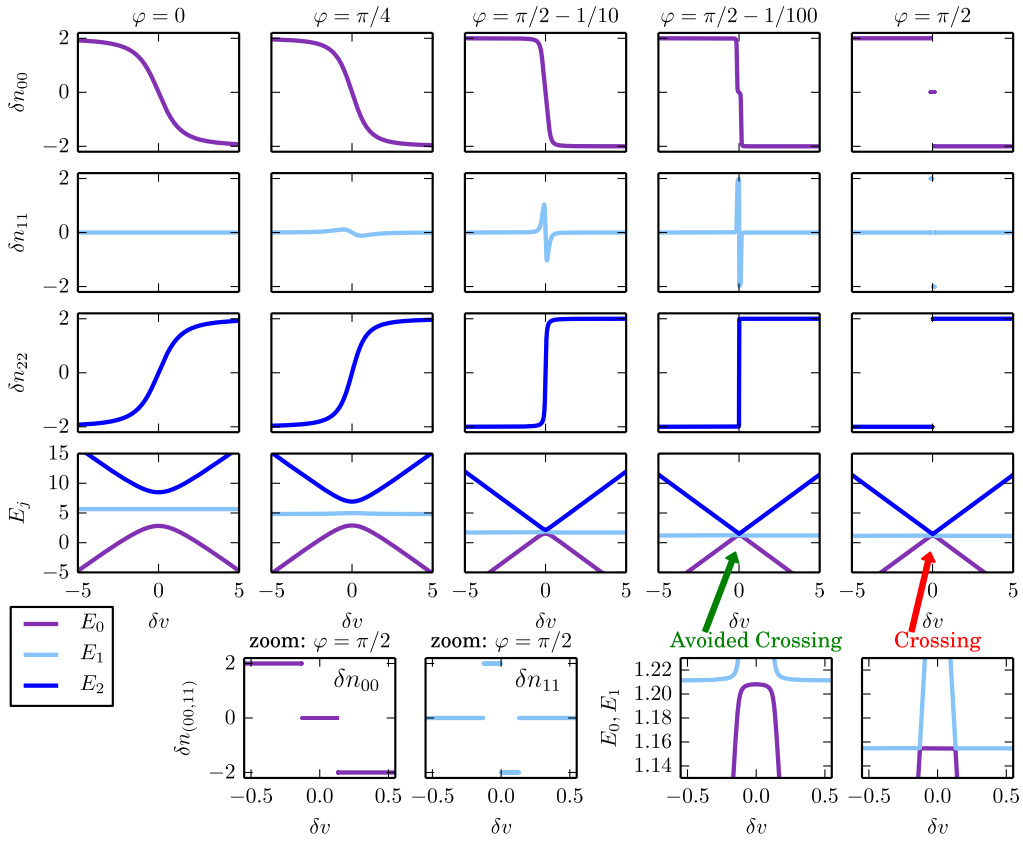

Figure 17: Maps of two electrons in a singlet state on a one-dimensional lattice with two sites. From left to right with increasing φ the electron-electron soft-Coulomb interaction and the static correlation between both sites increases. We plot the following quantities as function of the external potential. First row: Ground-state density in purple, second row: first excited-state density in light blue, third row: second excited-state density in dark blue, fourth row: ground- and excited state energies in corresponding colors of the density, fifth row: Zoomed frames on the scale $\delta v = \pm 0.5$ in the limit of $\varphi = \frac{\pi}{2}$ for the ground- and first excited state density on the left and their corresponding energies on the right that show an avoided crossing for $\varphi = \frac{\pi}{2} - \frac{1}{100}$ and a real crossing for $\varphi = \frac{\pi}{2}$. This figure is adapted from Ref. [116].

gradient of the density-to-potential maps plotted in Fig. 14 and Fig. 17 steepens carrying the signature of the static correlation between the subsystems within the system. This is nicely illustrated in the fourth row of Fig. 17 that displays the eigenenergies of the two-particle singlet states E_0, E_1 and E_2 as function of the external potential.

INTRASYSTEM STEEPENING With increasing value of φ the eigenenergies of the two-particle singlet states approach a degeneracy as indicated by a green arrow in Fig. 17 that points out the avoided crossing around $\delta v = 0$ in the limit of $\varphi = \frac{\pi}{2} - \frac{1}{100}$. This signature of the static correlation is captured in the gradient of the effective density-to-potential map that steepens as the eigenenergies approach the degeneracy. We have introduced this feature as intrasystem steepening. Similar the intrasystem steepening shows up while the fragments in Fig. 14

are stretched in space. Note, on the scale from $\delta v = -5$ to $\delta v = -5$, for $d = 8$ in Fig. 14 it resembles that the gradient looses its one-to-one character in the vicinity of $\delta v = 0$ (almost vertical lines in the map). However, this is solely a scaling question. On the scale[1] of the coupling strength between the fragments, the map is still smooth and the relation between δn and δv is indeed one-to-one. For finite coupling strength this map is invertible and the domain and co-domain of the selected independent variable can be swapped. Fig. 14 and Fig. 17 show

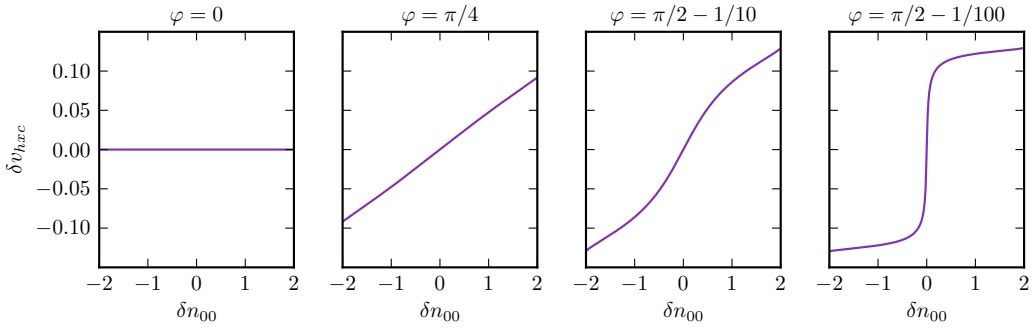

Figure 18: Exact Hartree xc potential as function of the density difference between two sites in the lattice that host two electrons in a singlet state. From left to right with increasing φ the electron-electron soft-Coulomb interaction and the static correlation between both sites increases. This figure is adapted from Ref. [116].

the density as function of the external potential, but density functional theory is rather considered about the inverse map. For $\varphi \neq \frac{\pi}{2}$, the domain and the co-domain of our maps can be swapped [2] by exchanging the x- and y-axis as we have done in Fig. 18 that shows the inverse map δv_{hxc}-to-δn_{00}. Note, Fig. 18 shows only the exact Hartree xc part of the external potential as function of the ground-state density that we have constructed by using the exact expression provided by Ref. [182]. The Hartree xc potential is the sum of the Hartree and the xc potential given in Eq. 131 and Eq. 132. In the case of non-interacting electrons $\varphi = 0$, the xc part vanishes.

DISCONNECTED LIMIT For fully decoupled fragments, where each fragment can be treated as isolated system, the Hilbert spaces of the fragments are disjoint. In the two-site model, the isolated systems would be represented by two fully disconnected individual sites. In this limit the particle exchange between the sites is prohibited. The particle number of each isolated system can only take integer values and the allowed discrete values of δn_{00} are therefore ± 2 and 0. Note, the meaning of δn_{00} that we have introduced as a quantity of the combined system defined in the joint Hilbert space of both sites is no longer valid. Each

1 Numerically, for increasing values of d the step size in the region around $\delta v = 0$ has to be significantly reduced. This leads to an increase of the number of iteration steps required and comes at increasing computational costs with increasing values of d. Therefore, to efficiently construct the points of the map, we use an adaptive step size. While the step size of δv is reduced whenever the density difference is above a threshold, δv is increased whenever the density difference is significantly below the threshold.

2 Note, earlier we have restricted the domain of φ to $[0, \frac{\pi}{2}]$. In general, the map is not invertible whenever the value of φ is a multiple of $\frac{\pi}{2}$.

site represents a disjoint physical systems with zero to two electrons. The HK theorem applies for each site separately, but not to both uncoupled sites. The density-to-potential map along the variable N is given by a set of discrete points at integer values that without introducing a coupling can not be connected. In the case of the hydrogen molecule this limit is reached at infinite separation of the fragments, where each fragment is represented by an isolated hydrogen atom.

INTERSYSTEM DERIVATIVE DISCONTINUITY In the strictly-localized limit, where $\varphi = \frac{\pi}{2}$, the electrons on the two sites kinetically decouple. However, both electrons are still coupled via the non-local electron-electron interaction and the external potential. This coupling between the two subsystems allows us to interpret one of the sites as a system that is coupled to an external particle bath represented by the remaining site in the lattice. Therefore, the particle number of the individual subsystems can also take fractional values and the discrete variable δn_{00} becomes a continuous variable with values in between -2, 0, and $+2$. The three two-particle singlet eigenstates represent three different physical systems. The first and the second eigenstate of the Hamiltonian[3]

$$\left|\phi_1^{\varphi=\frac{\pi}{2}}\right\rangle = \hat{c}_{1\downarrow}^\dagger \hat{c}_{1\uparrow}^\dagger \left|0\right\rangle, \text{ and } \left|\phi_2^{\varphi=\frac{\pi}{2}}\right\rangle = \hat{c}_{2\downarrow}^\dagger \hat{c}_{2\uparrow}^\dagger \left|0\right\rangle \tag{197}$$

correspond to a system where both electrons are located either on site one or two in the lattice leading to the density difference $\delta n_{00} = \pm 2$. The third eigenstate describes a system in which the electrons are delocalized over both sites and the density difference between the sites becomes $\delta n_{00} = 0$, i.e.

$$\left|\phi_3^{\varphi=\frac{\pi}{2}}\right\rangle = \frac{1}{\sqrt{2}}\left(\hat{c}_{1\downarrow}^\dagger \hat{c}_{2\uparrow}^\dagger - \hat{c}_{1\uparrow}^\dagger \hat{c}_{2\downarrow}^\dagger\right)\left|0\right\rangle. \tag{198}$$

The corresponding eigenergies of the eigenstates are plotted in the fourth row of Fig. 17. Except in the points of the degeneracy, each fixed value of the external potential favors one of the three different values of $\delta n_{00} = \pm 2, 0$ and the ground-state of one of the three described configurations becomes energetically more favorable. In the moment where the value of δv switches its sign, the eigenstates change their role and the eigenstate that has been the ground-state becomes the second excited-state of the system and vice versa. In Fig. 17, we have highlighted the ground-state energy in purple E_0, the first excited-state energy in light-blue E_1 and the second excited-state energy in dark blue E_2. In the strictly localized limit $\varphi = \frac{\pi}{2}$ the ground-state of the system becomes energetically degenerate in two points around $\delta v = \delta n_{00} = 0$ indicated by the red arrow in the fourth row of Fig. 17 that points out the real-crossing of eigenenergies. Due to the degeneracy of the eigenenergies, the density and the corresponding density functionals along the cut in δn_{00} can be constructed as convex combination in the degenerate subspace of the system using Eq. 112.

LEGENDRE TRANSFORMATION IN DENSITY FUNCTIONAL THEORY The Legendre transformation of $E[v, N]$ is $F_{\text{HK}}[n, N]$. The energy $E[v, N]$ is concave in

3 For $\varphi = \frac{\pi}{2}$ the hopping parameter is set to zero. The remaining Hamiltonian $\hat{H}^{\varphi=\frac{\pi}{2}} = \hat{W} + \hat{V}$ commutes with the position operator $\hat{x} = \sum_{m=1}^{M} \sum_\sigma x_m \hat{c}_{m,\sigma}^\dagger \hat{c}_{m,\sigma}$ with $x_m = -(M+1)/2dx + mdx$.

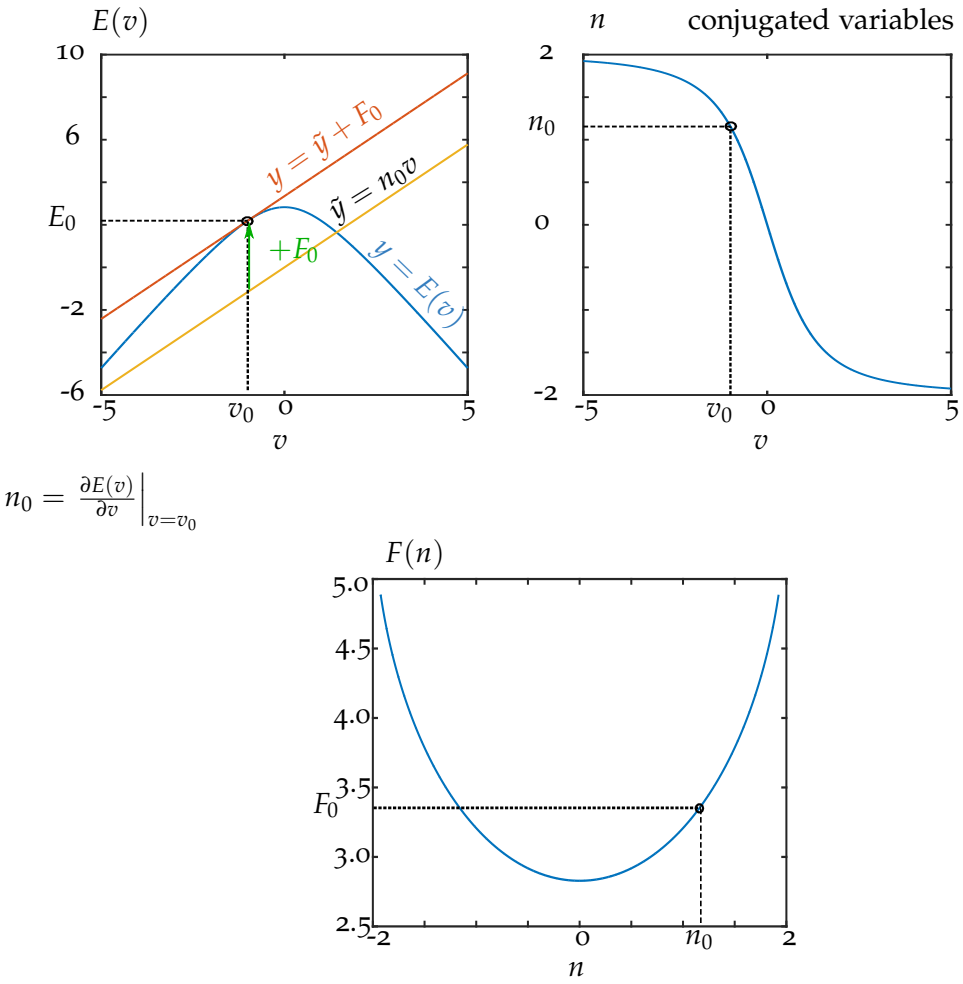

Figure 19: Graphical illustration of the variable transformation in DFT in terms of the Legendre transformation.

v [141] as can be seen in Fig. 19, where we have explicitly constructed $E[v]$ for the two-site lattice model system. Further, the energy $E[v]$ is convex in the variable N [141]. The negative of the ground-state density $-n$ is the dual variable to v [141]. The functional F_{HK} is concave in the variable n as can be seen in Fig. 19 which also shows $F_{\text{HK}}[n]$ as the Legendre transformation of $E[v, N]$. The convexity of $F_{\text{HK}}[n]$ guarantees the existence of a global minimum and formally underpins the HK theorem (the ground-state density n_{00} minimizes the $F_{\text{HK}}[n]$). Density-to-potential maps that can be reformulated in terms of the Legendre transformation have well-defined domains and analytic properties. Not only that the formulation of density functional theory in terms of the Legendre transformation circumvents the problem of v-representability as discussed in Sec. 3.2.4, but also it provides an additional criteria to differentiate between the intrasystem steepening and the intersystem derivative discontinuity. The intrasystem steepening is present in density-to-potential maps that have an exact one-to-one correspondence. For maps that show the intrasystem steepening the Legendre transformation exists. The uniqueness condition breaks down in the case

of density-to-potential maps that show the derivative discontinuity. Such maps are constructible as convex combination in the degenerate subspace of ground-state densities as defined in Eq. 112. Therefore, density-to-potential maps that show the intersystem derivative discontinuity can not be formulated in terms of the Legendre transformation. For the two particle singlet electrons on the two site lattice model, we can explicitly construct the Legendre transformation of $E[v]$. Fig. 19 and Fig. 20 graphically illustrate the variable transformation between the set of conjugated variables δv and δn for a few selected points v_j and n_j. The figure on the left in the first row displays the energy as function of the external potential color coded in blue. We explicitly construct the Legendre transformation for the point $E_0 = E(v = v_0)$ highlighted by a circle and the dashed lines. The figure on the right shows the conjugated pair of variables given by the ground-state density n and the external potential v. The conjugated variable of v_0 highlighted by a circle and dashed lines is explicitly given by

$$n_0 = \left.\frac{\partial E(v)}{\partial v}\right|_{v=v_0} . \tag{199}$$

The resulting linear equation $\tilde{y} = n_0 v$ is plotted in the figure on the left color coded in yellow. The shift highlighted in light-green in the figure on the left is given by the HK functional evaluated at the point $F_0 = F(n = n_0)$. The complete Legendre transformation that is given by the HK functional $F(n)$ is graphically illustrated in the figure below. Fig. 20 illustrates the same procedure for two additional points v_1 and v_2.

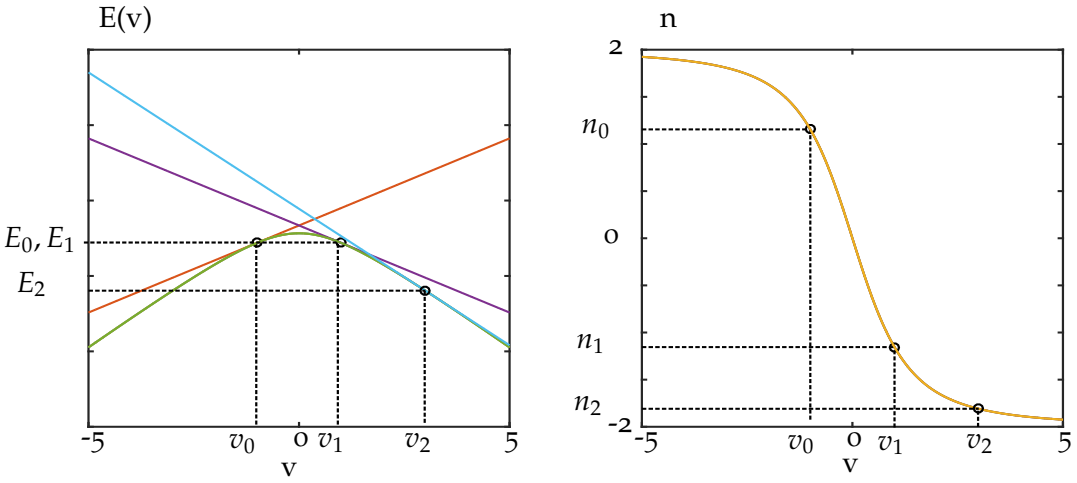

Figure 20: Graphical illustration of the variable transformation in ground-state density functional theory given by the Legendre transformation exemplified for three different points $v_j \leftrightarrow n_j$, where $j = 0, 1, 2$.

6.3 SIGNATURES OF STATIC CORRELATION IN DENSITY FUNCTIONALS

Features of the density-to-potential map carry the relevant information about the static correlation in the system. In Sec. 6.2.2 we have identified these features with the intra-system steepening and the inter-system derivative discontinuity.

Both features directly transmit to the CI coefficients α_q^φ of the wave function as function of the density difference as we will exemplify for the two site model in Sec. 6.3.1. As a consequence expectation values of arbitrary operators as functional of the ground-state density also carry such signatures of the static correlation along the cut in δn_{00}. For the two-site model, we exemplify this inheritance for the expectation values and transition matrix elements as function of δn_{00} for selected operators, i.e. in Sec. 6.3.2 and Sec. 6.3.3 for the ground- and excited state energies and densities along the cut in δn_{00}.

6.3.1 *Exact density-to-wavefunction map*

The exact ground-state density fully determines the external potential and in principle, even fully determines the electronic ground-state wave function of the system. In theory, the ground-state wave function can be considered as a functional of the ground-state density. In practice, the explicit density dependence of the wave function, i.e. the wave"functional" form of $\Psi_0[n_{00}]$ remains unknown. Further, as highlighted in Ref. [125], the inverse map $\Psi_0 \to n_{00}$ is not unique and - in contrast to the HK functional- the wavefunctional lacks well-defined domains and analytic properties [125]. However, the wavefunctional formally connects the fundamental descriptor $\Psi[v]$ of Schrödinger wave mechanics with the fundamental descriptor of density functional theory $n_{00}[v]$ allowing us to get direct insight how properties of a quantum mechanical system such as static correlation transmit from the wave function based methods to the density based ones. The same discussion holds for the ground-state as well as for the excited-state wavefunctionals $\Psi_j[n_{00}]$. For our model system we explicitly construct the wave function as functional of the ground-state density. We illustrate that features such as the intrasystem steepening and the intersystem derivative discontinuity of the density-to-potential map directly transmit to the density-to-wavefunction map and hence, to arbitrary density-to-observable maps which can be directly connected to the wavefunctional via $O_{kl}[n_{00}] = \langle \Psi_k[n_{00}] | \hat{O} | \Psi_l[n_{00}] \rangle$.

EXACT CONFIGURATION INTERACTION COEFFICIENTS AS FUNCTIONALS OF THE GROUND-STATE DENSITY The ground- and excited-state wavefunctionals are graphically well illustrated by the density dependence of their CI coefficients. For fixed φ, the CI coefficients of the exact ground- ($k = 0$) and excited-state ($k = 1, 2$) wave functions are given by the projection of the interacting wave function onto a complete set of Slater determinants $|\Phi_q\rangle$, i.e. explicitly given by

$$\alpha_q^{\varphi,k}[\delta n_{00}, N] = \langle \Phi_q | \, \Psi_k^\varphi[\delta n_{00}, N] \rangle \, . \tag{200}$$

A different choice of the set of Slater determinants leads to a different set of CI coefficients. Fig. 21 shows the CI coefficients, where we have projected the two-particle singlet ground-state wave function of the two-site lattice Hamiltonian onto the three two-particle singlet eigenstates of the kinetic operator $\hat{T}$. Fig. 21 shows the CI coefficients for different coupling strengths between the two sites. Since all three CI coefficients are symmetric around δn_{00}, the density functionals of other observables are also symmetric around $\delta n_{00} = 0$.

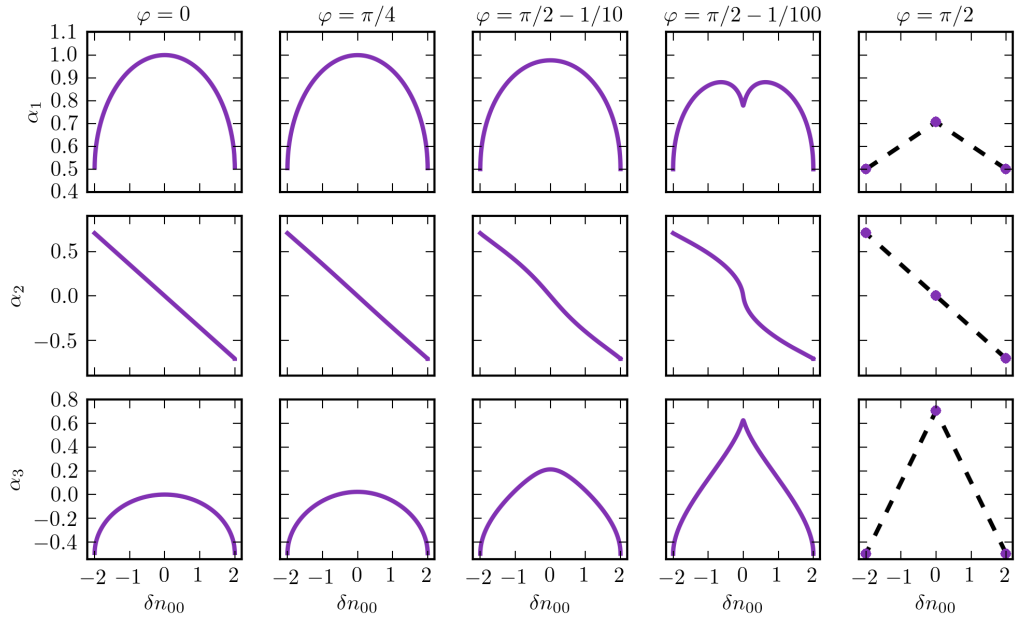

Figure 21: CI coefficients of the two-particle ground-state wave function. This figure is adapted from Ref. [116].

INTRASYSTEM STEEPENING OF THE CI COEFFICIENTS Going from the non-interacting limit on the left to the strictly-localized limit on the right of Fig. 21, the static correlation between the sites grows and the gradient of the CI coefficient steepens.

INTERSYSTEM DERIVATIVE DISCONTINUITY OF THE CI COEFFICIENTS Each of the three different physical systems, where the value of δn_{00} is fixed at -2, 0, or $+2$, and can be fully represented by a complete set of CI coefficients $\{\alpha_1, \alpha_2, \alpha_3\}$ indicated by the dots in Fig. 21. The CI coefficients in the strictly-localized limit are explicitly given by

$$\alpha_1^{\varphi=\frac{\pi}{2}}[\delta n_{00}] = \begin{cases} \frac{1}{2}, & \text{for } \delta n_{00} = -2 \\ \frac{1}{\sqrt{2}}, & \text{for } \delta n_{00} = 0 \\ \frac{1}{2}, & \text{for } \delta n_{00} = +2, \end{cases}$$

$$\alpha_2^{\varphi=\frac{\pi}{2}}[\delta n_{00}] = \begin{cases} \frac{1}{\sqrt{2}}, & \text{for } \delta n_{00} = -2 \\ 0, & \text{for } \delta n_{00} = 0 \\ -\frac{1}{\sqrt{2}}, & \text{for } \delta n_{00} = +2, \end{cases}$$

$$\alpha_3^{\varphi=\frac{\pi}{2}}[\delta n_{00}] = \begin{cases} -\frac{1}{2}, & \text{for } \delta n_{00} = -2 \\ \frac{1}{\sqrt{2}}, & \text{for } \delta n_{00} = 0 \\ -\frac{1}{2}, & \text{for } \delta n_{00} = +2, \end{cases}$$

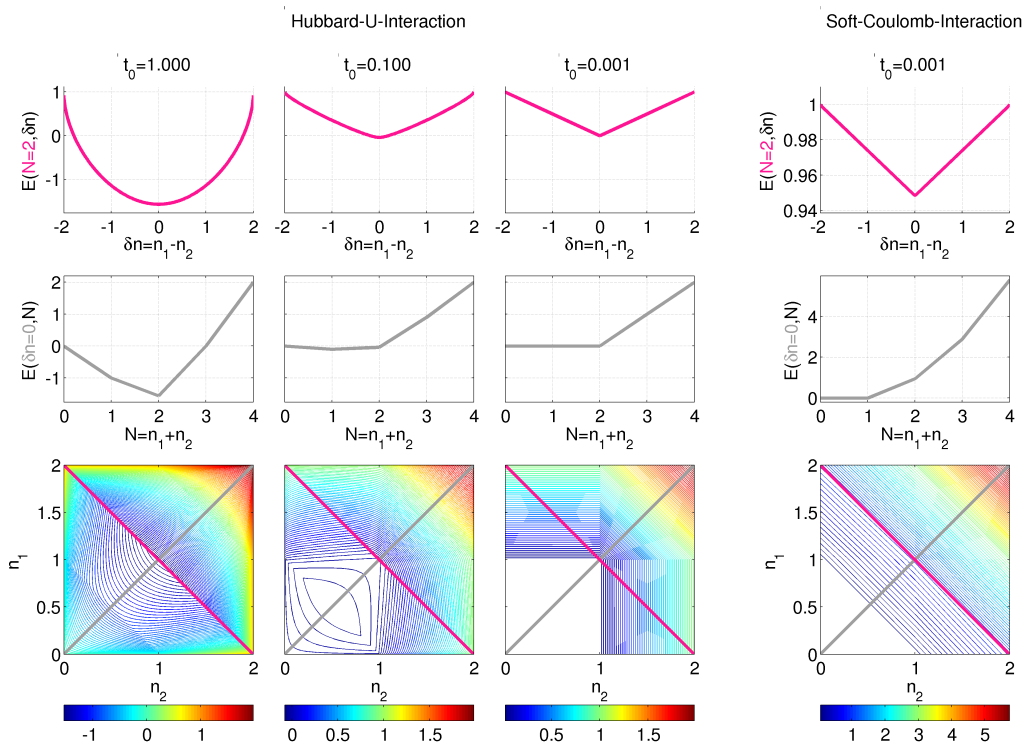

Figure 22: Exact HK energy as functional of the on-site densities $n_{00,1}$ and $n_{00,2}$ for different coupling strengths. First three columns Hubbard-U-interaction and fourth column soft-Coulomb. First row: Cut along the density difference between the sites δn_{00} while the particle number is kept fixed at $N = 2$ Second row: cut along the particle number N while the density difference is kept fixed $\delta n_{00} = 0$ Third row: complete HK functional, pink diagonal highlights cut plotted in first row, grey diagonal highlights cut in second row.

Using a linear interpolation indicated by the dashed-line style, we connect the three dots that represent the CI coefficients at different integer values of δn_{00}.

6.3.2 *Exact ground- and excited-state energy functionals*

The HK functional that is the universal part of the ground- state energy functional ($j = 0$) and the excited-state energy functional ($j = 1, 2$) are given by the expectation value

$$F^{\varphi}_{jj}[\delta n_{00}] = \left\langle \Psi^{\varphi}_{2s,j} \middle| \lambda_t(\varphi)\hat{T} + \lambda_w(\varphi)\hat{W} \middle| \Psi^{\varphi}_{2s,j} \right\rangle . \tag{201}$$

Fig. 22 shows the ground-state HK functional of the two-particle singlet states for different kinetic coupling strengths between the two sites. From left to right the static correlation between the sites grows. As we have seen the static correlation directly affects the density-to-potential map. The density dependence that carries the signatures of the static correlation enters the wave function, and hence the expectation value of Eq. 201. The third row of Fig. 22 shows a contour plot of the ground-state HK energy as function of both on-site densities $n_{00,1}$ and $n_{00,2}$, i.e. the functional form in complete real-space of the system. The first three columns

show the functional for two electrons interacting via the on-site Hubbard interaction, while the fourth column shows the functional for two electrons that interact via the non-local soft-Coulomb interaction. Both diagonals of the contour plot represent specific cuts of the functional. In particular, the diagonal highlighted in pink represents the cut along the variable δn_{00} and the grey diagonal represents the cut along the particle number N. Both cuts are explicitly shown in the first and second row of Fig. 22.

NON-LOCAL VERSUS LOCAL ELECTRON-ELECTRON INTERACTION From left to right the sites kinetically decouple and the kinetic energy distribution tends to zero while $t_0 \to 0$. Approaching this limit, the expectation value in Eq. 201 is dominated by the value of the electron-electron repulsion energy. This allows us to illustrate how the local and non-local electron-electron interaction affect the value of the HK functional. The third column of the second row shows $F_{HK}[N, \delta n_{00} = 0]$ in the limit $t_0 = 0.001$ for the Hubbard-interaction. In the local on-site Hubbard-interaction a term is added to the value of F_{HK} whenever two electrons populate the same site. Therefore, the value of F_{HK} is zero for $N < 2$. In contrast, the non-local soft-Coulomb interaction contributes to F_{HK} for $N > 1$.

INTRASYSTEM STEEPENING OF THE HOHENBERG-KOHN FUNCTIONAL The first row of Fig. 22 shows the cut of the HK functional along the density difference between the sites δn_{00}, while the particle number of the total system is kept fixed at $N = 2$. The intrasystem steepening that we have already seen in the density-to-potential map in Fig. 17 is also visible in the HK functional. Note, while t_0 approaches zero, the ground-state energy comes close to a degeneracy and the cut along δn_{00} of the HK functional approaches the straight-line behavior. Nevertheless for infinitesimal small values of $t_0 \neq 0$, the HK functional shown in the first row has a well-defined gradient around integer values of δn_{00} [4] as can be seen in the third and fourth row of Fig. 23.

INTRASYSTEM STEEPENING EXCITED-STATE ENERGY FUNCTIONALS Besides the intrasystem steepening of the HK functional, i.e. a ground-state property of the system, the first and the second row of Fig. 23 also illustrate the intrasystem steepening of the first and second excited-state energy functional. The left figure of the fourth row shows a zoom of the ground-state HK functional colored in purple. The figure on the right shows the zoom of the first-excited energy functional colored in light-blue. The solid and the dashed line in both figures show a comparison between the limit of the intrasystem steepening, where $\varphi = \frac{\pi}{2} - \frac{1}{100}$, and the limit of the straight-line behavior that is related to the intersystem derivative discontinuity where $\varphi = \frac{\pi}{2}$.

4 This can be formally shown by perturbation theory. We have perturbed the strictly localized states by an infinitesimal small value of t_0. The discrete set of values of δn than transitions into a continuous variable that captures the functional behavior of the density-to-potential map in the highly-localized electron limit, e.g. for $\varphi = \frac{\pi}{2}$. The corresponding density functionals of arbitrary observables along the cut in the variable δn_{00} have a smooth behavior with a well-defined gradient. [The perturbation idea was suggested in a personal communication by V. Attalla]

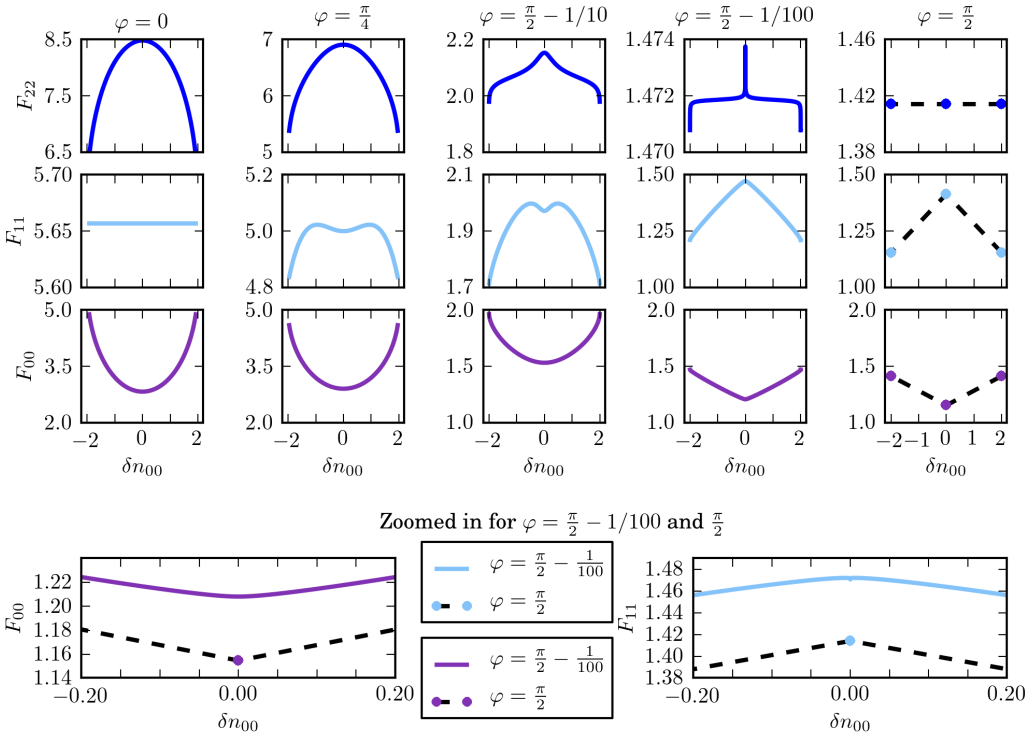

Figure 23: Universal part of the exact ground- and excited-state energy as functional of the density difference between the sites for the two-particle singlet states with soft-Coulomb interaction. From top to bottom: The first row shows the second excited-state energy functional, the second row shows the first excited-state energy functional and the third row shows the ground-state HK energy functional. The figure on the left in the fourth row shows the ground-state energy functional, while the figure on the right shows the first excited-state energy functional in the limit $\varphi = \frac{\pi}{2} - \frac{1}{100}$ and $\varphi = \frac{\pi}{2}$. The solid-line style corresponds to the intrasystem steepening and the dashed-line to the straight-line behavior that is related to the derivative discontinuity. From left to right the static correlation in the system increases from the non-interacting limit, where $\varphi = 0$ to the strictly-localized limit, where $\varphi = \frac{\pi}{2}$. This figure is adapted from Ref. [116].

INTERSYSTEM DERIVATIVE DISCONTINUITY OF THE HOHENBERG-KOHN FUNCTIONAL The cut along the particle number in the second row of Fig. 22 shows the HK functional as functional of N, while the density difference between the sites is kept fixed at $\delta n_{00} = 0$. At integer values of N, the ground-state of the N- and $N \pm 1$-particle system of the considered two-site model becomes degenerate, allowing to construct the HK functional as convex combination in the degenerate subspace as defined in Eq. 112. As a consequence, the HK functional along the cut in the variable N is piecewise linear and the straight-lines change their slope at integer values of N. At these points, the derivative along the cut in N becomes discontinues. This illustrates the well-known concept of the derivative discontinuity.

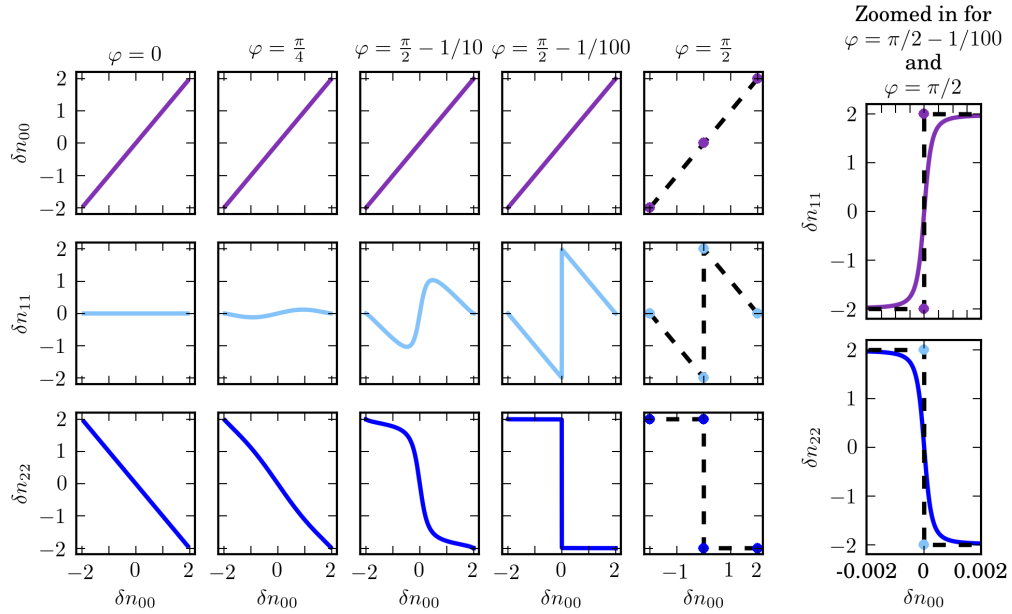

Figure 24: Ground- and excited state densities as functional of the ground-state density of the two-particle singlet states on two sites with soft-Coulomb electron-electron interaction. From top to bottom: The first row shows the ground-state density functional, the second row the first and the third row the second excited-state density functionals. A detailed view of the intra-system steepening (solid line style) in the limit $\varphi = \frac{\pi}{2} - \frac{1}{100}$) and the inter-system derivative discontinuity (dashed line style) in the limit of the excited-state densities can be found in the figures on the right. This figure is adapted from Ref. [116].

6.3.3 *Exact excited- and transition-state density functionals*

The excited- ($k = j = 1, 2$) and transition-state ($k \neq j = 0, 1, 2$) densities as functional of the ground-state density are given by

$$\delta n_{kj}[\delta n_{00}] = \langle \Psi_k[\delta n_{00}, N] | \hat{O} | \Psi_j[\delta n_{00}, N] \rangle . \tag{202}$$

EXCITED-STATE DENSITY FUNCTIONALS The first row in Fig. 24 shows the ground-state density, the second row the first excited- and the third row the second excited-state density as functional of the ground-state density. Clearly, the trivial functional behavior of the ground-state density in the first row remains linear for different values of φ. However, in the limit of $\varphi = \frac{\pi}{2}$, following Eq. 112, we have constructed the linear behavior by connecting the distributional points via straight-lines indicated by the dashed-line. From left to right with increasing static correlation in the system, the gradient of both excited-state densities steepens until the gradient shows a discontinuity in the limit of $\varphi = \frac{\pi}{2}$. A detailed view of the critical region of the excited density functionals is given on the right-hand side of Fig. 24. While the intra-system steepening of the functional in solid line style has a well defined gradient around $\delta n_{00} = 0$, the dashed line illustrates the inter-system derivative discontinuity of the functional along the cut in $\delta n_{00} = 0$ for $\varphi = \frac{\pi}{2}$.

TRANSITION-STATE DENSITY FUNCTIONALS Practical linear response calculations in the framework of TDDFT usually replace the phase-dependent transition densities by the phase-independent excited-state densities. For our model system, Fig. 25 displays the absolute value of the transition-state densities from the first to the second excited-state and from the the ground- to the first excited-state as functional of the ground-state density. In the limit where $\varphi = \frac{\pi}{2}$ the transition state densities vanish. Both transition densities between the different states show the clear features of the static correlation at points where their corresponding eigenvalues come close to a degeneracy. For example, the detailed view of the avoided crossing in Fig. 17 shows that the ground- and the first excited-state have two symmetric points around $\delta v = 0$, where the corresponding eigenenergies come close to a degeneracy. The corresponding transition-state density between the ground- and the first excited-state shows a double-well structure as can be seen in the second row of Fig. 25.

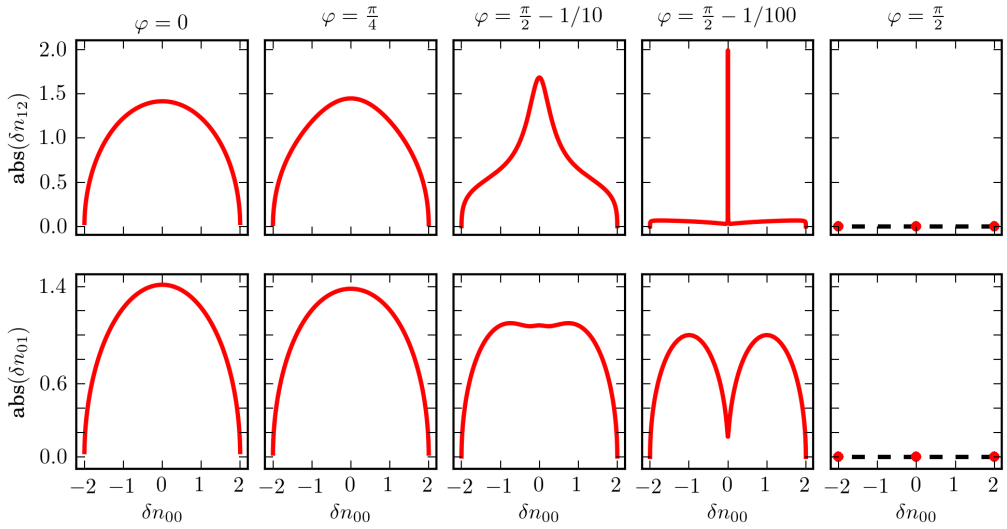

Figure 25: Absolute value of the transition state densities as functional of the ground-state density of the two-particle singlet states on two sites with soft-Coulomb electron-electron interaction. First row: Exact transition density from the first to the second excited-state as functional of the ground-state density $\delta n_{12}(\delta n_{00})$. Second row: Exact transition density from the ground- to the first excited-state as functional of the ground-state density $\delta n_{01}(\delta n_{00})$. This figure is adapted from Ref. [116].

6.3.4 *Exact correlation entropy functional*

We have introduced the intra-system steepening and the intersystem derivative discontinuity as signatures of the effective density-to-potential map that carry the relevant information about the static correlation in the system. Of particular relevance is the correlation entropy that is a measure of the correlation and entanglement present in a many-body system [81] and the Slater rank [81, 82]. Fig. 26 displays the correlation entropy which increases with the mixing of the

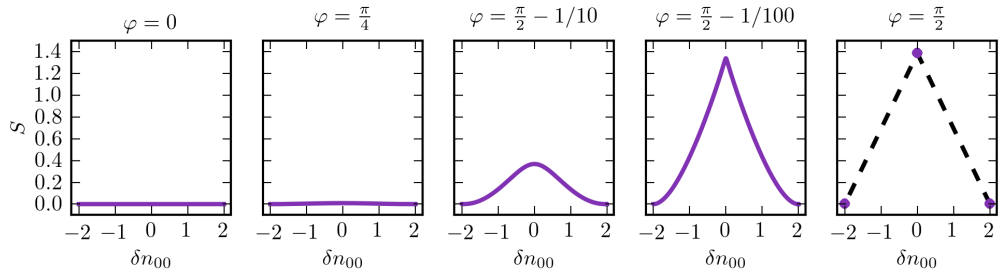

Figure 26: Intrasystem steepening and intersystem derivative discontinuity of the correlation entropy as functional of the ground-state density.This figure is adapted from Ref. [116].

eigenstates as can be seen in the lower panel and the inset of Fig. 17. In the limit of non-interacting electrons on the left, the correlation is zero. From left to right, the gradient of the correlation entropy functional shows the intra-system steepening until the functional can be constructed as convex combination due to the degeneracy of the ground-state for $\varphi = \frac{\pi}{2}$. The maximum value of the correlation entropy is reached in the strictly localized limit for $\delta n_{00} = 0$ where all three eigenenergies are degenerate.

6.4 SUMMARY

In this chapter, we have used the concept of the effective density-to-potential map to analyze the correlation between subsystems within the system. We have introduced the concept of the intrasystem steepening that is connected to the electron localization over the subsystems within the system. We have shown that the effective density-to-potential map of the LDA density lacks the intrasystem steepening. Further, we have illustrated how the intrasystem steepening and the intersystem derivative discontinuity directly translate to the wavefunctional and the functionals of arbitrary observables. A lack of the intrasystem steepening of approximate functionals therefore results in errors in their corresponding observables.

7

INTRASYSTEM STEEPING RELOADED - EXACT DENSITY MAPS IN CORRELATED ELECTRON-PHOTON SYSTEMS

7.1 INTRODUCTION

In this chapter, we illustrate that the intrasystem steepening of the effective density-to-potential maps discussed in the previous two chapters also shows up in the maps of correlated electron-photon systems. The intrasystem steepening is connected to the real-space signatures of the exact Kohn-Sham potential observed in Ref. [170]. The Kohn-Sham system is designed to yield the exact density of an interacting many-body system. These steps and peaks are then universal features in a sense that they are not only present in the xc potential of static and dynamic processes within conventional ground-state DFT of purely electronic systems, but are also present in the Kohn-Sham systems of arbitrary correlated interacting systems. The question arises whether, and if yes, under which conditions these real-space signatures appear in the xc potential of purely bosonic systems or coupled fermionic-bosonic systems. Such systems include purely phononic or photonic systems as well as coupled electron-phonon or coupled electron-photon systems. The correlation in phononic systems has been studied in Ref. [252–255]. We show that features such as the intrasystem steepening and the intersystem derivative discontinuity are also present in the cut along the particle number of the density-to-potential map as well as the density functionals of arbitrary observables. In this chapter, we study the maps of electron-photon systems in the framework of QEDFT.

7.2 DENSITY-TO-POTENTIAL MAP FOR A SINGLE ELECTRON

We employ the Rabi-Hubbard model as discussed in Sec. 4.2, where a single electron is coupled to the photon mode. In Fig. 27 (a), we show the case, where we have a single electron on two sites, without electron-photon interaction, i.e. $\lambda = 0$. Since electrons and photons do not couple, varying j_{ext} has no effect on the density-to-potential map $\Delta n[v_{ext}]$. Therefore, the density-to-potential map is determined by the external potential v_{ext} alone. The dependency of $\Delta n[v_{ext}]$ on v_{ext} is shown in the lower plot. We find a continuous and rather smooth mapping. Since, we have restricted ourselves to a single electron, the density Δn can have values between $[-1, 1]$, i.e. at these maxima values the electron is located on one of the two sites. In Fig. 27 (b), we now introduce a finite λ, here $\lambda = 0.1$. Now, if we couple the electronic and the photonic system (even for infinitesimal

The following chapter is based on the work of Dimitrov et al. to be submitted to Ref. [251].

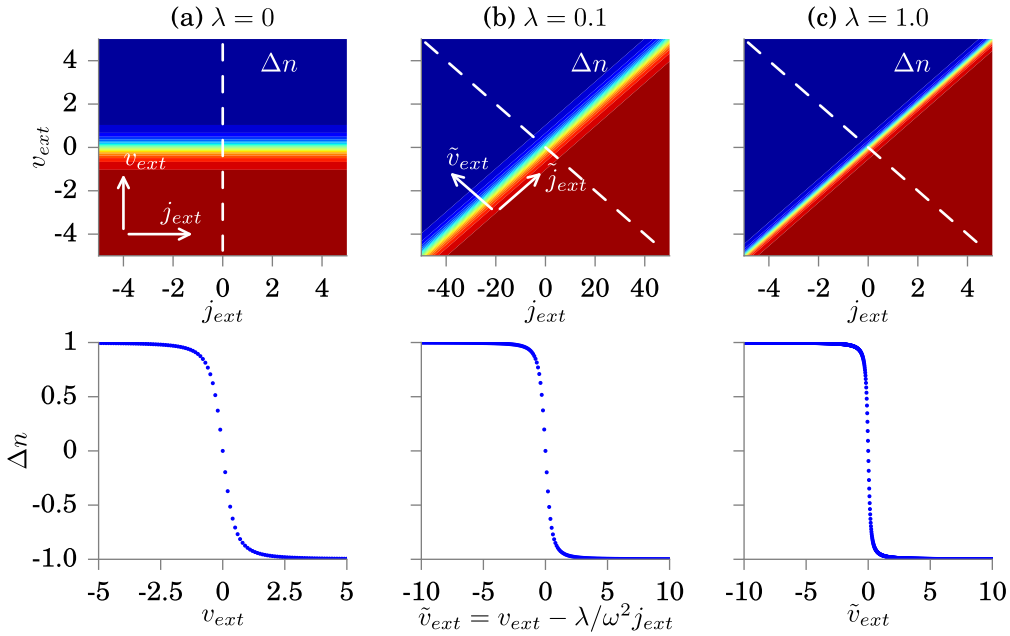

Figure 27: Single electron: the electron density Δn as function of the external variables (v_{ext}, j_{ext}) is shown in the first row. The second row shows the cut of $\Delta n(v_{ext}, j_{ext})$ as indicated by the dashed line in the upper plot both for different coupling strength of (a) $\lambda = 0$, (b) $\lambda = 0.1$, and (c) $\lambda = 1$.

coupling strength), we find that new normal modes are emerging, due to the electron-photon correlation. In Fig. 27 (b), we plot the two-dimensional density-to-potential map $\Delta n[v_{ext}, j_{ext}]$ for $v_{ext} = [-5, 5]$, $j_{ext} = [-50, 50]$, $\omega = 1$ and $t_0 = 1$. The first emerging feature in the plot is that two new normal modes appear [161, 256], i.e. the photon and electron degrees of freedom become correlated. This electron-photon correlation tildes the map as shown in the contour plot in the top of Fig. 27. The antidiagonal cut in the plot is the new polaritonic degree of freedom as shown in Fig. 27 on the bottom. We find a broad smearing of the density-to-potential map. For the diagonal and the antidiagonal cut in Fig. 27, we find the conditions

$$\tilde{v}_{\text{ext}} = v_{\text{ext}} - \tilde{\lambda} j_{\text{ext}} \text{ and } \tilde{j}_{\text{ext}} = j_{\text{ext}} + \tilde{\lambda} v_{\text{ext}} \text{ with } \tilde{\lambda} = \frac{\lambda}{\omega^2}. \tag{203}$$

These new coordinates are the new normal modes that are also illustrated in Fig. 28. Due to the linear relation of v_{ext} and j_{ext}, we find a horizontal plot for $\lambda = 0$, where the electrons and photons do not couple, and hence the photon field has no influence on the electron density. The opposite limit is given if λ approaches ∞ ($\lambda \to \infty$), where we find a vertical plot in Fig. 28 and the electronic Hamiltonian is negligible compared to the electron-photon interaction in the Hamiltonian.

Fig. 27 (c) shows the map for $\lambda = 1$. The plot is shown for $v_{ext} = [-5, 5]$ and $j_{ext} = [-5, 5]$, hence the photon external variable is narrower. In comparison to $\lambda = 0.1$, we find a steepening of the gradient in the density-to-potential plot. However, we emphasize that the map for this setup is still continuous, in contrast to a true intersystem derivative-discontinuity, where we would find a dis-

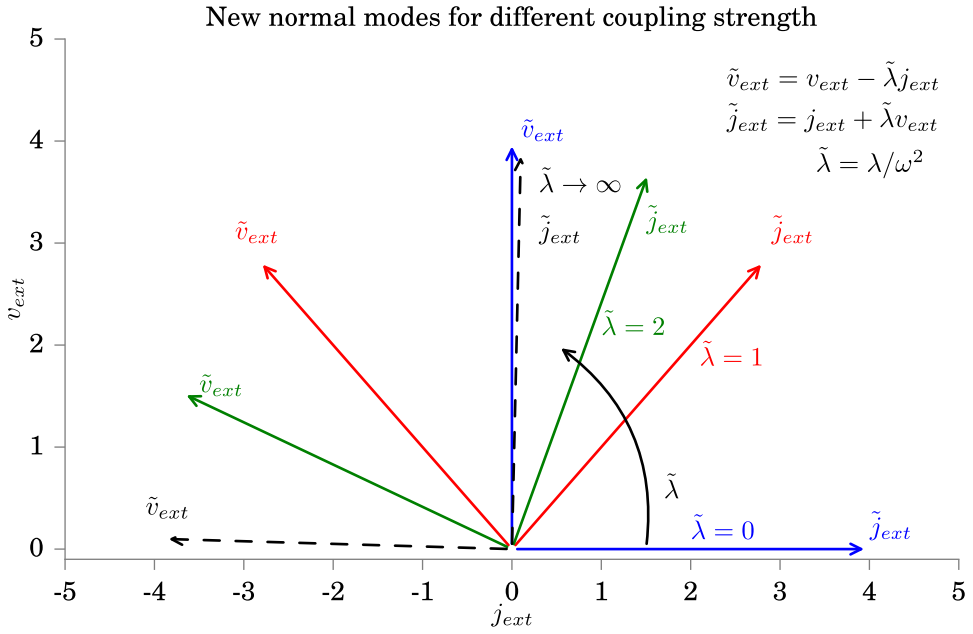

Figure 28: New normal mode for coupled electron-photon system.

continuous graph. We can conclude that the mapping becomes sharper for increasing electron-photon coupling strength λ reminiscent to the case of static correlation [116] as discussed in the previous chapter.

7.3 DENSITY-TO-POTENTIAL MAP FOR TWO ELECTRONS

Next, we analyze the two-site Rabi-Hubbard model in the two-electron subspace. The density-to-potential map is plotted in Fig. 29. In (a), we show the mapping for a electron-photon coupling strength of $\lambda = 0.1$, hence a weak coupling setup. As in the case of the single electron, we also find here electron-photon correlation by the appearance of new normal modes. While the upper panel shows the two-dimensional mapping $\Delta n[v_{ext}, j_{ext}]$, the lower panel shows a antidiagonal cut along the new normal mode. The most noticeable difference to Fig. 27 is that Δn can now acquire values between -2 and $+2$ and in the mapping an intermediate step appears, where $\Delta n \approx 0$. If we now increase the electron-photon coupling strength λ to $\lambda = 1$, we find a steeper density-to-potential map. Also the intermediate step is reduced in size. In Fig. 27 (c), we plot the mapping for $\lambda = 2$. Here, we find that the intermediate step vanishes and around $v_{ext} = j_{ext} = 0$, the mapping is very steep. In the Hubbard model discussed in the previous chapter, the length of the intermediate step is directly connected to the parameter of the Hubbard interaction U_0. Thus since, for strong electron-photon coupling this intermediate step vanishes, we can conclude that the electron-photon interaction is capable of effectively reducing the electron-electron repulsion of the Hubbard term in Eq. 180. Formulated differently, the electron-photon interaction mediates an effective attraction between the two electrons with the effect that both occupy the same site. Physically, we may interpret this finding such that the photons cloud (screen) the electrons in the ground state, which effectively causes a reduc-

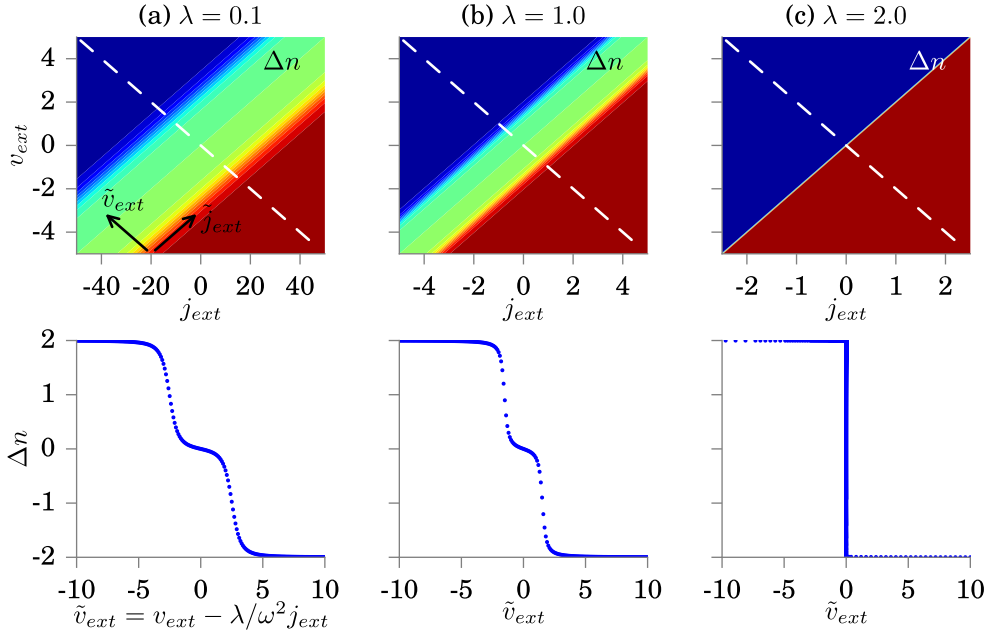

Figure 29: Two electrons with $U_0 = 5$: the electron density Δn as function of the external variables (v_{ext}, j_{ext}) is shown in the first row. The second row shows the antidiagonal cut of $\Delta n(v_{ext}, j_{ext})$ as indicated by the dashed line in the upper plot both for different coupling strength of (a) $\lambda = 0.1$, (b) $\lambda = 1$, and (c) $\lambda = 2$.

tion in the electron-electron repulsion. Next, we analyze the density-to-potential

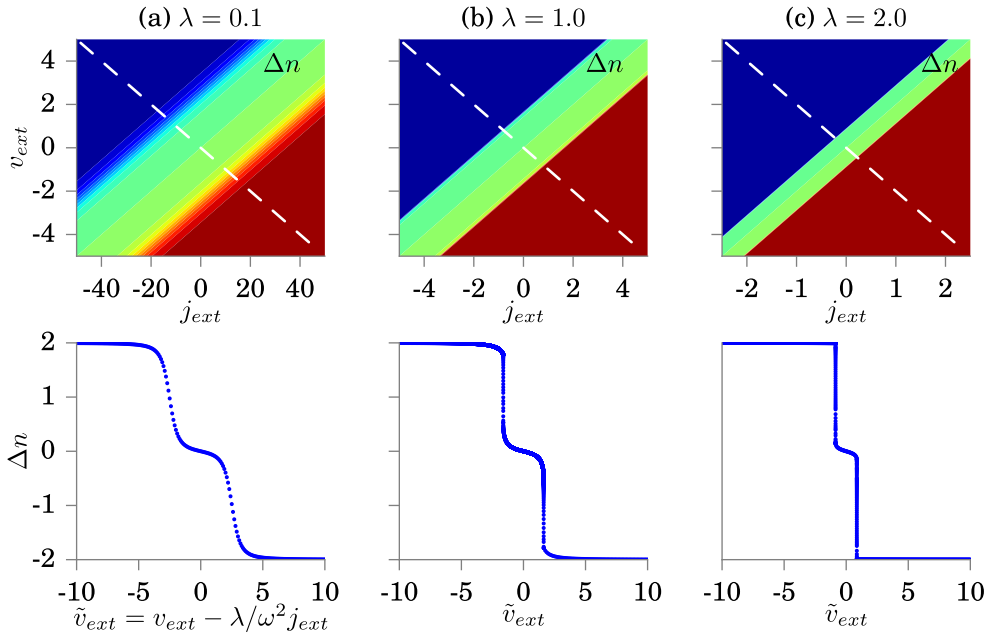

Figure 30: Two electrons with $U_0 = 5$ in mean-field approximation: the electron density Δn as function of the external variables (v_{ext}, j_{ext}) is shown in the first row. The second row shows the antidiagonal cut of $\Delta n(v_{ext}, j_{ext})$ as indicated by the dashed line in the upper plot both for different coupling strength of (a) $\lambda = 0.1$, (b) $\lambda = 1$, and (c) $\lambda = 2$.

map in the mean-field (classical) approximation, introduced in Eqns. 179-180. In Fig. 30 (a), we plot the density-to-potential map in the regime of weak-coupling ($\lambda = 0.1$). For the weak-coupling regime, we find a good agreement to the exact calculations shown in Fig. 29. The first differences become more pronounced in Fig. 30 (b). For the stronger coupling of $\lambda = 1$, we find in comparison to Fig. 29 (b) a broader intermediate step and also a lesser steepening in the map. The most significant differences are clearly visible in the strong-coupling limit for $\lambda = 2$. While in Fig. 29 (c) for the exact quantum calculation, we have seen the complete vanishing of the intermediate step, in Fig. 30 we find still a remaining (finite) step if the classical approximation is employed. Similarly, in Fig. 31 we show the exact and in Fig. 32 the mean-field approximated photon displacement variable as functional of the external potentials. In both figures, from (a) to (c), we increase the electron-photon coupling strength. Again the mean-field approximation fails to describe the vanishing of the intermediate step in the strong-coupling limit as can be seen by comparing Fig. 31 (c) with Fig. 32 (c). This clearly shows the breakdown of the classical approximation. Only in the limit of $\lambda \to \infty$, the classical approximation can correctly predict the vanishing intermediate step. This brings us to the conclusion that this feature can be only correctly captured, if electron-photon exchange correlation is taken into account. Thus, approximate exchange-correlation functionals have to be developed to correctly predict such features.

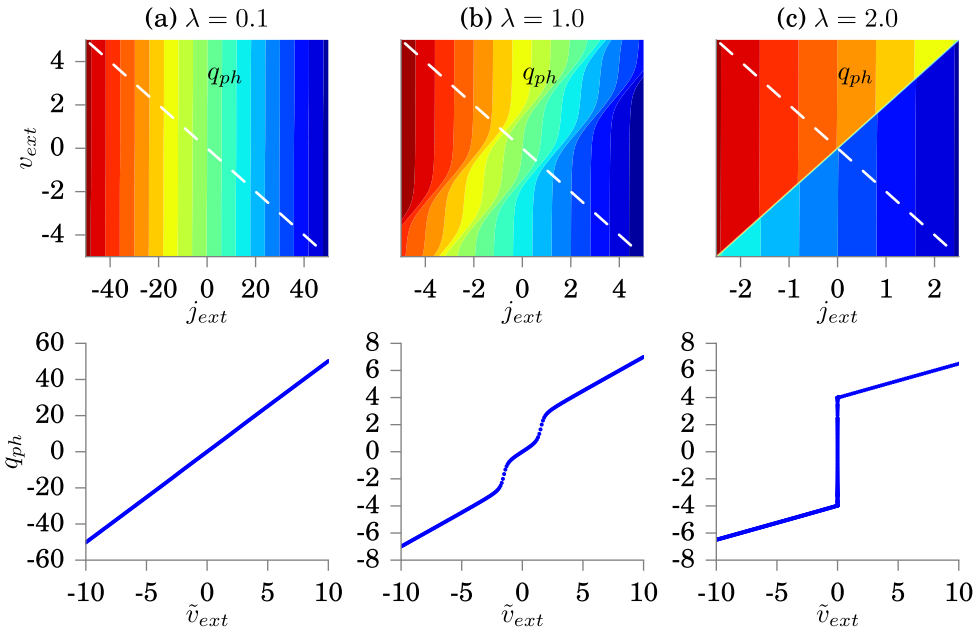

Figure 31: Two electrons with $U_0 = 5$: the photon displacement variable as function of the external variables $q_{ph}(v_{ext}, j_{ext})$ is shown in the first row. The second row shows the antidiagonal cut of $q_{ph}(v_{ext}, j_{ext})$ as indicated by the dashed line in the upper plot.

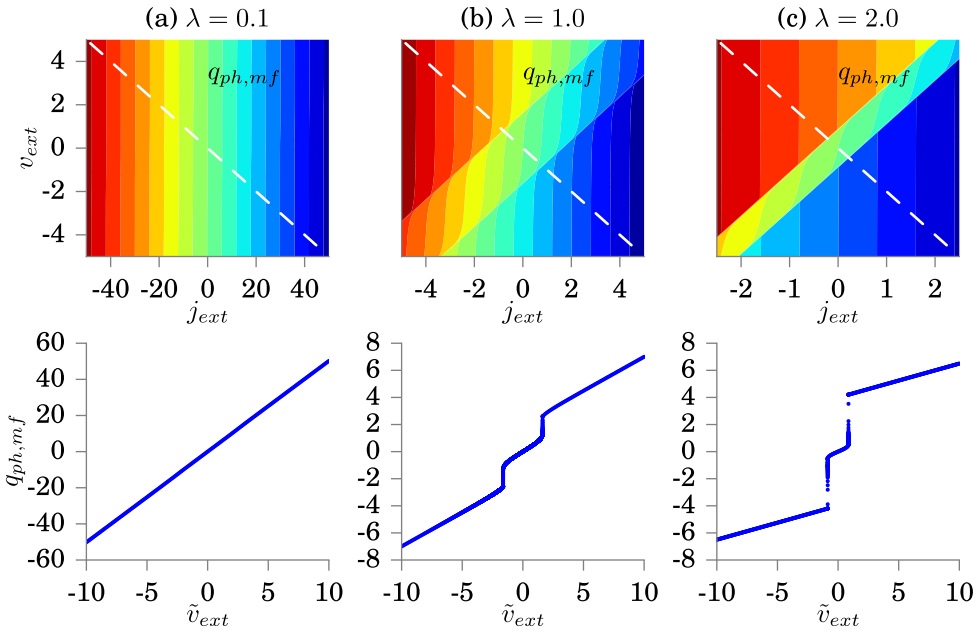

Figure 32: Two electrons with $U_0 = 5$: the photon displacement variable as function of the external variables $q_{ph}(v_{ext}, j_{ext})$ in mean-field approximation is shown in the first row. The second row shows the antidiagonal cut of $q_{ph}(v_{ext}, j_{ext})$ as indicated by the dashed line in the upper plot.

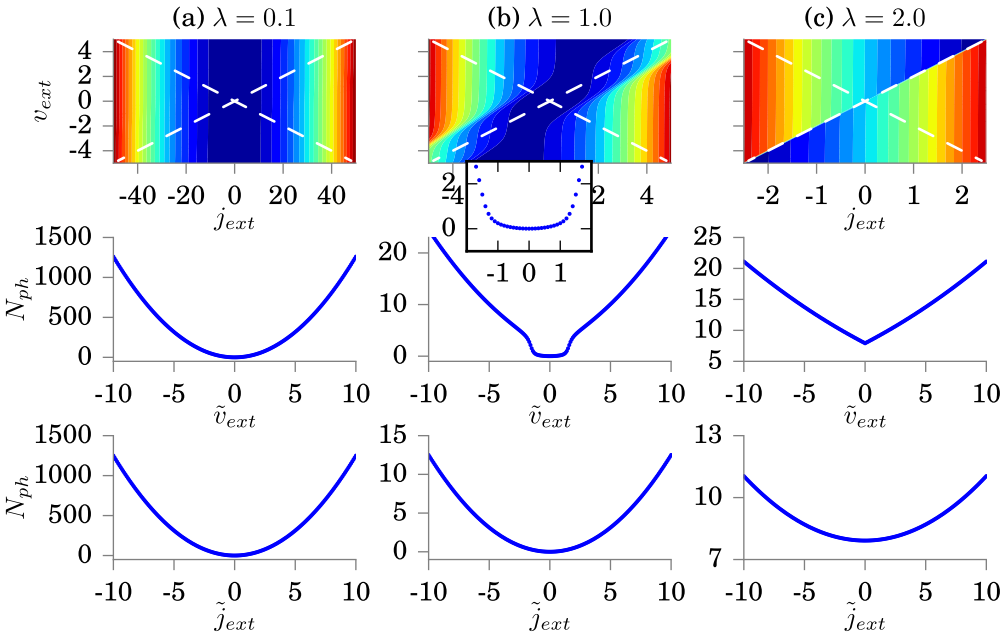

Figure 33: Two electrons with $U_0 = 5$: the photon number $N = \langle \hat{a}^\dagger \hat{a} \rangle$ as function of the external variables (v_{ext}, j_{ext}) is shown in the first row. The second row shows the antidiagonal cut of $N(v_{ext}, j_{ext})$ as indicated by the dashed line in the upper plot. The third row shows the diagonal cut of $N(v_{ext}, j_{ext})$. All plots for different coupling strength of (a) $\lambda = 0.1$, (b) $\lambda = 1$, and (c) $\lambda = 2$.

7.4 OBSERVABLES IN QEDFT

In the remaining part of this section, we now study the implications of the features of the density-to-potential map on observables. The first observable, we study is the photon number in the system $\langle \hat{N} \rangle = \langle \hat{a}^\dagger \hat{a} \rangle$. In general, and in difference to electronic observables, such as Δn, the photonic observables are unbound due to their underlying bosonic nature. In Fig. 33 (a), we show N as functional of the external potentials, $N[v_{ext}, j_{ext}]$. In Fig. 33 (a), in the weak-coupling limit for $\lambda = 0.1$, we find that the external potential v_{ext} has no large overall influence on this observable and the harmonic nature of this observable is given by the external current j_{ext}. In the two lower panels, we plot the diagonal and the antidiagonal cut. Since the observable is unbound, we can excite very high photon numbers, up to 1200 for the studied examples. Next in Fig. 33 (b), we show the case for $\lambda = 1$. Here, we find that the external potential v_{ext} can alter this observable in cases, where N is small. Around $j_{ext} \sim 0$, we find a funnel-type structure of this observable which is connected to the intermediate step of the density-to-potential mapping shown in Fig. 29. In Fig. 33 (c), we show the strong-coupling limit for $\lambda = 2$. Here, we find for the antidiagonal cut of the $N[v_{ext}, j_{ext}]$ map a sharp feature around $j_{ext} \sim 0$. However, we emphasize that this sharp feature is still continuous. Again this is connected to the sharp features in the density-to-potential map. Also the new normal mode is clearly visible along the antidiagonal. In Fig. 34 we now show the dependency of $N[\Delta n, q_\alpha]$ on the internal

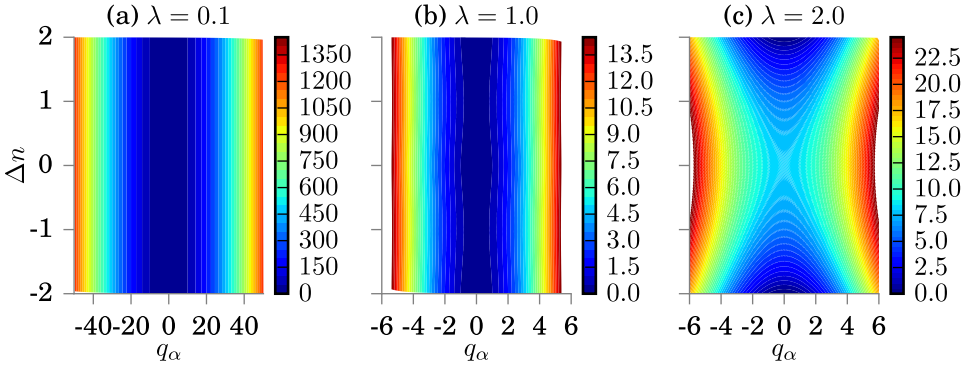

Figure 34: Two electrons with $U_0 = 5$: the photon number $N = \langle \hat{a}^\dagger \hat{a} \rangle$ as function of the internal variables $(\Delta n, q)$ is shown for different coupling strength of (a) $\lambda = 0.1$, (b) $\lambda = 1$, and (c) $\lambda = 2$.

variables. Here, we find that the appearing normal modes vanish for all three coupling strength. Qualitatively the weak-coupling $\lambda = 0.1$ and the strong-coupling for $\lambda = 1$ behave similarly, while the mapping for $\lambda = 2$ has a constricted shape. In Fig. 35, we plot the Hohenberg-Kohn functional [257] F_{HK} as function of the external variables v_{ext} and j_{ext} for the different coupling strength. The cut along the new normal mode is shown in the bottom. In the weak-coupling limit, for $\lambda = 0.1$, we find a rather smooth and harmonic curvature. For $\lambda = 1$, we find a similar feature as in Fig. 33. In the strong-coupling limit, we again find a smooth map, however the amplitude is smaller as for $\lambda = 0.1$. In Fig. 36, we show the total energy, i.e. $E_{tot} = \langle \Psi_0 | \hat{H} | \Psi_0 \rangle$. From the weak- to the strong-coupling limit,

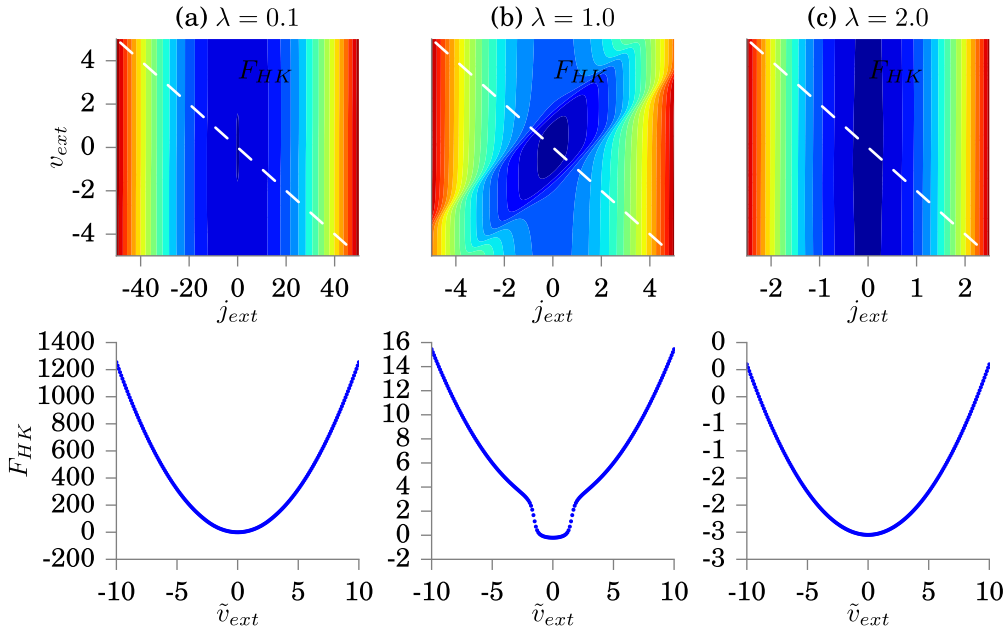

Figure 35: Two electrons with $U_0 = 5$: the Hohenberg-Kohn functional F_{HK} as function of the external variables (v_{ext}, j_{ext}) is shown in the first row. The second row shows the antidiagonal cut of $F_{HK}(v_{ext}, j_{ext})$ as indicated by the dashed line in the upper plot. The third row shows the diagonal cut of $F_{HK}(v_{ext}, j_{ext})$. From left to right the coupling strength is equal to (a) $\lambda = 0.1$, (b) $\lambda = 1$, and (c) $\lambda = 2$.

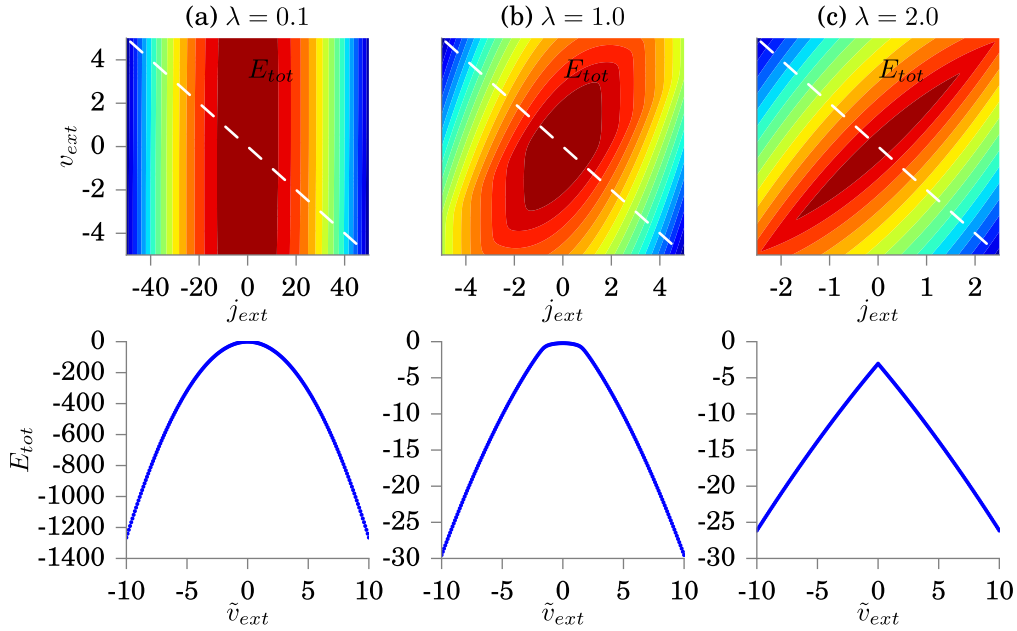

Figure 36: Two electrons with $U_0 = 5$: the total energy E_{tot} as function of the external variables (v_{ext}, j_{ext}) is shown in the first row. The second row shows the antidiagonal cut of $E_{tot}(v_{ext}, j_{ext})$ as indicated by the dashed line in the upper plot. The third row shows the diagonal cut of $E_{tot}(v_{ext}, j_{ext})$. From left to right the coupling strength is equal to (a) $\lambda = 0.1$, (b) $\lambda = 1$, and (c) $\lambda = 2$.

we find a rotation in the contour plots in the upper part of Fig. 36 that is the strongest for $\lambda = 2.0$. In the cut along the normal mode for $\lambda = 2$ we find that the sharpening of the observable-to-potential maps is also visible in the density-to-potential map.

The next observable we study is the interaction energy E_{int} that can be defined from Eq. 174 by $E_{\text{int}} = \omega\langle\hat{q}\,\hat{d}\rangle$. It is connected to the exchange-correlation energy by

$$E_{\text{xc}} = E_{\text{int}} - E_{\text{int, mf}} = \omega\left(\langle\hat{q}\,\hat{d}\rangle - q\,d\right) \tag{204}$$

The interaction energy $E_{int}[v_{ext}, j_{ext}]$ for the two-site Rabi-Hubbard model is shown

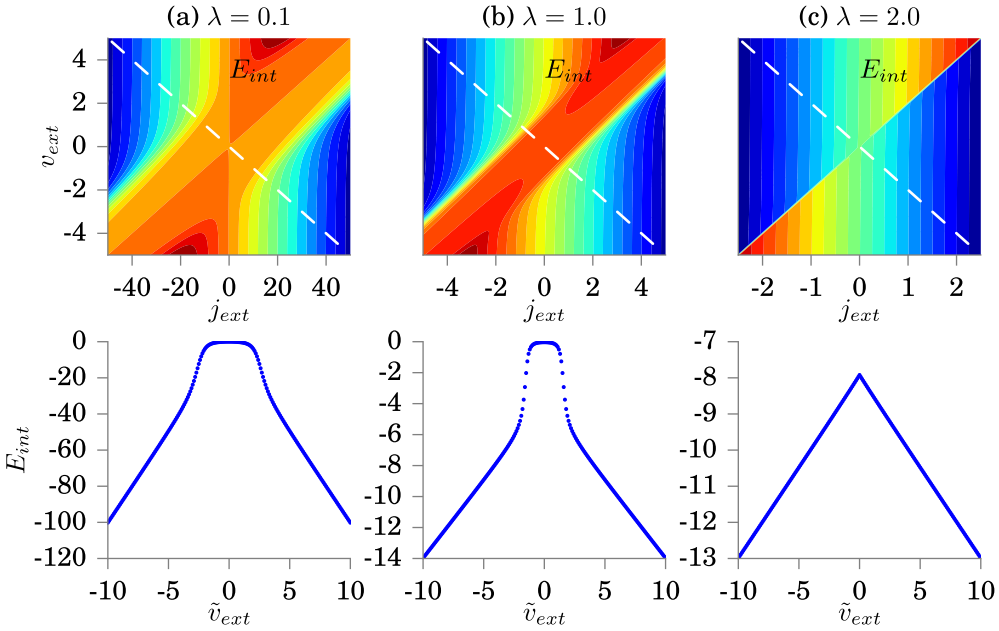

Figure 37: Two electrons with $U_0 = 5$: the interaction energy $E_{int} = \omega\langle\hat{q}\hat{d}\rangle$ as function of the external variables (v_{ext}, j_{ext}) is shown in the first row. The second row shows the antidiagonal cut of $E_{int}(v_{ext}, j_{ext})$ as indicated by the dashed line in the upper plot. The third row shows the diagonal cut of $E_{int}(v_{ext}, j_{ext})$. From left to right the coupling strength is equal to (a) $\lambda = 0.1$, (b) $\lambda = 1$, and (c) $\lambda = 2$.

in Fig. 37 and the corresponding observable in mean-field approximation is shown in Fig. 38. In (a), the weak-coupling is shown. We find here the new normal coordinates and the intermediate step causes a distinguishable behavior around $\tilde{v}_{\text{ext}} \sim 0$. This intermediate step becomes smaller for $\lambda = 1$ shown in (b). In the strong-coupling limit, the interaction energy has a vanishing step in the exact solution of the problem shown in Fig. 37 (c). In contrast the mean-field solution fails to correctly reproduce the exact sharp feature of the interaction energy. For $\lambda = 1$ the failure of the mean-field approximation can be traced back to the mean-field energies that are plotted in Fig. 9. We find while the exact energy is a concave function in $\tilde{v}_{\text{ext}}$, the mean-field energy shows a loop-like function in the area highlighted in red in Fig. 9.

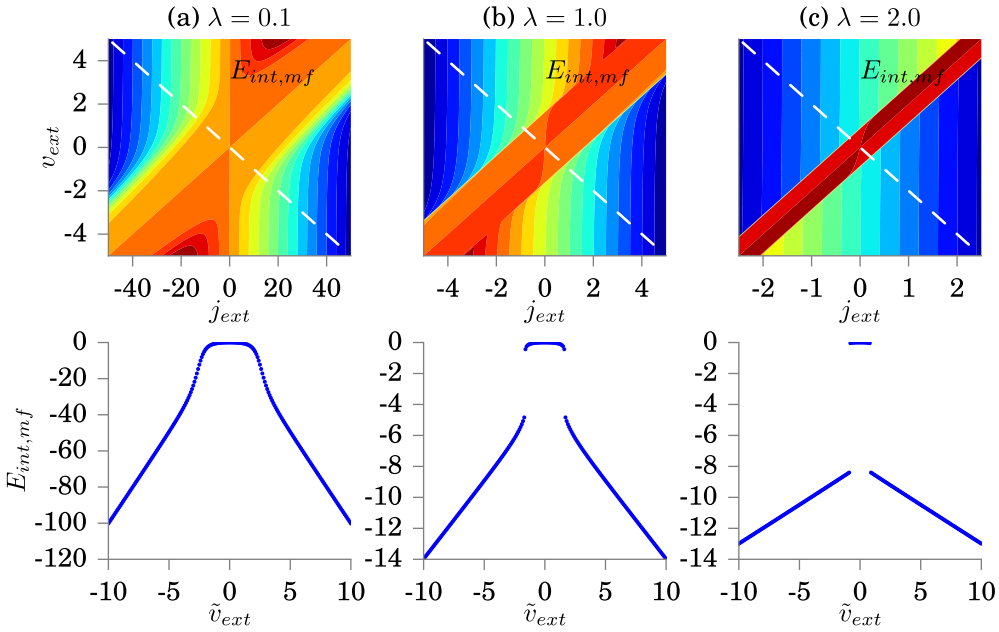

Figure 38: Two electrons with $U_0 = 5$: the interaction energy $E_{int,mf} = \omega q d$ in mean-field approximation as function of the external variables (v_{ext}, j_{ext}) is shown in the first row. The second row shows the antidiagonal cut of $E_{int,mf}(v_{ext}, j_{ext})$ as indicated by the dashed line in the upper plot. The third row shows the diagonal cut of $E_{int,mf}(v_{ext}, j_{ext})$. All plots for different coupling strength of (a) $\lambda = 0.1$, (b) $\lambda = 1$, and (c) $\lambda = 2$.

7.5 FOUR-SITE RABI-HUBBARD MODEL

In the following, we consider a four-site Rabi-Hubbard model. We use this section to demonstrate the implications of the discussed modifications of the density-to-potential map under strong light-matter coupling. The extension of Eq. 174 to four sites is straightforward and the Hamiltonian for half-filling (four electrons) reads explicitly

$$\hat{H}_0 = -t_0 \sum_{i=1}^{3} \sum_{\sigma=\uparrow,\downarrow} \left(\hat{c}^\dagger_{i,\sigma} \hat{c}_{i+1,\sigma} + \hat{c}^\dagger_{i+1,\sigma} \hat{c}_{i,\sigma} \right) + U_0 \sum_{i=1}^{4} \hat{n}_{i,\uparrow} \hat{n}_{i,\downarrow} + \omega \hat{a}^\dagger \hat{a} + \omega \lambda \hat{q} \hat{d} + \frac{j_{\text{ext}}}{\omega} \hat{q} + v_{\text{ext}} \hat{d} \tag{205}$$

with $\hat{d} = d_0 \left(3n_1 + n_2 - n_3 - 3n_4\right)$. In this case, v_{ext} effectively is an external electric field, as routinely studied in electronic-structure calculations. Physically the gradient of the dipole moment to the external electric field describes the electric polarizability α [258]. In this spirit, we define the electric polarizability as follows

$$\alpha[v_{\text{ext}}] = \frac{\delta d}{\delta v_{\text{ext}}}, \tag{206}$$

where v_{ext} describes the external electric field applied to the system as defined by Eq. 205. We note that for the two-site Rabi-Hubbard model studied in the previous section, the polarizability α is the gradient of the density-to-potential

map. Thus, the larger the gradient in the mapping becomes, the larger values for the polarizability are obtained. In conducting polymers, it has been demonstrated that this high polarizability is directly connected to charge-transfer, i.e. conductivity [258–260]. In Fig. 39, we show how the dipole moment d and the

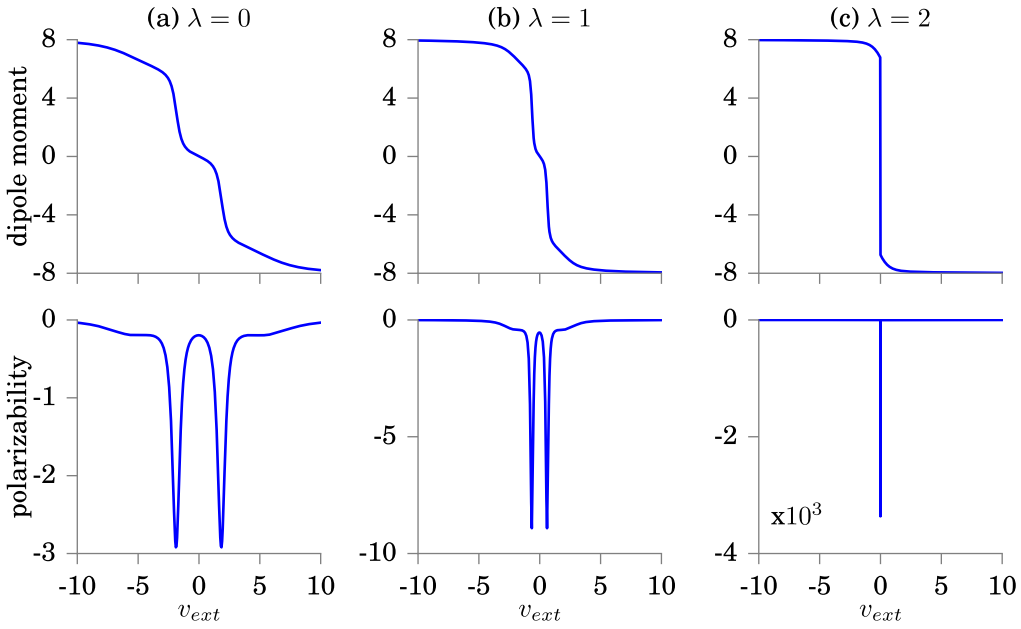

Figure 39: Four electrons with $U_0 = 2$: the dipole moment d as function of the electric field v_{ext} is shown in the first row. The second row shows the polarizability α as defined in the main text. All plots for different coupling strength of (a) $\lambda = 0$, (b) $\lambda = 1$, and (c) $\lambda = 2$.

polarizability α as function of the applied external potential v_{ext} change under strong light-matter coupling. Without coupling, shown in Fig. 39 (a), we find that the dipole moment develops three quasi-stationary regions and can take values between -8 and 8. These extremal values correspond to the situation, where two electrons occupy the outermost site and the other two electrons occupy the neighboring site. In the lower panel of the figure, we plot the polarizability α as defined in Eq. 206. We find two peaks in between the stationary regions of the dipole moment. If we now increase the electron-photon coupling, shown in Fig. 39 (b) for the case of $\lambda = 1$, we find that similarly as reported in the previous section, the dipole moment as function of the external potential steepens and the step around $v_{\text{ext}} \sim 0$ becomes narrower. Accordingly, the two peaks in the polarization shown in the bottom panel are closer together and have larger amplitudes in comparison to the setup in Fig. 39 (a). In the strong-coupling limit ($\lambda = 2$) shown in Fig. 39 (c), we find that the middle step completely vanishes and the two peaks shown in the bottom panel collapse into a single high amplitude peak. This can be interpret such that for neutral systems that do not have a permanent dipole moment, we find a very high polarizability, if the system is strongly coupled to a single photon mode.

7.6 SUMMARY

In this chapter, we have generalized the concept of the intra-system steepening and demonstrated its applicability for strong light-matter coupling. We have shown how the density-to-potential map in ground-state QEDFT can be expressed as functionals of the internal variables. For a two site model, we have demonstrated how this mapping is modified under strong-light matter coupling. Additionally, we demonstrated how this affects observables that are functional of the internal and the external variables. For a four-site model with four electrons, we have explicitly constructed the electric dipole moment as function of the external electric field and the polarizability of the system under strong light-matter interaction. These results of the increase in the polarizability are directly relevant for experiments such as in Ref. [49], where an increase in conductivity for organic semiconductors in strong coupling was measured.

Part IV

SUMMARY&OUTLOOK- GOING BEYOND MODEL SYSTEMS

8

SUMMARY AND OUTLOOK

In this work, we have illustrated fundamental concepts of DFT and ground-state QEDFT by investigating their underlying fundamental maps. While DFT exploits the map between the ground-state density and the local external potential, ground-state QEDFT exploits the map between the set of internal variables $(n(\vec{r}), q_\alpha)$ and the set of external variables $(v_{\text{ext}}(\vec{r}), j_{\text{ext}}^{(\alpha)})$. For simple but general interacting lattice models we have constructed and analyzed the relevant maps in DFT and QEDFT from weak to strong coupling between fragments within the system. Of particular interest is the electronic ground-state density that is the internal variable in DFT as well as one of the internal variables in QEDFT. The exact xc potential of realistic systems is unknown. The exact density-to-potential map as well as the effective density-to-potential of model systems help to learn about the unknown xc potential of realistic systems.

Furthermore the density-to-potential map helps to develop observable functionals. Such functional expressions of arbitrary observables are a crucial ingredient for the practicability of DFT and QEDFT. Additionally, the density-to-potential map helps to identify and understand novel physical effects and situations such as the reduced dipole map in the four-particle case, where a very high polarizability is found in the strong-coupling case. These results of the increase in the polarizability are directly relevant for experiments such as in Ref. [49], where an increase in conductivity for organic semiconductors in strong coupling was measured. Constructing the density-to-potential map helps us to identify and understand such drastic changes.

In particular, we have used the concept of the effective density-to-potential map to illustrate how static correlation is captured in the exact maps between conjugated pairs of variables. As subsystems in DFT, we refer to the spatially separated fragments that contain different electrons, e.g. atoms in a molecule or the individual sites in a two-site lattice model. In the models that we have used to illustrate the concepts of DFT, we have tuned the correlation by the parameter d and φ that determine the spatial distance between the subsystems and the ratio between electron-electron repulsion and the kinetic energy. As subsystems in QEDFT we refer to the individual fragments of the matter part and to the field part. To study the correlation in the models that we have used to illustrate the concepts of QEDFT we have tuned the parameter λ that determines the coupling strength between the matter and field part, and the ratio between electron-electron repulsion and the kinetic energy. To characterize the correlation between the above defined subsystems, we have introduced the concept of the intrasystem steepening and discussed how it relates to the well-known intersystem derivative discontinuity. Both features are features of the effective density-to-potential map along specific cuts of the real-space density that are linked to the electron localization

over subsystems within the system. The intersystem derivative discontinuity describes the functional behavior along the particle number of the total system while the system is weakly coupled to an external bath (due to the coupling we regard both as subsystems otherwise the particle number of the system could not change). The straight-line behavior with the related intersystem derivative discontinuity is an exact condition whenever the ground-state energy as function of the external potential coincides with a real degeneracy. The intrasystem steepening instead shows the functional behavior along the cut in the variable δn, i.e. the density difference between weakly-to-strongly coupled subsystems with non-degenerate ground-state. With increasing coupling strength, the intrasystem steepening is a feature that sharpens whenever the eigenenergies as function of the external potential approach a degeneracy. In the limit, when the eigenenergies show a real-degeneracy, the intrasystem steepening transitions into the well-known intersystem derivative discontinuity, and functionals $F[\delta n]$ show the straight-line behavior. Both features are related to processes which change the particle number of an subsystem in time and characterize the static correlation between the subsystems.

We carved out that the intrasystem steepening and the intersystem derivative discontinuity are conceptually different features within DFT. Furthermore, we illustrated that the features of the density-to-potential map directly transmit to the wavefunction-to-density map. For our model systems, we have constructed the ground-state wavefunctional and the functional dependency of selected observables. As examples for electronic observables we have shown the density dependency of the ground- and excited state energies, the ground- and excited state densities, and the correlation entropy. As example of photonic observables we have shown the photon number. All of the shown functionals are affected by the intrasystem steepening and the intersystem derivative discontinuity.

The intrasystem steepening is linked to processes where particles are transferred from one fragment to another fragment within a system of fixed particle number such as stretched molecules, charge-transfer processes and any problem involving highly localized electrons. We expect approximate functionals may fail to describe such problems because of the lack of the intrasystem steepening feature. Given the relevance of the above mentioned problems it is crucial to develop improved density functionals that capture this exact condition of the exact density-to-potential and density-to-wavefunction maps. In the highly localized electron limit the exact xc-functional does not present a straight line behavior but rather a sharp but differentiable one. To improve the accuracy of DFT and QEDFT observables, approximate functionals should capture both, the intersystem derivative discontinuity and the intrasystem steepening respectively.

For future work, these ideas will have impact on the role of the electron-electron interactions within the functional development of conventional density-functional theory and we will study the density-to-potential maps in full real-space. We are optimistic that the development of functionals in the case of the electron-photon interaction can be complementary to the functional development of electron-

electron interaction and thus allows for new routes in the search of novel functionals. With this in mind the results of model systems as the ones we have studied in this work can be extrapolated to larger, i.e. more realistic molecular systems.

Our results allow to learn about the exact properties of any desired functional, to test approximate functionals and how the approximate functional perform to describe the properties of different types of systems, in particular from weak to strong coupling. Our approach e.g. allows to learn about the kinetic energy functional which is of interest in orbital free DFT [261]. Further, our results also allow to get insight about spin DFT functionals as the magnetization of the N electron system can be written in terms of the ground-state density similar to the observables we discussed in this thesis. This is a way to tackle the known problems of spin DFT [123, 262] that will require going beyond present adiabatic functionals. Many physical processes can be theoretically analyzed and understood by studying simplified model systems such as exactly solvable one-dimensional lattice models. In this thesis we have analyzed an important exact condition of the density-to-potential map. The next step is to transfer the gained insight from the lattice model Hamiltonians to real continuous systems. Such realistic systems are in contact with their environment and can change in time. Therefore, the intrasystem steepening should be also studied within the framework of TDDFT.

As seen in Fig. 16 the effective density-to-potential map in the LDA approximation lacks the intrasystem steepening directly leading to errors in the dissociation energy as shown in Fig. 12. Beyond the results shown in this thesis we have tried different ways to fix this shortcoming of LDA by employing the insights from the exact maps of the two-site lattice model. Using the LDA allows to study large realistic systems, where no exact solution can be obtained. However, for strongly correlated systems we have discussed that the LDA can lead to wrong results. Therefore, we aim at curing the LDA density of the realistic system within the self-consistent cycle at each iteration step. The idea is to relate the LDA system to a two-site system that can be solved exactly. This exact solution then leads to corrections for the LDA solution. One of the major problems we encountered is how to relate the model parameters of the real-space description to the reduced few-site model. We find that simple schemes such as using the LDA kinetic and electron electron interaction energy of the real-space model as input parameters for the reduced few-site model could not correctly reproduce the features of the exact density-to-potential map. Therefore, we have come to the conclusion that more sophisticated methods that allow to construct the mapping from real-space to few sites in a consistent manner should be applied. Such methods are for instance embedding and coarse grained methods, e.g. DMET [153, 263, 264] that allows to decompose the system by applying the Schmidt decomposition. We are optimistic that in this way the insight from the model systems can be directly transferred to more realistic systems. The framework of DMET allows to go from model systems to realistic three-dimensional systems in a consistent manner. Work along these lines is in progress.

BIBLIOGRAPHY

[1] H. Czichos, T. Saito, and L. Smith, *Springer handbook of materials measurement methods*, vol. 978, Springer Berlin, 2006 (cit. on p. 1).

[2] F. David, *The Formalisms of Quantum Mechanics*, Springer International Publishing, 2016, DOI: 10.1007/978-3-319-10539-0 (cit. on p. 1).

[3] G Binning and H Rohrer, *Scanning tunneling microscopy*, Springer, 1986, 40–54 (cit. on p. 2).

[4] I. I. Rabi, J. R. Zacharias, S. Millman, and P. Kusch, *A New Method of Measuring Nuclear Magnetic Moment*, Phys. Rev. **53**, 4, 318–318 (1938), DOI: 10.1103/PhysRev.53.318 (cit. on p. 2).

[5] J. Bardeen and W. H. Brattain, *The Transistor, A Semi-Conductor Triode*, Phys. Rev. **74**, 2, 230–231 (1948), DOI: 10.1103/PhysRev.74.230 (cit. on p. 2).

[6] M. A. Kastner, *The single-electron transistor*, Rev. Mod. Phys. **64**, 3, 849–858 (1992), DOI: 10.1103/RevModPhys.64.849 (cit. on p. 2).

[7] N. Zheludev, *The life and times of the LED — a 100-year history*, Nature Photonics **1**, 4, 189–192 (2007), DOI: 10.1038/nphoton.2007.34 (cit. on p. 2).

[8] I. Robel, V. Subramanian, M. Kuno, and P. V. Kamat, *Quantum Dot Solar Cells. Harvesting Light Energy with CdSe Nanocrystals Molecularly Linked to Mesoscopic TiO2Films*, Journal of the American Chemical Society **128**, 7, 2385–2393 (2006), DOI: 10.1021/ja056494n (cit. on p. 2).

[9] G. R. Fleming and G. D. Scholes, *Physical chemistry: Quantum mechanics for plants*, Nature **431**, 7006, 256–257 (2004), DOI: 10.1038/431256a (cit. on p. 2).

[10] N. Lambert, Y.-N. Chen, Y.-C. Cheng, C.-M. Li, G.-Y. Chen, and F. Nori, *Quantum biology*, Nature Physics **9**, 1, 10–18 (2012), DOI: 10.1038/nphys2474 (cit. on p. 2).

[11] J. Bardeen, L. N. Cooper, and J. R. Schrieffer, *Theory of Superconductivity*, Phys. Rev. **108**, 5, 1175–1204 (1957), DOI: 10.1103/PhysRev.108.1175 (cit. on p. 2).

[12] P Kapitza, *Viscosity of liquid helium below the λ-point*, Nature **141**, 3558, 74 (1938) (cit. on p. 2).

[13] J. Allen and A. Misener, *Flow phenomena in liquid helium II*, Nature **142**, 3597, 643–644 (1938) (cit. on p. 2).

[14] M. W. Zwierlein, J. R. Abo-Shaeer, A. Schirotzek, C. H. Schunck, and W. Ketterle, *Vortices and superfluidity in a strongly interacting Fermi gas*, Nature **435**, 7045, 1047–1051 (2005) (cit. on p. 2).

[15] J. D. Macomber and R. Lynch, *Squeezed spin states*, The Journal of Chemical Physics **83**, 12, 6514–6519 (1985), DOI: 10.1063/1.449838 (cit. on p. 2).

[16] M. Kitagawa and M. Ueda, *Squeezed spin states*, Phys. Rev. A **47**, 6, 5138–5143 (1993), DOI: 10.1103/PhysRevA.47.5138 (cit. on p. 2).

[17] J. Franck and G. Hertz, *Über Zusammenstöße zwischen Elektronen und den Molekülen des Quecksilberdampfes und die Ionisierungsspannung desselben*, Physik Journal **23**, 7, 294–301 (1967), DOI: 10.1002/phbl.19670230702 (cit. on p. 2).

[18] W. Gerlach and O. Stern, *Der experimentelle Nachweis des magnetischen Moments des Silberatoms*, Zeitschrift für Physik **8**, 1, 110–111 (1922), DOI: 10.1007/BF01329580 (cit. on p. 2).

[19] B. Friedrich and D. Herschbach, *Stern and Gerlach: How a bad cigar helped reorient atomic physics*, Physics Today **56**, 12, 53–59 (2003), DOI: http://dx.doi.org/10.1063/1.1650229 (cit. on p. 2).

[20] H. Hertz, *Ueber einen Einfluss des ultravioletten Lichtes auf die electrische Entladung*, Annalen der Physik **267**, 8, 983–1000 (1887), DOI: 10.1002/andp.18872670827 (cit. on p. 2).

[21] R. A. Millikan, *A Direct Determination of "h."* Phys. Rev. **4**, 1, 73–75 (1914), DOI: 10.1103/PhysRev.4.73.2 (cit. on p. 2).

[22] A. H. Compton, *A Quantum Theory of the Scattering of X-rays by Light Elements*, Phys. Rev. **21**, 5, 483–502 (1923), DOI: 10.1103/PhysRev.21.483 (cit. on p. 2).

[23] A. Einstein, *Über einen die Erzeugung und Verwandlung des Lichtes betreffenden heuristischen Gesichtspunkt*, Annalen der Physik **322**, 6, 132–148 (1905), DOI: 10.1002/andp.19053220607 (cit. on p. 2).

[24] C. Davisson and L. H. Germer, *Diffraction of Electrons by a Crystal of Nickel*, Phys. Rev. **30**, 6, 705–740 (1927), DOI: 10.1103/PhysRev.30.705 (cit. on p. 2).

[25] I. Estermann and O. Stern, *Beugung von Molekularstrahlen*, Zeitschrift für Physik **61**, 1, 95–125 (1930), DOI: 10.1007/BF01340293 (cit. on p. 2).

[26] H. v. Halban and P. Preiswerk, *Preuve expérimentale de la diffraction des neutrons*, C. R. Acad. Sci. Paris **203**, 73–75 (1936) (cit. on p. 2).

[27] M. Arndt, O. Nairz, J. Vos-Andreae, C. Keller, G. van der Zouw, and A. Zeilinger, *Wave–particle duality of C60 molecules*, Nature **401**, 6754, 680–682 (1999), DOI: 10.1038/44348 (cit. on p. 2).

[28] E. Schrödinger, *Der stetige Übergang von der Mikro- zur Makromechanik*, Naturwissenschaften **14**, 28, 664–666 (1926), DOI: 10.1007/BF01507634 (cit. on p. 2).

[29] E. Schrödinger, *An Undulatory Theory of the Mechanics of Atoms and Molecules*, Phys. Rev. **28**, 6, 1049–1070 (1926), DOI: 10.1103/PhysRev.28.1049 (cit. on p. 2).

[30] E. Schrödinger, *Über das Verhältnis der Heisenberg-Born-Jordanschen Quantenmechanik zu der meinem*, Annalen der Physik **384**, 8, 734–756 (1926), DOI: 10.1002/andp.19263840804 (cit. on p. 2).

[31] W. Heisenberg, *Über quantentheoretische Umdeutung kinematischer und mechanischer Beziehungen.* Zeitschrift für Physik **33**, 1, 879–893 (1925), DOI: 10.1007/BF01328377 (cit. on p. 2).

[32] M. Born and P. Jordan, *Zur Quantenmechanik*, Zeitschrift für Physik **34**, 1, 858–888 (1925), DOI: 10.1007/BF01328531 (cit. on p. 2).

[33] M. Born, W. Heisenberg, and P. Jordan, *Zur Quantenmechanik. II.* Zeitschrift für Physik **35**, 8, 557–615 (1926), DOI: 10.1007/BF01379806 (cit. on p. 2).

[34] A. Einstein, B. Podolsky, and N. Rosen, *Can Quantum-Mechanical Description of Physical Reality Be Considered Complete?* Phys. Rev. **47**, 10, 777–780 (1935), DOI: 10.1103/PhysRev.47.777 (cit. on pp. 2, 12).

[35] N. Bohr, *Can Quantum-Mechanical Description of Physical Reality be Considered Complete?* Phys. Rev. **48**, 8, 696–702 (1935), DOI: 10.1103/PhysRev.48.696 (cit. on p. 2).

[36] N. Bohr, *Discussion with Einstein on epistemological problems in atomic physics*, University of Copenhagen, 1949 (cit. on p. 2).

[37] A. C. de la Torre, A Daleo, and I García-Mata, *The photon-box Bohr-Einstein debate demythologized*, European Journal of Physics **21**, 3, 253–260 (2000), DOI: 10.1088/0143-0807/21/3/308 (cit. on p. 2).

[38] N. R. Hanson, *Copenhagen interpretation of quantum theory*, American Journal of Physics **27**, 1, 1–15 (1959) (cit. on p. 2).

[39] L. E. Ballentine, *The Statistical Interpretation of Quantum Mechanics*, Rev. Mod. Phys. **42**, 4, 358–381 (1970), DOI: 10.1103/RevModPhys.42.358 (cit. on p. 2).

[40] H. Everett, *"Relative State" Formulation of Quantum Mechanics*, Rev. Mod. Phys. **29**, 3, 454–462 (1957), DOI: 10.1103/RevModPhys.29.454 (cit. on p. 2).

[41] B. DeWitt and N. Graham, *The Many-Worlds Interpretation of Quantum Mechanics*, Princeton Series in Physics, Princeton University Press, ISBN: 9780783719429 (cit. on p. 2).

[42] D. Bohm, *A Suggested Interpretation of the Quantum Theory in Terms of "Hidden" Variables. I*, Phys. Rev. **85**, 2, 166–179 (1952), DOI: 10.1103/PhysRev.85.166 (cit. on p. 2).

[43] D. Bohm, *A Suggested Interpretation of the Quantum Theory in Terms of "Hidden" Variables. II*, Phys. Rev. **85**, 2, 180–193 (1952), DOI: 10.1103/PhysRev.85.180 (cit. on p. 2).

[44] R. J. Bartlett and M. Musiał, *Coupled-cluster theory in quantum chemistry*, Reviews of Modern Physics **79**, 1, 291 (2007) (cit. on p. 3).

[45] C. Møller and M. S. Plesset, *Note on an Approximation Treatment for Many-Electron Systems*, Phys. Rev. **46**, 7, 618–622 (1934), DOI: 10.1103/PhysRev.46.618 (cit. on p. 3).

[46] R. A. Friesner, *Ab initio quantum chemistry: Methodology and applications*, Proceedings of the National Academy of Sciences **102**, 19, 6648–6653 (2005), DOI: 10.1073/pnas.0408036102 (cit. on p. 3).

[47] W. Kohn, *Nobel Lecture: Electronic structure of matter—wave functions and density functionals*, Rev. Mod. Phys. **71**, 5, 1253–1266 (1999), DOI: 10.1103/RevModPhys.71.1253 (cit. on pp. 3, 7, 44).

[48] M. Slootsky, X. Liu, V. M. Menon, and S. R. Forrest, *Room Temperature Frenkel-Wannier-Mott Hybridization of Degenerate Excitons in a Strongly Coupled Microcavity*, Phys. Rev. Lett. **112**, 7, 076401 (2014), DOI: 10.1103/PhysRevLett.112.076401 (cit. on p. 3).

[49] E. Orgiu, J. George, J. A. Hutchison, E. Devaux, J. F. Dayen, B. Doudin, F. Stellacci, C. Genet, J. Schachenmayer, C. Genes, G. Pupillo, P. Samorì, and T. W. Ebbesen, *Conductivity in organic semiconductors hybridized with the vacuum field*, Nat. Mater. **14**, 11, 1123–1129 (2015), DOI: 10.1038/nmat4392 (cit. on pp. 3, 98, 101).

[50] A. Shalabney, J. George, J. Hutchison, G. Pupillo, C. Genet, and T. W. Ebbesen, *Coherent coupling of molecular resonators with a microcavity mode*, Nat. Commun. **6**, 5981 (2015), DOI: 10.1038/ncomms6981 (cit. on p. 3).

[51] A. Shalabney, J. George, H. Hiura, J. A. Hutchison, C. Genet, P. Hellwig, and T. W. Ebbesen, *Enhanced Raman Scattering from Vibro-Polariton Hybrid States*, Angewandte Chemie **127**, 27, 8082–8086 (2015), DOI: 10.1002/ange.201502979 (cit. on p. 3).

[52] J. George, A. Shalabney, J. A. Hutchison, C. Genet, and T. W. Ebbesen, *Liquid-Phase Vibrational Strong Coupling*, The Journal of Physical Chemistry Letters **6**, 6, 1027–1031 (2015), DOI: 10.1021/acs.jpclett.5b00204 (cit. on p. 3).

[53] J. George, T. Chervy, A. Shalabney, E. Devaux, H. Hiura, C. Genet, and T. W. Ebbesen, *Multiple Rabi Splittings under Ultrastrong Vibrational Coupling*, Phys. Rev. Lett. **117**, 15, 153601 (2016), DOI: 10.1103/PhysRevLett.117.153601 (cit. on p. 3).

[54] A. Thomas, J. George, A. Shalabney, M. Dryzhakov, S. J. Varma, J. Moran, T. Chervy, X. Zhong, E. Devaux, C. Genet, J. A. Hutchison, and T. W. Ebbesen, *Ground-State Chemical Reactivity under Vibrational Coupling to the Vacuum Electromagnetic Field*, Angewandte Chemie International Edition **55**, 38, 11462–11466 (2016), DOI: 10.1002/anie.201605504 (cit. on p. 3).

[55] R. Chikkaraddy, B. de Nijs, F. Benz, S. J. Barrow, O. A. Scherman, E. Rosta, A. Demetriadou, P. Fox, O. Hess, and J. J. Baumberg, *Single-molecule strong coupling at room temperature in plasmonic nanocavities*, Nature **535**, 7610, 127–130 (2016), DOI: 10.1038/nature17974 (cit. on p. 3).

[56] E. J. Baerends and O. V. Gritsenko, *A Quantum Chemical View of Density Functional Theory*, The Journal of Physical Chemistry A **101**, 30, 5383–5403 (1997), DOI: 10.1021/jp9703768 (cit. on pp. 3, 25).

[57] K. Capelle, *A bird's-eye view of density-functional theory*, Brazilian Journal of Physics **36**, 4a, 1318–1343 (2006), DOI: 10.1590/s0103-97332006000700035 (cit. on pp. 3, 25, 31, 32).

[58] T. Ziegler, *Approximate density functional theory as a practical tool in molecular energetics and dynamics*, Chemical Reviews **91**, 5, 651–667 (1991), DOI: 10.1021/cr00005a001 (cit. on pp. 3, 25).

[59] W. Kohn, A. D. Becke, and R. G. Parr, *Density Functional Theory of Electronic Structure*, The Journal of Physical Chemistry **100**, 31, 12974–12980 (1996), DOI: 10.1021/jp960669l (cit. on pp. 3, 25).

[60] A. Pribram-Jones, D. A. Gross, and K. Burke, *DFT: A Theory Full of Holes?* Annual Review of Physical Chemistry **66**, 1, 283–304 (2015) (cit. on p. 3).

[61] G. E. Scuseria and V. N. Staroverov, *Progress in the development of exchange-correlation functionals*, Theory and applications of computational chemistry: the first **40**, 669–724 (2005) (cit. on pp. 3, 40, 42).

[62] N. D. Mermin, *What is quantum mechanics trying to tell us?* American Journal of Physics **66**, 9, 753–767 (1998), DOI: http://dx.doi.org/10.1119/1.18955 (cit. on p. 9).

[63] V. Apel, S. Curilef, and A. Plastino, *Entanglement and the process of measuring the position of a quantum particle*, Annals of Physics **354**, 570 –589 (2015), DOI: http://dx.doi.org/10.1016/j.aop.2015.01.019 (cit. on p. 9).

[64] C. M. Bender and S. Boettcher, *Real Spectra in Non-Hermitian Hamiltonians Having $\mathcal{PT}$ Symmetry*, Phys. Rev. Lett. **80**, 24, 5243–5246 (1998), DOI: 10.1103/PhysRevLett.80.5243 (cit. on p. 9).

[65] C. M. Bender, *Introduction to $\mathcal{PT}$-symmetric quantum theory*, Contemporary Physics **46**, 4, 277–292 (2005), DOI: 10.1080/00107500072632 (cit. on p. 9).

[66] A. K. Pati, U. Singh, and U. Sinha, *Measuring non-Hermitian operators via weak values*, Phys. Rev. A **92**, 5, 052120 (2015), DOI: 10.1103/PhysRevA.92.052120 (cit. on p. 9).

[67] R. Shoemaker and E. Van Stryland, *Direct measurements of transition dipole matrix elements using optical nutation*, The Journal of Chemical Physics **64**, 4, 1733–1740 (1976) (cit. on p. 10).

[68] J. P. Perdew, R. G. Parr, M. Levy, and J. L. Balduz, *Density-Functional Theory for Fractional Particle Number: Derivative Discontinuities of the Energy*, Phys. Rev. Lett. **49**, 23, 1691–1694 (1982) (cit. on pp. 11, 35, 36, 46).

[69] D. Dubbers and H.-J. Stöckmann, *"Spooky Action at a Distance"*, in: *Quantum Physics: The Bottom-Up Approach: From the Simple Two-Level System to Irreducible Representations*, Berlin, Heidelberg: Springer Berlin Heidelberg, 2013, 93–100, ISBN: 978-3-642-31060-7, DOI: 10.1007/978-3-642-31060-7_9 (cit. on p. 12).

[70] A. Ekert and P. L. Knight, *Entangled quantum systems and the Schmidt decomposition*, American Journal of Physics **63**, 5, 415–423 (1995), DOI: http://dx.doi.org/10.1119/1.17904 (cit. on p. 12).

[71] E. Schrödinger, *Die gegenwärtige Situation in der Quantenmechanik*, Naturwissenschaften **23**, 49, 823–828 (1935) (cit. on p. 12).

[72] K Eckert, J. Schliemann, D Bruss, and M Lewenstein, *Quantum correlations in systems of indistinguishable particles*, Annals of Physics **299**, 1, 88–127 (2002) (cit. on pp. 12, 13).

[73] M. B. Plenio and S. S. Virmani, "An Introduction to Entanglement Theory," in: *Quantum Information and Coherence*, Springer, 2014, 173–209 (cit. on p. 12).

[74] R. Horodecki, P. Horodecki, M. Horodecki, and K. Horodecki, *Quantum entanglement*, Rev. Mod. Phys. **81**, 2, 865–942 (2009), DOI: 10.1103/RevModPhys.81.865 (cit. on p. 12).

[75] L. Amico, R. Fazio, A. Osterloh, and V. Vedral, *Entanglement in many-body systems*, Rev. Mod. Phys. **80**, 2, 517–576 (2008), DOI: 10.1103/RevModPhys.80.517 (cit. on p. 12).

[76] H. Lo, T. Spiller, and S. Popescu, *Introduction to Quantum Computation and Information*, World Scientific, 1998, ISBN: 9789810244101 (cit. on p. 12).

[77] O. Sinanoğlu, *Many-Electron Theory of Atoms, Molecules and Their Interactions*, in: *Advances in Chemical Physics*, John Wiley & Sons, Inc., 2007, 315–412, ISBN: 9780470143520, DOI: 10.1002/9780470143520.ch7 (cit. on pp. 12, 23).

[78] O. Sinanogulu and D. F. tai Tuan, *Many-Electron Theory of Atoms and Molecules. III. Effect of Correlation on Orbitals*, The Journal of Chemical Physics **38**, 7, 1740 (1963), DOI: 10.1063/1.1776948 (cit. on p. 12).

[79] K. Boguslawski, P. Tecmer, Örs Legeza, and M. Reiher, *Entanglement Measures for Single- and Multireference Correlation Effects*, The Journal of Physical Chemistry Letters **3**, 21, 3129–3135 (2012), DOI: 10.1021/jz301319v (cit. on p. 12).

[80] N. C. Handy and A. J. Cohen, *Left-right correlation energy*, Molecular Physics **99**, 5, 403–412 (2001), DOI: 10.1080/00268970010018431 (cit. on p. 12).

[81] P. Ziesche, O. Gunnarsson, W. John, and H. Beck, *Two-site Hubbard model, the Bardeen-Cooper-Schrieffer model, and the concept of correlation entropy*, Phys. Rev. B **55**, 16, 10270–10277 (1997) (cit. on pp. 13, 84).

[82] J. Schliemann, J. I. Cirac, M. Ku ś, M. Lewenstein, and D. Loss, *Quantum correlations in two-fermion systems*, Phys. Rev. A **64**, 2, 022303 (2001) (cit. on pp. 13, 84).

[83] I. Franco and H. Appel, *Reduced purities as measures of decoherence in many-electron systems*, The Journal of Chemical Physics **139**, 9, 094109 (2013) (cit. on p. 13).

[84] P.-O. Löwdin, *Quantum Theory of Many-Particle Systems. I. Physical Interpretations by Means of Density Matrices, Natural Spin-Orbitals, and Convergence Problems in the Method of Configurational Interaction*, Phys. Rev. **97**, 6, 1474–1489 (1955), DOI: 10.1103/PhysRev.97.1474 (cit. on p. 13).

[85] S. Sharma, J. K. Dewhurst, N. N. Lathiotakis, and E. K. U. Gross, *Reduced density matrix functional for many-electron systems*, Phys. Rev. B **78**, 20, 201103 (2008), DOI: 10.1103/PhysRevB.78.201103 (cit. on p. 13).

[86] J. Schliemann, J. I. Cirac, M. Ku ś, M. Lewenstein, and D. Loss, *Quantum correlations in two-fermion systems*, Phys. Rev. A **64**, 2, 022303 (2001), DOI: 10.1103/PhysRevA.64.022303 (cit. on p. 13).

[87] J. D. Jackson, *Classical Electrodynamics*, 3rd ed., John Wiley & Sons, Inc., 1991 (cit. on p. 14).

[88] G. D. Mahan, *Many-particle physics*, Springer Science & Business Media, 2013 (cit. on p. 14).

[89] W. Vogel and D.-G. Welsch, *Quantum optics*, John Wiley & Sons, 2006 (cit. on pp. 14, 15, 17, 18).

[90] C. Cohen-Tannoudji, J. Dupont-Roc, and G. Grynberg, *Lagrangian and Hamiltonian Approach to Electrodynamics, The Standard Lagrangian and the Coulomb Gauge*, in: *Photons and Atoms*, Wiley-VCH Verlag GmbH, 2007, 79–168, ISBN: 9783527618422, DOI: 10.1002/9783527618422.ch2 (cit. on pp. 15–17).

[91] B. Huttner and S. M. Barnett, *Quantization of the electromagnetic field in dielectrics*, Phys. Rev. A **46**, 7, 4306–4322 (1992), DOI: 10.1103/PhysRevA.46.4306 (cit. on p. 15).

[92] L. A. Gergely, *On Hamiltonian Formulations of the Schrödinger System*, Annals of Physics **298**, 2, 394 –402 (2002), DOI: http://dx.doi.org/10.1006/aphy.2002.6262 (cit. on p. 15).

[93] C. Cohen-Tannoudji, B. Diu, and F. Laloë, *Quantenmechanik*, 2.Auflage, Wiley, 1999, ISBN: 3110164582 (cit. on p. 16).

[94] D. Craig and T. Thirunamachandran, *Molecular Quantum Electrodynamics*, Dover Books on Chemistry, Dover Publications, 2012, ISBN: 9780486135632 (cit. on pp. 18, 19, 21).

[95] F. Mandl and G. Shaw, *Quantum field theory*, John Wiley & Sons, 2010 (cit. on p. 21).

[96] J. R. Ackerhalt and P. W. Milonni, *Interaction Hamiltonian of quantum optics*, J. Opt. Soc. Am. B **1**, 1, 116–120 (1984), DOI: 10.1364/JOSAB.1.000116 (cit. on p. 21).

[97] M Babiker and R Loudon, "Derivation of the Power-Zienau-Woolley Hamiltonian in quantum electrodynamics by gauge transformation," in: *Proceedings of the Royal Society of London A: Mathematical, Physical and Engineering Sciences*, vol. 385, 1789, The Royal Society, 1983, 439–460 (cit. on p. 21).

[98] F. H. Faisal, *Theory of multiphoton processes*, Springer Science & Business Media, 2013 (cit. on p. 21).

[99] E. Gross, E. Runge, and O. Heinonen, *Many-Particle Theory*, Taylor & Francis, 1991, ISBN: 9780750301558 (cit. on pp. 21, 23).

[100] M. Born and R. Oppenheimer, *Zur Quantentheorie der Molekeln*, Annalen der Physik **389**, 20, 457–484 (1927), DOI: 10.1002/andp.19273892002 (cit. on p. 21).

[101] E. Engel and R. M. Dreizler, *Density functional theory: an advanced course*, Springer Science & Business Media, 2011 (cit. on pp. 21, 22, 44).

[102] J. C. Slater, *A Simplification of the Hartree-Fock Method*, Phys. Rev. **81**, 3, 385–390 (1951), DOI: 10.1103/PhysRev.81.385 (cit. on pp. 22, 23).

[103] V. Fock, *Näherungsmethode zur Lösung des quantenmechanischen Mehrkörperproblems*, Zeitschrift für Physik **61**, 1, 126–148 (1930), DOI: 10.1007/BF01340294 (cit. on p. 22).

[104] K. Ramachandran, G. Deepa, and K. Namboori, *Computational Chemistry and Molecular Modeling: Principles and Applications*, in: Berlin, Heidelberg: Springer Berlin Heidelberg, 2008, chap. Hartree-Fock Theory, 93–113, ISBN: 978-3-540-77304-7, DOI: 10.1007/978-3-540-77304-7_5 (cit. on pp. 22, 23).

[105] A. Szabo and N. Ostlund, *Modern Quantum Chemistry: Introduction to Advanced Electronic Structure Theory*, Dover Books on Chemistry, Dover Publications, 2012, ISBN: 9780486134598 (cit. on p. 23).

[106] R. McWeeny, *Methods in Computational Molecular Physics*, in: Boston, MA: Springer US, 1992, chap. The Electron Correlation Problem, 47–56, ISBN: 978-1-4615-7419-4, DOI: 10.1007/978-1-4615-7419-4_4 (cit. on p. 23).

[107] T. Helgaker, P. Jorgensen, and J. Olsen, *Molecular Electronic-Structure Theory*, Wiley, 2014, ISBN: 9781119019558 (cit. on p. 23).

[108] A. Pribram-Jones, D. A. Gross, and K. Burke, *DFT: A Theory Full of Holes?* Annual Review of Physical Chemistry **66**, 1, 283–304 (2015), DOI: 10.1146/annurev-physchem-040214-121420 (cit. on p. 25).

[109] P. Hohenberg and W. Kohn, *Inhomogeneous Electron Gas*, Phys. Rev. **136**, 3B, B864–B871 (1964) (cit. on pp. 25, 26, 28).

[110] E. Runge and E. K. Gross, *Density-functional theory for time-dependent systems*, Physical Review Letters **52**, 12, 997 (1984) (cit. on p. 25).

[111] E. Gross and W Kohn, *Time-dependent density-functional theory*, Advances in quantum chemistry **21**, 255–291 (1990) (cit. on p. 25).

[112] M. A. Marques and E. Gross, *Time-dependent density functional theory*, Annu. Rev. Phys. Chem. **55**, 427–455 (2004) (cit. on p. 25).

[113] C. A. Ullrich, *Time-dependent density-functional theory: concepts and applications*, OUP Oxford, 2011 (cit. on p. 25).

[114] M. Ruggenthaler, M. Penz, and R. van Leeuwen, *Existence, uniqueness, and construction of the density-potential mapping in time-dependent density-functional theory*, Journal of Physics: Condensed Matter **27**, 20, 203202 (2015) (cit. on pp. 25, 37, 38).

[115] T. Heaton-Burgess, P. Ayers, and W. Yang, *Spin-Potential Functional Formalism for Current-Carrying Noncollinear Magnetic Systems*, Phys. Rev. Lett. **98**, 3, 036403 (2007), DOI: 10.1103/PhysRevLett.98.036403 (cit. on p. 25).

[116] T. Dimitrov, H. Appel, J. I. Fuks, and A. Rubio, *Exact maps in density functional theory for lattice models*, New Journal of Physics **18**, 8, 083004 (2016) (cit. on pp. 27, 50, 56, 67, 69, 70, 72–74, 79, 82–85, 89, 129).

[117] E. S. Kryachko and E. V. Ludea, *Formulation of N - and v -representable density-functional theory. I. Ground states*, Phys. Rev. A **43**, 5, 2179–2193 (1991), DOI: 10.1103/PhysRevA.43.2179 (cit. on p. 27).

[118] W. Kohn, *v-Representability and Density Functional Theory*, Phys. Rev. Lett. **51**, 17, 1596–1598 (1983), DOI: 10.1103/PhysRevLett.51.1596 (cit. on p. 27).

[119] H Englisch and R Englisch, *V-representability in finite-dimensional spaces*, Journal of Physics A: Mathematical and General **16**, 18, L693 (1983) (cit. on pp. 27, 32).

[120] H. Englisch and R. Englisch, *Hohenberg-Kohn theorem and non-V-representable densities*, Physica A: Statistical Mechanics and its Applications **121**, 1–2, 253 –268 (1983) (cit. on pp. 27, 31, 32).

[121] J. Chayes, L. Chayes, and M. Ruskai, *Density functional approach to quantum lattice systems*, Journal of Statistical Physics **38**, 3-4, 497–518 (1985), DOI: 10.1007/BF01010474 (cit. on pp. 27, 32).

[122] N. Bourbaki, *Theory of Sets*, in: *Theory of Sets*, Berlin, Heidelberg: Springer Berlin Heidelberg, 2004, 65–129, ISBN: 978-3-642-59309-3, DOI: 10.1007/978-3-642-59309-3_3 (cit. on p. 27).

[123] K. Capelle and G. Vignale, *Nonuniqueness of the Potentials of Spin-Density-Functional Theory*, Phys. Rev. Lett. **86**, 24, 5546–5549 (2001) (cit. on pp. 27, 29, 103).

[124] R. Dreizler and E. Gross, *Density Functional Theory: An Approach to the Quantum Many-Body Problem*, Springer Berlin Heidelberg, 2012, ISBN: 9783642861055 (cit. on p. 28).

[125] W. Kutzelnigg, *Density functional theory in terms of a Legendre transformation for beginners*, Journal of Molecular Structure **768**, 1–3, 163 –173 (2006) (cit. on pp. 29, 30, 32, 33, 78).

[126] X.-Y. Pan and V. Sahni, *New perspectives on the fundamental theorem of density functional theory*, International Journal of Quantum Chemistry **108**, 15, 2756–2762 (2008), DOI: 10.1002/qua.21826 (cit. on p. 29).

[127] J. Tao, J. P. Perdew, V. N. Staroverov, and G. E. Scuseria, *Climbing the Density Functional Ladder: Nonempirical Generalized Gradient Approximation Designed for Molecules and Solids*, Phys. Rev. Lett. **91**, 14, 146401 (2003), DOI: 10.1103/PhysRevLett.91.146401 (cit. on p. 30).

[128] P. W. Ayers, *Axiomatic formulations of the Hohenberg-Kohn functional*, Phys. Rev. A **73**, 1, 012513 (2006), DOI: 10.1103/PhysRevA.73.012513 (cit. on pp. 31, 42).

[129] P. W. Ayers and S. Liu, *Necessary and sufficient conditions for the N-representability of density functionals*, Phys. Rev. A **75**, 2, 022514 (2007), DOI: 10.1103/PhysRevA.75.022514 (cit. on p. 31).

[130] J. Chen and M. Stott, *v-representability for noninteracting systems*, Physical Review A **47**, 1, 153 (1993) (cit. on pp. 31, 32).

[131] T. Gilbert, *Hohenberg-Kohn theorem for nonlocal external potentials*, Physical Review B **12**, 2111–2120 (1975) (cit. on p. 31).

[132] J. E. Harriman, *Orthonormal orbitals for the representation of an arbitrary density*, Phys. Rev. A **24**, 2, 680–682 (1981), DOI: 10.1103/PhysRevA.24.680 (cit. on p. 31).

[133] M. Levy, *Mathematical thoughts in DFT*, International Journal of Quantum Chemistry **116**, 11, 802–804 (2016) (cit. on p. 31).

[134] M. Levy, *Electron densities in search of Hamiltonians*, Phys. Rev. A **26**, 3, 1200–1208 (1982) (cit. on p. 31).

[135] E. H. Lieb, *Density functionals for coulomb systems*, International Journal of Quantum Chemistry **24**, 3, 243–277 (1983), DOI: 10.1002/qua.560240302 (cit. on pp. 31–34).

[136] M. Levy, *Universal variational functionals of electron densities, first-order density matrices, and natural spin-orbitals and solution of the v-representability problem*, Proceedings of the National Academy of Sciences **76**, 12, 6062–6065 (1979) (cit. on p. 32).

[137] P. W. Ayers and P. Fuentealba, *Density-functional theory with additional basic variables: Extended Legendre transform*, Phys. Rev. A **80**, 3, 032510 (2009), DOI: 10.1103/PhysRevA.80.032510 (cit. on pp. 32, 33).

[138] L. D. Site, *Levy–Lieb constrained-search formulation as a minimization of the correlation functional*, Journal of Physics A: Mathematical and Theoretical **40**, 11, 2787 (2007) (cit. on p. 32).

[139] T. T. Nguyen-Dang, R. F. W. Bader, and H. Essén, *Some properties of the Lagrange multiplier μ in density functional theory*, International Journal of Quantum Chemistry **22**, 5, 1049–1058 (1982), DOI: 10.1002/qua.560220517 (cit. on pp. 32, 33).

[140] R. F. Nalewajski and R. G. Parr, *Legendre transforms and Maxwell relations in density functional theory*, Journal of Chemical Physics **77**, 399–407 (1982) (cit. on pp. 32, 33).

[141] H. Eschrig, *The Fundamentals of Density Functional Theory*, in: Wiesbaden: Vieweg+Teubner Verlag, 1996, chap. Density Functional Theory by Lieb, 127–142, ISBN: 978-3-322-97620-8, DOI: 10.1007/978-3-322-97620-8_7 (cit. on pp. 32, 33, 76).

[142] G. P., D. P. F., and L. W., *Conceptual Density Functional Theory*, Chemical Reviews **103**, 5, 1793–1874 (2003), DOI: 10.1021/cr990029p (cit. on pp. 32, 33).

[143] C. A. Ullrich and W. Kohn, *Degeneracy in Density Functional Theory: Topology in the v and n Spaces*, Phys. Rev. Lett. **89**, 15, 156401 (2002), DOI: 10.1103/PhysRevLett.89.156401 (cit. on p. 32).

[144] P. E. Lammert, *Coarse-grained V representability*, The Journal of Chemical Physics **125**, 7, 074114, – (2006), DOI: http://dx.doi.org/10.1063/1.2336211 (cit. on p. 32).

[145] S. M. Valone, *Consequences of extending 1state representable to all ensemble representable 1 matrices*, The Journal of Chemical Physics **73**, 3, 1344–1349 (1980), DOI: http://dx.doi.org/10.1063/1.440249 (cit. on p. 33).

[146] S. M. Valone, *A one-to-one mapping between one-particle densities and some n-particle ensembles*, The Journal of Chemical Physics **73**, 9, 4653–4655 (1980) (cit. on p. 33).

[147] E. Chamorro, P. Fuentealba, and R. Contreras, *Higher order derivatives for nuclear indexes in the framework of density functional theory*, The Journal of Chemical Physics **115**, 15, 6822–6826 (2001), DOI: http://dx.doi.org/10.1063/1.1394755 (cit. on p. 34).

[148] W. Yang, Y. Zhang, and P. W. Ayers, *Degenerate Ground States and a Fractional Number of Electrons in Density and Reduced Density Matrix Functional Theory*, Phys. Rev. Lett. **84**, 22, 5172–5175 (2000) (cit. on pp. 35, 36).

[149] N. D. Mermin, *Thermal Properties of the Inhomogeneous Electron Gas*, Phys. Rev. **137**, 5A, A1441–A1443 (1965), DOI: 10.1103/PhysRev.137.A1441 (cit. on p. 36).

[150] M. A. Mosquera, D. Jensen, and A. Wasserman, *Fragment-Based Time-Dependent Density Functional Theory*, Phys. Rev. Lett. **111**, 2, 023001 (2013), DOI: 10.1103/PhysRevLett.111.023001 (cit. on pp. 36, 55).

[151] P. Elliott, K. Burke, M. H. Cohen, and A. Wasserman, *Partition density-functional theory*, Physical Review A **82**, 2, 024501 (2010) (cit. on p. 36).

[152] A. Krishtal, D. Sinha, A. Genova, and M. Pavanello, *Subsystem density-functional theory as an effective tool for modeling ground and excited states, their dynamics and many-body interactions*, Journal of Physics: Condensed Matter **27**, 18, 183202 (2015) (cit. on pp. 36, 37).

[153] G. Knizia and G. K.-L. Chan, *Density Matrix Embedding: A Simple Alternative to Dynamical Mean-Field Theory*, Phys. Rev. Lett. **109**, 18, 186404 (2012), DOI: 10.1103/PhysRevLett.109.186404 (cit. on pp. 36, 103).

[154] W. Yang, *Direct calculation of electron density in density-functional theory*, Phys. Rev. Lett. **66**, 11, 1438–1441 (1991), DOI: 10.1103/PhysRevLett.66.1438 (cit. on p. 36).

[155] F. L. Hirshfeld, *Bonded-atom fragments for describing molecular charge densities*, Theoretica chimica acta **44**, 2, 129–138 (1977) (cit. on p. 37).

[156] J. Nafziger and A. Wasserman, *Density-Based Partitioning Methods for Ground-State Molecular Calculations*, The Journal of Physical Chemistry A **118**, 36, 7623–7639 (2014), DOI: 10.1021/jp504058s (cit. on p. 37).

[157] R. F. W. Bader, P. M. Beddall, and P. E. Cade, *Partitioning and characterization of molecular charge distributions*, Journal of the American Chemical Society **93**, 13, 3095–3107 (1971) (cit. on p. 37).

[158] C. R. Jacob and L. Visscher, *A subsystem density-functional theory approach for the quantum chemical treatment of proteins*, The Journal of Chemical Physics **128**, 15, 155102 (2008), DOI: http://dx.doi.org/10.1063/1.2906128 (cit. on p. 37).

[159] I. V. Tokatly, *Time-Dependent Density Functional Theory for Many-Electron Systems Interacting with Cavity Photons*, Phys. Rev. Lett. **110**, 23, 233001 (2013), DOI: 10.1103/PhysRevLett.110.233001 (cit. on pp. 37, 38).

[160] C. Pellegrini, J. Flick, I. V. Tokatly, H. Appel, and A. Rubio, *Optimized Effective Potential for Quantum Electrodynamical Time-Dependent Density Functional Theory*, Phys. Rev. Lett. **115**, 9, 093001 (2015), DOI: 10.1103/PhysRevLett.115.093001 (cit. on pp. 37, 38, 55, 57).

[161] J. Flick, M. Ruggenthaler, H. Appel, and A. Rubio, *Atoms and Molecules in Cavities: From Weak to Strong Coupling in QED Chemistry*, arXiv:1609.03901 [quant-ph] arXiv: 1609.03901 (quant-ph) (2016) (cit. on pp. 37, 88).

[162] M. Ruggenthaler, F. Mackenroth, and D. Bauer, *Time-dependent Kohn-Sham approach to quantum electrodynamics*, Phys. Rev. A **84**, 4, 042107 (2011), DOI: 10.1103/PhysRevA.84.042107 (cit. on p. 38).

[163] M. Ruggenthaler, J. Flick, C. Pellegrini, H. Appel, I. V. Tokatly, and A. Rubio, *Quantum-electrodynamical density-functional theory: Bridging quantum optics and electronic-structure theory*, Phys. Rev. A **90**, 1, 012508 (2014), DOI: 10.1103/PhysRevA.90.012508 (cit. on pp. 38, 42, 56).

[164] K. Yabana, T. Sugiyama, Y. Shinohara, T. Otobe, and G. F. Bertsch, *Time-dependent density functional theory for strong electromagnetic fields in crystalline solids*, Phys. Rev. B **85**, 4, 045134 (2012), DOI: 10.1103/PhysRevB.85.045134 (cit. on p. 38).

[165] Y. Li, S. He, A. Russakoff, and K. Varga, *Accurate time propagation method for the coupled Maxwell and Kohn-Sham equations*, Phys. Rev. E **94**, 2, 023314 (2016), DOI: 10.1103/PhysRevE.94.023314 (cit. on p. 38).

[166] S. Kurth and J. P. Perdew, *Role of the exchange–correlation energy: Nature's glue*, International Journal of Quantum Chemistry **77**, 5, 814–818 (2000) (cit. on p. 40).

[167] A. Görling, *Kohn-Sham potentials and wave functions from electron densities*, Physical Review A **46**, 7, 3753 (1992) (cit. on p. 40).

[168] K. Burke et al., *The abc of dft*, Department of Chemistry, University of California (2007) (cit. on p. 40).

[169] W. Kohn and L. J. Sham, *Self-Consistent Equations Including Exchange and Correlation Effects*, Phys. Rev. **140**, 4A, A1133–A1138 (1965) (cit. on pp. 40, 45).

[170] J. Flick, M. Ruggenthaler, H. Appel, and A. Rubio, *Kohn–Sham approach to quantum electrodynamical density-functional theory: Exact time-dependent effective potentials in real space*, Proceedings of the National Academy of Sciences **112**, 50, 15285–15290 (2015), DOI: 10.1073/pnas.1518224112 (cit. on pp. 42, 55–57, 87).

[171] M. Ernzerhof and G. E. Scuseria, *Assessment of the PerdewErnzerhof exchange-correlation functional*, The Journal of Chemical Physics **110**, 11, 5029–5036 (1999), DOI: http://dx.doi.org/10.1063/1.478401 (cit. on p. 43).

[172] L. O. Wagner, E. M. Stoudenmire, K. Burke, and S. R. White, *Reference electronic structure calculations in one dimension*, Phys. Chem. Chem. Phys. **14**, 24, 8581–8590 (2012) (cit. on pp. 43, 63, 65).

[173] K. Capelle, N. Lima, M. Silva, and L. Oliveira, "Density-Functional Theory for the Hubbard Model: Numerical Results for the Luttinger Liquid and the Mott Insulator," in: *The Fundamentals of Electron Density, Density Matrix and Density Functional Theory in Atoms, Molecules and the Solid State*, ed. by N. Gidopoulos and S. Wilson, vol. 14, Progress in Theoretical Chemistry

and Physics, Springer Netherlands, 2003, 145–168, ISBN: 978-90-481-6508-7 (cit. on p. 43).

[174] D. J. Carrascal and J. Ferrer, *Exact Kohn-Sham eigenstates versus quasiparticles in simple models of strongly correlated electrons*, Phys. Rev. B **85**, 4, 045110 (2012) (cit. on p. 43).

[175] D. J. Carrascal, J. Ferrer, J. C. Smith, and K. Burke, *The Hubbard dimer: a density functional case study of a many-body problem*, Journal of Physics: Condensed Matter **27**, 39, 393001 (2015) (cit. on p. 43).

[176] J. I. Fuks, M. Farzanehpour, I. V. Tokatly, H. Appel, S. Kurth, and A. Rubio, *Time-dependent exchange-correlation functional for a Hubbard dimer: Quantifying nonadiabatic effects*, Physical Review A **88**, 6, 062512 (2013) (cit. on pp. 43, 54).

[177] J. I. Fuks and N. T. Maitra, *Challenging adiabatic time-dependent density functional theory with a Hubbard dimer: the case of time-resolved long-range charge transfer*, Phys. Chem. Chem. Phys. **16**, 28, 14504–14513 (2014) (cit. on p. 43).

[178] J. I. Fuks and N. T. Maitra, *Charge transfer in time-dependent density-functional theory: Insights from the asymmetric Hubbard dimer*, Phys. Rev. A **89**, 6, 062502 (2014), DOI: 10.1103/PhysRevA.89.062502 (cit. on p. 43).

[179] J. I. Fuks, P Elliott, A Rubio, and N. T. Maitra, *Dynamics of Charge-Transfer Processes with Time-Dependent Density Functional Theory*, J. Phys. Chem. Lett. **4**, 5, 735–739 (2013) (cit. on pp. 43, 65).

[180] O. V. Gritsenko, R. v. Leeuwen, and E. J. Baerends, *Molecular exchange-correlation Kohn–Sham potential and energy density from ab initio first-and second-order density matrices: Examples for XH (X= Li, B, F)*, The Journal of chemical physics **104**, 21, 8535–8545 (1996) (cit. on p. 43).

[181] M. A. Buijse, E. J. Baerends, and J. G. Snijders, *Analysis of correlation in terms of exact local potentials: Applications to two-electron systems*, Phys. Rev. A **40**, 8, 4190–4202 (1989) (cit. on p. 43).

[182] N. Helbig, I. V. Tokatly, and A. Rubio, *Exact Kohn–Sham potential of strongly correlated finite systems*, The Journal of Chemical Physics **131**, 22, 224105, – (2009), DOI: http://dx.doi.org/10.1063/1.3271392 (cit. on pp. 43, 44, 74).

[183] R. van Leeuwen, O. Gritsenko, and E. J. Baerends, *Step structure in the atomic Kohn-Sham potential*, Zeitschrift für Physik D Atoms, Molecules and Clusters **33**, 4, 229–238 (1995) (cit. on p. 44).

[184] M. J. P. Hodgson, J. D. Ramsden, and R. W. Godby, *Origin of static and dynamic steps in exact Kohn-Sham potentials*, Phys. Rev. B **93**, 15, 155146 (2016), DOI: 10.1103/PhysRevB.93.155146 (cit. on p. 44).

[185] J. Walkenhorst, *Analysis and Control of Transient Spectra Using Time-Dependent Density Functional Theory*, PhD thesis, Universidad del País Vasco, 2016 (cit. on pp. 44, 71).

[186] P Gori-Giorgi and A Savin, *Degeneracy and size consistency in electronic density functional theory*, Journal of Physics: Conference Series **117**, 1, 012017 (2008) (cit. on p. 44).

[187] P. Ziesche, S. Kurth, and J. P. Perdew, *Density functionals from {LDA} to {GGA}*, Computational Materials Science **11**, 2, 122 –127 (1998), DOI: http://dx.doi.org/10.1016/S0927-0256(97)00206-1 (cit. on p. 44).

[188] L. H. Thomas, *The calculation of atomic fields*, Mathematical Proceedings of the Cambridge Philosophical Society **23**, 05, 542–548 (1927), DOI: 10.1017/S0305004100011683 (cit. on p. 45).

[189] P. A. M. Dirac, *Note on Exchange Phenomena in the Thomas Atom*, **26**, 3, 376–385 (1930), DOI: 10.1017/S0305004100016108 (cit. on p. 45).

[190] A. D. Becke, *Density-functional exchange-energy approximation with correct asymptotic behavior*, Phys. Rev. A **38**, 6, 3098–3100 (1988), DOI: 10.1103/PhysRevA.38.3098 (cit. on p. 45).

[191] M. Gell-Mann and K. A. Brueckner, *Correlation Energy of an Electron Gas at High Density*, Phys. Rev. **106**, 2, 364–368 (1957), DOI: 10.1103/PhysRev.106.364 (cit. on p. 45).

[192] W. J. Carr, *Energy, Specific Heat, and Magnetic Properties of the Low-Density Electron Gas*, Phys. Rev. **122**, 5, 1437–1446 (1961), DOI: 10.1103/PhysRev.122.1437 (cit. on p. 45).

[193] D. M. Ceperley and B. J. Alder, *Ground State of the Electron Gas by a Stochastic Method*, Phys. Rev. Lett. **45**, 7, 566–569 (1980), DOI: 10.1103/PhysRevLett.45.566 (cit. on p. 45).

[194] T. Chachiyo, *Communication: Simple and accurate uniform electron gas correlation energy for the full range of densities*, The Journal of Chemical Physics **145**, 2, 021101 (2016), DOI: http://dx.doi.org/10.1063/1.4958669 (cit. on p. 45).

[195] S. H. Vosko, L. Wilk, and M Nusair, *Accurate spin-dependent electron liquid correlation energies for local spin density calculations: a critical analysis*, Canadian Journal of physics **58**, 8, 1200–1211 (1980) (cit. on p. 45).

[196] M. A. Marques, M. J. Oliveira, and T. Burnus, *Libxc: A library of exchange and correlation functionals for density functional theory*, Computer Physics Communications **183**, 10, 2272 –2281 (2012), DOI: http://dx.doi.org/10.1016/j.cpc.2012.05.007 (cit. on p. 45).

[197] M. Casula, S. Sorella, and G. Senatore, *Ground state properties of the one-dimensional Coulomb gas using the lattice regularized diffusion Monte Carlo method*, Phys. Rev. B **74**, 24, 245427 (2006), DOI: 10.1103/PhysRevB.74.245427 (cit. on p. 45).

[198] N. Helbig, J. I. Fuks, M. Casula, M. J. Verstraete, M. A. L. Marques, I. V. Tokatly, and A. Rubio, *Density functional theory beyond the linear regime: Validating an adiabatic local density approximation*, Phys. Rev. A **83**, 3, 032503 (2011) (cit. on p. 45).

[199] J. P. Perdew and K. Schmidt, "Jacob's ladder of density functional approximations for the exchange-correlation energy," in: *DENSITY FUNCTIONAL THEORY AND ITS APPLICATION TO MATERIALS*, vol. 577, 1, AIP Publishing, 2001, 1–20 (cit. on p. 45).

[200] D. C. Langreth and M. J. Mehl, *Beyond the local-density approximation in calculations of ground-state electronic properties*, Phys. Rev. B **28**, 4, 1809–1834 (1983), DOI: 10.1103/PhysRevB.28.1809 (cit. on p. 45).

[201] J. P. Perdew, K. Burke, and M. Ernzerhof, *Generalized Gradient Approximation Made Simple*, Phys. Rev. Lett. **77**, 18, 3865–3868 (1996) (cit. on p. 45).

[202] J. Sun, A. Ruzsinszky, and J. P. Perdew, *Strongly Constrained and Appropriately Normed Semilocal Density Functional*, Phys. Rev. Lett. **115**, 3, 036402 (2015), DOI: 10.1103/PhysRevLett.115.036402 (cit. on p. 45).

[203] J. Sun, R. C. Remsing, Y. Zhang, Z. Sun, A. Ruzsinszky, H. Peng, Z. Yang, A. Paul, U. Waghmare, X. Wu, M. L. Klein, and J. P. Perdew, *Accurate first-principles structures and energies of diversely bonded systems from an efficient density functional*, Nature Chemistry **8**, 9, 831–836 (2016), DOI: 10.1038/nchem.2535 (cit. on p. 45).

[204] R. Car, *Density functional theory: Fixing Jacob's ladder*, Nature Chemistry **8**, 9, 820–821 (2016) (cit. on p. 45).

[205] M. E. Casida, "Jacob's ladder for time-dependent density-functional theory: Some rungs on the way to photochemical heaven," in: *ACS Symposium Series*, vol. 828, Washington, DC; American Chemical Society; 1999, 2002, 199–220 (cit. on p. 45).

[206] A. D. Becke, *Density-functional thermochemistry. III. The role of exact exchange*, The Journal of Chemical Physics **98**, 7, 5648–5652 (1993) (cit. on p. 45).

[207] S. Kümmel and L. Kronik, *Orbital-dependent density functionals: Theory and applications*, Rev. Mod. Phys. **80**, 1, 3–60 (2008) (cit. on p. 45).

[208] J. Heyd, G. E. Scuseria, and M. Ernzerhof, *Hybrid functionals based on a screened Coulomb potential*, The Journal of Chemical Physics **118**, 18, 8207–8215 (2003) (cit. on p. 46).

[209] H. Xiao, J. Tahir-Kheli, and W. A. Goddard, *Accurate Band Gaps for Semiconductors from Density Functional Theory*, The Journal of Physical Chemistry Letters **2**, 3, 212–217 (2011) (cit. on p. 46).

[210] F. Caruso, D. R. Rohr, M. Hellgren, X. Ren, P. Rinke, A. Rubio, and M. Scheffler, *Bond Breaking and Bond Formation: How Electron Correlation is Captured in Many-Body Perturbation Theory and Density-Functional Theory*, Phys. Rev. Lett. **110**, 14, 146403 (2013) (cit. on p. 46).

[211] A. J. Cohen, P. Mori-Sánchez, and W. Yang, *Challenges for Density Functional Theory*, Chemical Reviews **112**, 1, 289–320 (2012) (cit. on p. 46).

[212] B. Champagne, E. A. Perpète, S. J. A. van Gisbergen, E.-J. Baerends, J. G. Snijders, C. Soubra-Ghaoui, K. A. Robins, and B. Kirtman, *Assessment of conventional density functional schemes for computing the polarizabilities and hyperpolarizabilities of conjugated oligomers: An ab initio investigation of polyacetylene chains*, The Journal of Chemical Physics **109**, 23, 10489–10498 (1998) (cit. on p. 46).

[213] S. J. A. van Gisbergen, P. R. T. Schipper, O. V. Gritsenko, E. J. Baerends, J. G. Snijders, B. Champagne, and B. Kirtman, *Electric Field Dependence of the Exchange-Correlation Potential in Molecular Chains*, Phys. Rev. Lett. **83**, 4, 694–697 (1999) (cit. on p. 46).

[214] C. R. Jacob and M. Reiher, *Spin in density-functional theory*, International Journal of Quantum Chemistry **112**, 23, 3661–3684 (2012) (cit. on p. 46).

[215] L. Kronik, T. Stein, S. Refaely-Abramson, and R. Baer, *Excitation Gaps of Finite-Sized Systems from Optimally Tuned Range-Separated Hybrid Functionals*, Journal of Chemical Theory and Computation **8**, 5, 1515–1531 (2012) (cit. on p. 46).

[216] E. Kraisler and L. Kronik, *Elimination of the asymptotic fractional dissociation problem in Kohn-Sham density-functional theory using the ensemble-generalization approach*, Phys. Rev. A **91**, 3, 032504 (2015) (cit. on p. 46).

[217] E. Kraisler and L. Kronik, *Piecewise Linearity of Approximate Density Functionals Revisited: Implications for Frontier Orbital Energies*, Phys. Rev. Lett. **110**, 12, 126403 (2013) (cit. on p. 46).

[218] C. Li, X. Zheng, A. J. Cohen, P. Mori-Sánchez, and W. Yang, *Local Scaling Correction for Reducing Delocalization Error in Density Functional Approximations*, Phys. Rev. Lett. **114**, 5, 053001 (2015) (cit. on p. 46).

[219] R. Armiento and S. Kümmel, *Orbital Localization, Charge Transfer, and Band Gaps in Semilocal Density-Functional Theory*, Phys. Rev. Lett. **111**, 3, 036402 (2013) (cit. on p. 46).

[220] H. van Aggelen, Y. Yang, and W. Yang, *Exchange-correlation energy from pairing matrix fluctuation and the particle-particle random-phase approximation*, Phys. Rev. A **88**, 3, 030501 (2013) (cit. on p. 46).

[221] M. Fuchs, Y.-M. Niquet, X. Gonze, and K. Burke, *Describing static correlation in bond dissociation by Kohn–Sham density functional theory*, The Journal of Chemical Physics **122**, 9, 094116 (2005), DOI: http://dx.doi.org/10.1063/1.1858371 (cit. on pp. 46, 64).

[222] A. J. Cohen, P. Mori-Sánchez, and W. Yang, *Insights into Current Limitations of Density Functional Theory*, Science **321**, 5890, 792–794 (2008) (cit. on pp. 46, 63).

[223] P. Mori-Sánchez, A. J. Cohen, and W. Yang, *Localization and Delocalization Errors in Density Functional Theory and Implications for Band-Gap Prediction*, Phys. Rev. Lett. **100**, 14, 146401 (2008) (cit. on p. 46).

[224] O. A. Vydrov and G. E. Scuseria, *Assessment of a long-range corrected hybrid functional*, The Journal of Chemical Physics **125**, 23, 234109 (2006) (cit. on p. 46).

[225] M. Seidl, *Strong-interaction limit of density-functional theory*, Phys. Rev. A **60**, 6, 4387–4395 (1999), DOI: 10.1103/PhysRevA.60.4387 (cit. on p. 46).

[226] M. Seidl, P. Gori-Giorgi, and A. Savin, *Strictly correlated electrons in density-functional theory: A general formulation with applications to spherical densities*, Phys. Rev. A **75**, 4, 042511 (2007) (cit. on p. 46).

[227] P. Gori-Giorgi, M. Seidl, and G. Vignale, *Density-Functional Theory for Strongly Interacting Electrons*, Phys. Rev. Lett. **103**, 16, 166402 (2009) (cit. on p. 46).

[228] A. Mirtschink, M. Seidl, and P. Gori-Giorgi, *Derivative Discontinuity in the Strong-Interaction Limit of Density-Functional Theory*, Phys. Rev. Lett. **111**, 12, 126402 (2013) (cit. on p. 46).

[229] G. Hautier, C. C. Fischer, A. Jain, T. Mueller, and G. Ceder, *Finding Nature's Missing Ternary Oxide Compounds Using Machine Learning and Density Functional Theory*, Chemistry of Materials **22**, 12, 3762–3767 (2010), DOI: 10.1021/cm100795d (cit. on p. 46).

[230] J. C. Snyder, M. Rupp, K. Hansen, K.-R. Müller, and K. Burke, *Finding Density Functionals with Machine Learning*, Phys. Rev. Lett. **108**, 25, 253002 (2012), DOI: 10.1103/PhysRevLett.108.253002 (cit. on p. 46).

[231] M. Rupp, A. Tkatchenko, K.-R. Müller, and O. A. von Lilienfeld, *Fast and Accurate Modeling of Molecular Atomization Energies with Machine Learning*, Phys. Rev. Lett. **108**, 5, 058301 (2012), DOI: 10.1103/PhysRevLett.108.058301 (cit. on p. 46).

[232] A. P. Bartók, M. J. Gillan, F. R. Manby, and G. Csányi, *Machine-learning approach for one- and two-body corrections to density functional theory: Applications to molecular and condensed water*, Phys. Rev. B **88**, 5, 054104 (2013), DOI: 10.1103/PhysRevB.88.054104 (cit. on p. 46).

[233] O. Gunnarsson and K. Schönhammer, *Density-Functional Treatment of an Exactly Solvable Semiconductor Model*, Phys. Rev. Lett. **56**, 18, 1968–1971 (1986), DOI: 10.1103/PhysRevLett.56.1968 (cit. on p. 49).

[234] K Schönhammer and O Gunnarsson, *Discontinuity of the exchange-correlation potential in density functional theory*, Journal of Physics C: Solid State Physics **20**, 24, 3675 (1987) (cit. on p. 49).

[235] I. V. Tokatly, *Time-dependent current density functional theory on a lattice*, Phys. Rev. B **83**, 3, 035127 (2011) (cit. on p. 49).

[236] P. Fulde, *Electron correlations in molecules and solids*, vol. 100, Springer Science & Business Media, 2012 (cit. on p. 52).

[237] Q. Su and J. H. Eberly, *Model atom for multiphoton physics*, Phys. Rev. A **44**, 9, 5997–6008 (1991), DOI: 10.1103/PhysRevA.44.5997 (cit. on p. 53).

[238] T. E. Baker, E. M. Stoudenmire, L. O. Wagner, K. Burke, and S. R. White, *One-dimensional mimicking of electronic structure: The case for exponentials*, Physical Review B **91**, 23, 235141 (2015) (cit. on p. 53).

[239] P. Mori-Sánchez and A. J. Cohen, *The derivative discontinuity of the exchange-correlation functional*, Phys. Chem. Chem. Phys. **16**, 28, 14378–14387 (2014) (cit. on pp. 53, 70, 72).

[240] A. J. Cohen and P. Mori-Sánchez, *Dramatic changes in electronic structure revealed by fractionally charged nuclei*, The Journal of Chemical Physics **140**, 4, – (2014) (cit. on pp. 53, 70, 72).

[241] B. W. Shore and P. L. Knight, *The jaynes-cummings model*, Journal of Modern Optics **40**, 7, 1195–1238 (1993) (cit. on p. 55).

[242] D. Braak, *Integrability of the Rabi Model*, Phys. Rev. Lett. **107**, 10, 100401 (2011), DOI: 10.1103/PhysRevLett.107.100401 (cit. on p. 55).

[243] A. Le Boité, M.-J. Hwang, H. Nha, and M. B. Plenio, *Fate of photon blockade in the deep strong-coupling regime*, Phys. Rev. A **94**, 3, 033827 (2016), DOI: 10.1103/PhysRevA.94.033827 (cit. on p. 55).

[244] J. Calderón and F. De Zela, *Geometric phases and the Rabi Hamiltonian*, Phys. Rev. A **93**, 3, 033823 (2016), DOI: 10.1103/PhysRevA.93.033823 (cit. on p. 55).

[245] Q. Xie, H. Zhong, M. T. Batchelor, and C. Lee, *The quantum Rabi model: solution and dynamics*, ArXiv e-prints arXiv: 1609.00434 (quant-ph) (2016) (cit. on p. 55).

[246] N. Säkkinen, Y. Peng, H. Appel, and R. van Leeuwen, *Many-body Green's function theory for electron-phonon interactions: Ground state properties of the Holstein dimer*, The Journal of Chemical Physics **143**, 23, 234101 (2015), DOI: 10.1063/1.4936142 (cit. on pp. 56, 59).

[247] N. Säkkinen, Y. Peng, H. Appel, and R. van Leeuwen, *Many-body Green's function theory for electron-phonon interactions: The Kadanoff-Baym approach to spectral properties of the Holstein dimer*, The Journal of Chemical Physics **143**, 23, 234102 (2015), DOI: 10.1063/1.4936143 (cit. on p. 56).

[248] M. Berciu, *Exact Green's functions for the two-site Hubbard-Holstein Hamiltonian*, Phys. Rev. B **75**, 8, 081101 (2007), DOI: 10.1103/PhysRevB.75.081101 (cit. on p. 56).

[249] J. Flick, H. Appel, and A. Rubio, *Nonadiabatic and Time-Resolved Photoelectron Spectroscopy for Molecular Systems*, J. Chem. Theory Comput. **10**, 4, 1665–1676 (2014), DOI: 10.1021/ct4010933 (cit. on p. 56).

[250] J. Calderón and F. De Zela, *Geometric phases and the Rabi Hamiltonian*, Phys. Rev. A **93**, 3, 033823 (2016), DOI: 10.1103/PhysRevA.93.033823 (cit. on p. 56).

[251] T. Dimitrov, J. Flick, M. Ruggenthaler, and A. Rubio, *Exact maps in correlated electron-photon systems*, to be submitted (2017) (cit. on pp. 69, 87, 129).

[252] G. Albareda, H. Appel, I. Franco, A. Abedi, and A. Rubio, *Correlated Electron-Nuclear Dynamics with Conditional Wave Functions*, Phys. Rev. Lett. **113**, 8, 083003 (2014), DOI: 10.1103/PhysRevLett.113.083003 (cit. on p. 87).

[253] G. Albareda, J. M. Bofill, I. Tavernelli, F. Huarte-Larrañaga, F. Illas, and A. Rubio, *Conditional Born–Oppenheimer Dynamics: Quantum Dynamics Simulations for the Model Porphine*, The Journal of Physical Chemistry Letters **6**, 9, 1529–1535 (2015), DOI: 10.1021/acs.jpclett.5b00422 (cit. on p. 87).

[254] A. Abedi, N. T. Maitra, and E. K. U. Gross, *Exact Factorization of the Time-Dependent Electron-Nuclear Wave Function*, Phys. Rev. Lett. **105**, 12, 123002 (2010), DOI: 10.1103/PhysRevLett.105.123002 (cit. on p. 87).

[255] E. Khosravi, A. Abedi, and N. T. Maitra, *Exact Potential Driving the Electron Dynamics in Enhanced Ionization of* H_2^+, Phys. Rev. Lett. **115**, 26, 263002 (2015), DOI: 10.1103/PhysRevLett.115.263002 (cit. on p. 87).

[256] J. Flick, H. Appel, M. Ruggenthaler, and A. Rubio, *Cavity Born-Oppenheimer Approximation for Correlated Electron-Nuclear-Photon Systems*, arXiv: 1611.09306 [quant-ph] arXiv: 1611.09306 (quant-ph) (2016) (cit. on p. 88).

[257] M. Ruggenthaler, *Ground-State Quantum-Electrodynamical Density-Functional Theory*, ArXiv e-prints arXiv: 1509.01417 (quant-ph) (2015) (cit. on p. 93).

[258] S. Kümmel, L. Kronik, and J. P. Perdew, *Electrical Response of Molecular Chains from Density Functional Theory*, Phys. Rev. Lett. **93**, 21, 213002 (2004), DOI: 10.1103/PhysRevLett.93.213002 (cit. on pp. 96, 97).

[259] V. Mujica, A. E. Roitberg, and M. Ratner, *Molecular wire conductance: Electrostatic potential spatial profile*, The Journal of Chemical Physics **112**, 15, 6834–6839 (2000), DOI: 10.1063/1.481258 (cit. on p. 97).

[260] S. K. S. Mazinani, R. V. Meidanshahi, J. L. Palma, P. Tarakeshwar, T. Hansen, M. A. Ratner, and V. Mujica, *Polarizability as a Molecular Descriptor for Conductance in Organic Molecular Circuits*, The Journal of Physical Chemistry C **120**, 45, 26054–26060 (2016), DOI: 10.1021/acs.jpcc.6b06241 (cit. on p. 97).

[261] V. L. Lignères and E. A. Carter, *An Introduction to Orbital-Free Density Functional Theory*, in: *Handbook of Materials Modeling: Methods*, ed. by S. Yip, Dordrecht: Springer Netherlands, 2005, 137–148, ISBN: 978-1-4020-3286-8, DOI: 10.1007/978-1-4020-3286-8_9 (cit. on p. 103).

[262] H. Eschrig and W. Pickett, *Density functional theory of magnetic systems revisited*, Solid State Communications **118**, 3, 123 –127 (2001) (cit. on p. 103).

[263] G. Knizia and G. K.-L. Chan, *Density matrix embedding: A strong-coupling quantum embedding theory*, Journal of chemical theory and computation **9**, 3, 1428–1432 (2013) (cit. on p. 103).

[264] S. Wouters, C. A. Jiménez-Hoyos, Q. Sun, and G. K.-L. Chan, *A practical guide to density matrix embedding theory in quantum chemistry*, Journal of chemical theory and computation (2016) (cit. on p. 103).

LIST OF FIGURES

LIST OF TABLES

ACRONYMS

CI configuration interaction

CSDFT current-spin density functional theory

DFT density-functional theory

DMET density-matrix embedding theory

DMRG Density-matrix renormalization group

GGA general gradient approximation

HK Hohenberg-Kohn

HEG homogeneous electron gas

KS Kohn-Sham

LDA local-density approximation

libxc library of exchange and correlation functionals

PBE Perdew-Burke-Ernzerhof

PDFT partitioning density-functional theory

QEDFT quantum-electrodynamical density-functional theory

QED quantum electrodynamics

QMC quantum Monte Carlo

RPA Random-phase approximation

RDFT relativistic density-functional theory

SCAN strongly constrained and appropriately normed

TDCDFT time-dependent current-density functional theory

TDDFT time-dependent density-functional theory

xc exchange-correlation

TALKS, POSTER & PUBLICATIONS

Some ideas and figures have been shown previously in the following talks, poster or publications:

2013

DPG Regensburg- Linear and non-linear responses in pump-probe spectroscopy (Talk)

Density Functional Theory: learning from the past, looking to the future, Berlin, The exact Hohenberg-Kohn functional for a lattice model (Poster)

2014

6th Time-Dependent Density Functional Theory: Prospects and Applications, Benasque - The exact Hohenberg-Kohn functional for a lattice model (Poster)

DinL Winterschool, Winkelmoos Alm, Exact Hohenberg-Kohn-Functional for a Lattice System (Talk)

DPG Dresden, The exact Hohenberg-Kohn functional for a lattice model (Talk)

White nights of materials science: From physics and chemistry to data analysis, and back, Saint Petersburg, Russia, Exact Hohenberg-Kohn-Functional for a Lattice Model (Poster)

2015

DPG Berlin, Exact functionals for a lattice model (Talk)

Publications

T. Dimitrov, H. Appel, J. I. Fuks, and A. Rubio, "Exact maps in density functional theory for lattice models", New Journal of Physics **18**, 8, 083004 (2016) [116]

T. Dimitrov, J. Flick, M. Ruggenthaler, and A. Rubio, "Exact maps in correlated electron-photon systems" (to be submitted) [251]

ACKNOWLEDGMENTS

I would like to thank Prof. Rubio for giving me the opportunity to write my PhD thesis under his supervision, for his support and ideas.
I thank Prof. Scheffler for giving me the opportunity to work in the FHI and for his support. The FHI always has been a great scientific and friendly environment with a great infrastructure. I really enjoyed working here.
I would like to thank Prof. Dähne for beeing the head of the PhD comitee.
I would like to thank Prof. Knorr for accepting me as a PhD student at the Technical University. The technical university has always been a stimulating environment during my studies, where I have learned a lot and where I have met a lot of friends.
I like to thank Dr. Appel for giving me the opportunity to write the PhD thesis under his supervision, for proofreading this thesis, for introducing me to the field of density functional theory and for helping me with his ideas and discussions.
For fruitful discussions and collaboration I would like to thank Dr. Ruggenthaler and Dr. Fuks. In particular, I would like to thank Dr. Fuks for her constant support during the preparation of the manuscript on the exact maps in DFT.
I really like to thank Julia and Birgit who helped me from the start to the end of my time at the FHI with organizational questions and who make the FHI to a very welcoming and friendly place.
I also like to thank Anne Hodgson and Heidi for helping me to improve my academic writing skills.
A big thanks goes also to Uyen, Lydia, Franz, Björn, Viktor, Karsten, Carsten, Rene, Wael, Markus, Fabio, Susmita, Amrita, Guillem, Christian, Jessica, Adriana, Sebastian, Arvid, Benjamin, Samara, Nora, Florian, Teresa, Uliana and Johannes.
I am super grateful that I am surrounded by constant support, love and friendship. Therefore, I would like to thank my family and in particular my parents, and Nicole, Shaela, Drake and Chris. I am lucky to have the greatest parents in the world, who unconditionally supported me and helped whenever needed. I also like to thank my sister Nicole who happens to always find the right words "Lass die Ohren nicht hängen". Thanks for always beeing there for me! A big thanks also to Bärbel and Detlef for their encouragement.
I also would like to thank my friends for their encouragement and support and for making my life so much happier: Many thanks to Isi, Conni, Tini, Kadi, Moritz, Nina, Jörg, Bekka, Lia, Justus, Robert, Diana, Björn, Nadine, Alex & Alex, Susi, Aylin, and Johannes.
A special thanks goes to Johannes, who constantly supported me, who proofread my manuscripts and this thesis, shared his enthusiasm about QEDFT, for scientific and numerical advices, for fruitful discussions and his countless ideas, for lots of fun, his encouragement and his unconditional love and support.

COLOPHON

This document was typeset using LaTeX and `classicthesis`.
The plots have been created using python 2.7.9. with matplotlib, SciPy, Inkscape, and TikZ.

Final Version as of January, 2017 (`Exact maps in density functional theory` version 1.0).